

AD-A992 241

MASSACHUSETTS INST OF TECH CAMBRIDGE DEPT OF MATERIALS-ETC F/6 11/9  
MOLECULAR FRACTION BEHAVIOR IN ORIENTED POLYMERS,(U)  
JUN 80 R K POPLI, D K ROYLANC

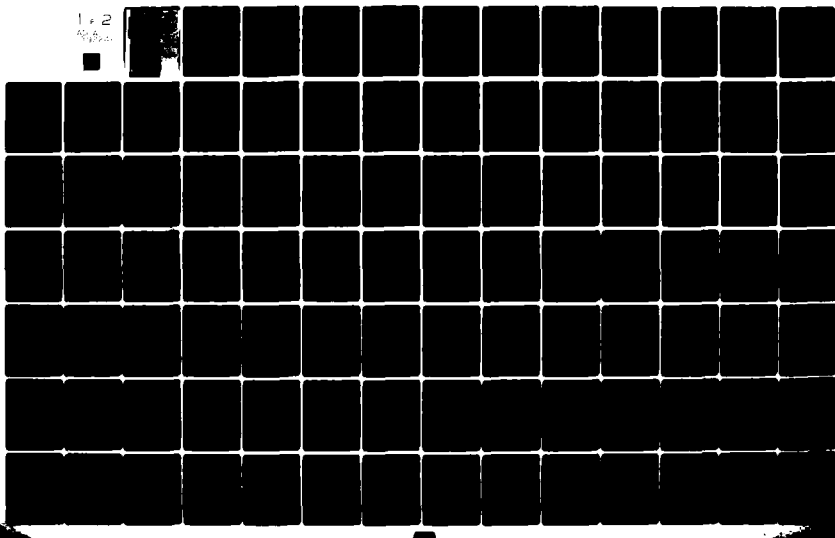
DAAG29-76-C-0044

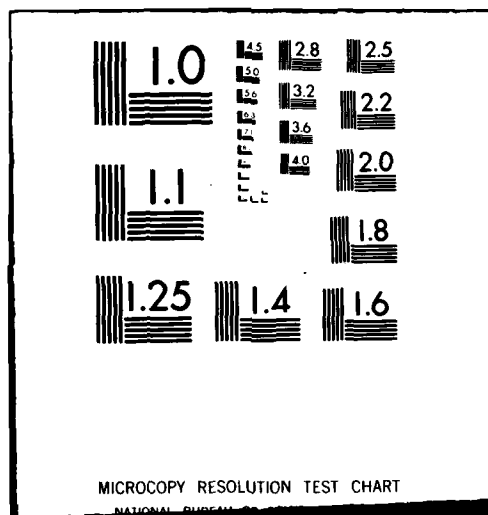
ARO-13630.3-MSX

NL

UNCLASSIFIED

1 & 2  
ARO-13630.3-MSX





MICROCOPY RESOLUTION TEST CHART  
NATIONAL BUREAU OF STANDARDS

AD A092241

LEVEL

ARO

(12)

MIT

MOLECULAR FRACTURE BEHAVIOR IN  
ORIENTED POLYMERS

Rakesh K. Popli  
David K. Roylance

June 1980

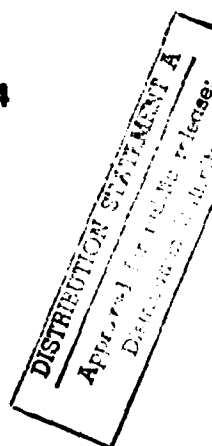
DEPARTMENT  
OF  
MATERIALS SCIENCE  
AND  
ENGINEERING

SCHOOL OF ENGINEERING  
MASSACHUSETTS INSTITUTE OF TECHNOLOGY  
Cambridge, Massachusetts 02139

Final Report  
Contract Number DAAG-29-76-C-0044

Approved for public release;  
distribution unlimited

Prepared for  
U.S. Army Research Office  
P.O. Box 12211  
Research Triangle Park, NC 27709



DDC FILE COPY

**UNCLASSIFIED**

SECURITY CLASSIFICATION OF THIS PAGE (When Data Entered)

(9) Final Rep. 11/1/76-31/May/79

REPORT DOCUMENTATION PAGE		READ INSTRUCTIONS BEFORE COMPLETING FORM
1. REPORT NUMBER	2. GOVT ACCESSION NO.	3. RECIPIENT'S CATALOG NUMBER
	AD-A092241	
4. TITLE (and Subtitle)	5. TYPE OF REPORT & PERIOD COVERED	
MOLECULAR FRACTURE BEHAVIOR IN ORIENTED POLYMERS.	Final 9/1/76-8/31/79	
7. AUTHOR(s)	6. PERFORMING ORG. REPORT NUMBER	
Rakesh K./Popli/ David K./Roylance	DAAG29-76-C-0044	
9. PERFORMING ORGANIZATION NAME AND ADDRESS	10. PROGRAM ELEMENT, PROJECT, TASK AREA & WORK UNIT NUMBERS	
Massachusetts Institute of Technology Department of Materials Science and Engineering ✓ 77 Massachusetts Ave. Cambridge, MA 02139	(13) 136	
11. CONTROLLING OFFICE NAME AND ADDRESS	12. REPORT DATE	
U.S. Army Research Office P.O. Box 12211 Research Triangle Park, NC 27709	June 1980	
14. MONITORING AGENCY NAME & ADDRESS(if different from Controlling Office)	13. NUMBER OF PAGES	
18/100 (13) 13630-3-15 X	134	
16. DISTRIBUTION STATEMENT (of this Report)	15. SECURITY CLASS. (of this report)	
Approved for public release; distribution unlimited.	U	
17. DISTRIBUTION STATEMENT (of the abstract entered in Block 20, if different from Report)	15a. DECLASSIFICATION/DOWNGRADING SCHEDULE	
18. SUPPLEMENTARY NOTES		
THE VIEW, OPINIONS, AND/OR FINDINGS CONTAINED IN THIS REPORT ARE THOSE OF THE AUTHOR(S) AND SHOULD NOT BE CONSTRUED AS AN OFFICIAL DEPARTMENT OF THE ARMY POSITION, POLICY, OR DE- CISION, UNLESS SO DESIGNATED BY OTHER DOCUMENTATION.		
19. KEY WORDS (Continue on reverse side if necessary and identify by block number)		
polymers, fracture, deformation, degradation, chromatography, spectroscopy, nylon		
20. ABSTRACT (Continue on reverse side if necessary and identify by block number)		
Fracture in polymers of fibrous morphology is accompanied by covalent bond scission. Gel permeation chromatography (GPC) was used to monitor the changes in molecular weight distribution upon fracture in nylon 6 fibers. The bond rupture of $2.3 \times 10^{18}$ per cm <sup>3</sup> measured from GPC is approximately five times the number of free radicals observed on fracture using electron spin resonance (ESR). GPC results showed that the high molecular weight component of the molecular weight distribution ruptures preferentially. Fourier transform infra-red		

SECURITY CLASSIFICATION OF THIS PAGE(When Data Entered)

spectroscopy (FTIS) observation of virgin, fractured, ground and irradiated nylon 6 fiber specimens provided additional evidence supporting the results of GPC and ESR. A quantitative measure of the bond rupture could not be obtained from FTIS measurements.

Some calculations for the structure of the fibrous morphology were performed: (1) Calculation for the number of tie molecules per gram. This was found to be approximately  $1 \times 10^{20}$  per gram in nylon 6 fibers. (2) Calculation for the contribution of various amorphous components like cilia, chain loops (folds), chain ends, and tie chains. (3) A model for the distribution of the tie chain lengths.

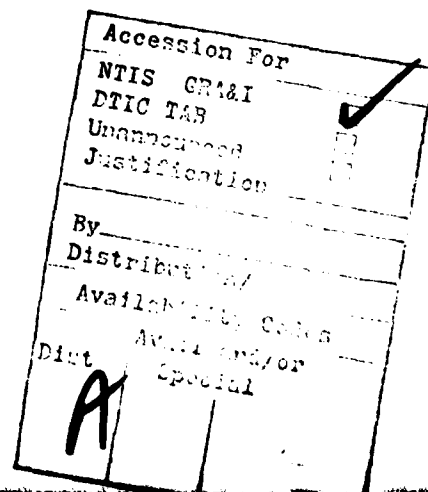
The experimental results of GPC and some of the calculations above were used to review the morphology and the fracture behavior of the fibrous structure. A new mechanism for the formation of submicroscopic cracks in stressed fibers is proposed.

UNCLASSIFIED

SECURITY CLASSIFICATION OF THIS PAGE(When Data Entered)

## CONTENTS

<b>1. Introduction .....</b>	<b>10</b>
<b>2. Background .....</b>	<b>12</b>
2.1 Classical Failure Criteria .....	12
2.2 Fracture Mechanics Approach .....	14
2.3 Viscoelastic Models .....	15
2.4 Kinetic Rate Process Theories of Fracture .....	16
2.5 Molecular-Morphological Models of Fracture .....	24
<b>3. Experimental Studies of Mechanochemical Degradation .....</b>	<b>36</b>
3.1 Introduction .....	36
3.2 ESR Studies .....	40
3.3 Infrared Spectroscopy of Nylon 6 and Polyethylene .....	45
3.4 Gel Permeation Chromatography .....	56
<b>4. Analysis of Tie Chain Scission .....</b>	<b>76</b>
4.1 Model for Tie Chain Length Distribution .....	76
4.2 Calculation for Number of Tie Molecules .....	94
4.3 Discussion .....	96
<b>Appendix I. Calculation for P(N,r) .....</b>	<b>108</b>
<b>Appendix II. Calculation for X .....</b>	<b>112</b>
<b>Appendix III. Calculation of Amorphous Components .....</b>	<b>114</b>
<b>Appendix IV. GPC Calibration .....</b>	<b>117</b>
<b>Appendix V. Median Rank Plotting .....</b>	<b>123</b>
<b>Appendix VI. Viscosity of Nylon 6 in Dilute Solutions .....</b>	<b>126</b>
<b>References .....</b>	<b>132</b>



## LIST OF FIGURES

Figure	Title	Page
1	Decay characteristics within a population of randomly oriented elements.	23
2	Simulated brittle fracture events in x-y plane as a function of $t/\tau$ .	23
3	Histograms of nylon 6 free radical concentration from step-strain at room temperature.	31
4	Distribution of relative chain lengths of tie molecules ( $L/L_0$ ) of nylon 6 fibers from step-strain data using Lloyd-DeVries model.	31
5	Four phase model of the fibrous structure.	32
6	Model of highly oriented semi-crystalline fiber.	33
7	Fibrillar model of the fibrous structure.	34
8	Crack coalescence mechanism - (A) radial, (B) axial direction of the fibrous structure.	35
9	Energetic characteristics due to rupture of molecules during loading of nylon 6.	35
10	Nylon 6 fiber tensile specimen.	39
11	Stress-strain curve for nylon 6 fibers.	39
12	ESR spectra of irradiated nylon 6 fibers at temperature of $298^0$ K.	42
13	ESR spectra of irradiated nylon 6 fibers at temperature of $269^0$ K.	42
14	ESR spectra of irradiated nylon 6 fibers at temperature of $242^0$ K.	43
15	ESR spectra of irradiated nylon 6 fibers at temperature of $188^0$ K.	43

16	Nylon 6 ESR calibration curve.	44
17	Kinetics of free radical decay.	44
18	IR spectra of virgin nylon 6 fibers.	47
19	IR spectra of fractured nylon 6 fibers.	48
20	IR spectra of ground nylon 6 fibers.	49
21	IR spectra of irradiated nylon 6 fibers.	50
22	Principles of Gel Permeation Chromatography (GPC).	58
23	Schematics of a GPC instrument.	58
24	GPC calibration curve for polystyrene at 25 <sup>0</sup> C.	61
25	Averaged molecular weight distribution (MWD) of virgin and crazed polystyrene at 25 <sup>0</sup> C.	62
26	Median rank plot for weight average molecular weight ( $\bar{M}_w$ ) of polystyrene.	64
27	Median rank plot for number average molecular weight ( $\bar{M}_n$ ) of polystyrene.	65
28	Averaged MWDs of virgin and fractured nylon 6 fibers.	68
29	Median rank plot for weight average molecular weight ( $\bar{M}_w$ ) for nylon 6 fibers.	70
30	Median rank plot for number average molecular weight ( $\bar{M}_n$ ) for nylon 6 fibers.	70
31	Median rank plot for polydispersity 'V' for nylon 6 fibers.	71
32	Calculation for the number of molecules ruptured per gram in nylon 6 fibers on fracture.	72
33	Distribution for the number of molecules per gram in virgin and fractured nylon 6 fibers.	73
34	Difference MWD = MWD of fractured nylon 6 fibers - MWD of virgin nylon 6 fibers.	74

35	Difference distribution = Number of molecules per gram in fractured nylon 6 fibers - Number of molecules per gram in virgin nylon 6 fibers.	74
36	Typical crystalline and amorphous regions of the fibrous structure.	78
37	Schematic drawing of a tie chain and the interfacial zone in an amorphous region.	78
38	Chain configurations not allowed in the amorphous region of a semi-crystalline polymer.	79
39	A view of the alternating crystalline and amorphous blocks in the fibrous structure.	79
39a	Cross-sectional view of the crystal face for computer modelling.	79
40	A drawing for calculation of RSQR(i,j) in the model for tie length distribution.	87
41	Fraction of tie molecules vs. relative lengths of tie molecules.	91
42	Cumulative fraction of tie molecules vs. relative lengths of tie molecules.	92
43	Fractional change in concentration vs. $\log_{10}$ (Molecular Weight).	106
44	Comparison of the cumulative tie chain distributions from Lloyd-DeVries model and theoretical model.	106
45	Comparison between the stress-strain behavior predicted by Lloyd-DeVries model and the experimentally measured one.	107
46	Viscosity of nylon 6 fibers in dilute solution of hexafluoro-iso-propanol (S-HFIP).	128
47	Viscosity of Allied nylon 6 in dilute solution of hexafluoro-iso-propanol (S-HFIP).	128
48	Viscosity of nylon 6 fibers in dilute solution of tetrafluoro-ethanol (S-TFE).	129
49	Viscosity of Allied nylon 6 in dilute solution of	

	tetrafluoro-ethanol (S-TFE).	129
50	Viscosity of nylon 6 fibers in dilute solution of formic acid (88%).	130
51	Viscosity of Allied nylon 6 in dilute solution of formic acid (88%).	130

LIST OF TABLES

Table	Title	Page
1	IR spectroscopy band assignment for nylon 6.	51
2	Changes in nylon 6 bands on irradiation.	52
3	Changes in nylon 6 IR bands on grinding.	53
4	Changes in the intensity of IR end-group bands on drawing of polyethylene.	55
5	Tabulation of number, weight average molecular weights and polydispersity for virgin and crazed polyethylene.	63
6	Tabulation of number, weight average molecular weights and polydispersity for virgin and fractured nylon 6 fibers.	69
7	Contribution of crystalline and various amorphous components (chain ends, chain loops (folds), cilia, and tie chains) to the semi-crystalline nylon 6 fiber morphology.	105
8	Universal Calibration equations.	122
9	Viscosity constants for nylon 6 fiber and Allied nylon 6 in hexafluoro-iso-propanol, tetrafluoro-ethanol, and aqueous formic acid (88%).	131

#### **ACKNOWLEDGEMENTS**

The authors wish to thank the many helpful contributions made to this work by Ms. Jeanne Counter, Prof. E.W. Merrill, and Prof. F.J. McGarry. We are also most grateful for the financial support and technical advice made available by the U.S. Army Research Office under Contract DAAG29-76-C-0040.

## **1. Introduction**

The increased use of polymers in structural applications puts a premium requirement on the desired mechanical properties of these materials. A basic understanding of the factors and processes governing the stress-strain characteristics and the fracture behavior is essential in this regard. It is generally believed that the stress-strain behavior is determined by the overall structure whereas the fracture characteristics are controlled by the critical phenomena in the material, for example, the longest flaw may determine the ultimate strength. A knowledge of the morphology and structure of the materials is essential to understanding of its mechanical response.

The study of fracture can be approached from two frames of reference:

(1). Macroscopic: The macroscopic viewpoint treats the material as a continuum containing flaws and other inhomogeneities. This is referred to as Fracture Mechanics and consists in devising a functional relationship between the properties and some parameter of the material on the basis of energy balance or an analysis of the stress intensity factor at the tip of the crack to deal with local stresses and strains. Fracture mechanics has very successfully provided many engineering criteria for failure and an extensive research effort is active in the area at the present time. Such a framework, however, fails to provide information regarding the molecular processes and interactions that govern and accompany the macroscopic failure of the materials.

(2). Molecular or Microscopic: The molecular approach relates observed macroscopic behavior to the scenarios being played at the molecular level. Such an understanding is tremendously important for the formulation of a structure-property relationship. The molecular understanding of the structure-property relationship will provide material scientists and engineers with an insight into the expected behavior under various mechanical stress histories. This will also provide the means for design of materials with superior properties and materials tailored to specific needs.

Such an endeavor towards understanding the molecular nature of fracture has been taken up by many researchers over the past two decades. The application of analytical means for study of molecular fracture in polymers was initiated with the use of Electron Spin Resonance (ESR) by Zhurkov and colleagues to measure the covalent bond scission caused by mechanical stress. Thereafter a large number of researchers have used ESR and other analytical methods for investigation of molecular fracture. These studies have related the observed mechanical response to the morphological structure of the materials but with partial success. It is an ongoing process and this research effort is another step in the same direction.

This research has introduced a new analytical technique - Gel Permeation Chromatography (GPC) - for the study of changes in the molecular weight distribution on fracture. GPC has been successfully used to determine the changes on fracture in nylon 6 fibers broken under uniaxial loading and polystyrene specimens where extensive damage was produced from multiple cracking. The results of GPC and IR spectroscopic investigations of this study for nylon 6 fibers are basically in agreement with the reported ESR measures of bond scission in the same material, and therefore allays generally expressed doubts regarding use of ESR. GPC studies have provided additional information regarding the role of different molecular weight components of the distribution in determining the fracture behavior.

A theoretical calculation for the distribution of the lengths of tie chains in the amorphous region is performed. This calculation gives information about the morphological structure of the amorphous regions of the semi-crystalline polymers and this morphological information is employed to obtain a description of the fracture behavior in fibrous morphology. A new means for the formation of submicroscopic cracks, which have been experimentally observed using Small Angle X-ray Scattering (SAXS), is suggested and discussed to indicate that it provides a better explanation for the observed fracture response.

## **2. Background**

Strength of materials and ways to improve it have been a matter of concern for man long since he moved from the stone age. Over the past few thousand years among different civilizations experience with the use of various materials has provided the major guidelines toward obtaining better materials. A scientific approach in this area had its beginnings in eighteenth century, along with the growing interest in other scientific disciplines such as physics, chemistry and biology. Earlier studies obtained a single material characteristic such as critical stress, strain, energy absorbed, etc. to determine a fracture criterion. Griffith's paper in 1920 started what has come to be known as Fracture Mechanics. Griffith's fracture criterion was based on an energy balance between the energy required to form the new surface ahead of a crack and a decrease in the elastically stored energy. Further investigations in the area have led to other criteria such as critical stress intensity factor  $K_{Ic}$ , energy release rate  $G_{Ic}$ , J-integral, Crack Opening Displacement, etc. Very active research in fracture mechanics is continuing at the present time.

Over the past forty years or so increasing attention has been devoted to understand the molecular nature of the fracture process. These molecular models of fracture are referred to as 'Kinetic Rate Process Models'; the earliest one is due to Tobolsky and Eyring, and others have been developed by Coleman, Bueche, Hsiao-Kausch, Lloyd-DeVries and Peterlin. These different approaches to fracture analysis are discussed in this chapter.

### **2.1 Classical Failure Criteria**

Classical continuum mechanics deals with homogeneous isotropic materials. Failure criteria in this approach are established on the basis that some strategic property of the material such as uniaxial tensile strength, shear strength, strain, energy stored or applied, reach a critical value. These kinds of criteria have been used to obtain failure surfaces in three-dimensional stress space.

Fracture manifests itself in different forms such as brittle, ductile or through plastic deformation or some kind of mixed mode. These different fracture modes result in different failure surfaces which may overlap and penetrate each other. Some of the principal classical criteria are the following:

1. Maximum Principal Stress Theory (Rankine's Theory) states that the largest principal stress component, say  $s_3$ , in the material determines failure regardless of other normal or shearing stress, i.e., the stability criterion is

$$s_3 < s^* \text{ where } s^* \text{ is a basic material property.}$$

2. Maximum Elastic Strain Theory (St. Venant's Theory) states that it is the largest principal strain that determines the failure, i.e.,

$$e_3 = 1/E [s_3 - v(s_1 + s_2)] < e^*$$

3. Constant Elastic Strain Energy of Distortion. Large amounts of elastic energy due to hydrostatic pressure may be stored without causing either fracture or permanent deformation. The energy criterion is based on the assumption that the energy of distortion  $W$  determines the criticality state of stress. For small elastic deformation one obtains:

$$6E * W/(1+v) = [(s_1 - s_2)^2 + (s_2 - s_3)^2 + (s_3 - s_1)^2] < 2(s^*)^2.$$

4. Coulomb Yield Criterion assumes a critical yield stress  $T^*$  which is pressure dependent in any plane and describes the failure mode.

$$(s_3 - s_1) < T^* = T_0 + \mu s_N$$

The latter two criteria have received the most experimental support. The above criteria do not have explicit time-dependence, but this may be obtained by considering that the critical value of the parameters are themselves time-dependent. Also, these failure criteria fail to take into account the complete stress state, thereby neglecting some of the stress effects.

## 2.2 Fracture Mechanics Approach

Real solids have flaws, voids, cracks or other inhomogeneities which distort a homogeneous applied stress field. The continuum mechanical approach which derives its criterion for crack stability from an energy balance consideration is a fracture mechanics approach. Griffith (1) fracture mechanics, the earliest approach in this direction, was based on the balance between the energy required to produce the new surface ahead of a crack and a decrease in the elastically stored energy. Griffith further proposed that the elastically stored energy is not distributed uniformly throughout the specimen but is concentrated in the neighborhood of small cracks. Fracture thus occurs by spreading of cracks which originate in the pre-existing flaws. The crack growth by a length  $dC$  is governed by the equation

$$-dU/dC = \gamma C(dA/dC)$$

For an elliptical crack of length  $2C$ , stressed at right angles to the major axis of the crack, the tensile strength  $S_b$  of the material is given as

$$S_b = [2\gamma E/C]^{0.5}$$

where  $E$  is the Young's modulus.

This shows that the observed macroscopic strength is much smaller than the theoretical strength of the flawless specimen. The problem has been generalized to three dimensions and alternative formulations like the one due to Irwin for stresses in a planar crack for plane strain and plane stress have been devised. For an infinite plate with a central crack of length  $2C$  subjected to a uniform stress, the Griffith and Irwin formulations are equivalent. Another fracture mechanics critical criterion is that fracture occurs when the strain energy release rate  $G$  (decrease in strain energy per unit increase in crack length) reaches a critical value  $G_c$ .

Except in the case of glass, the values for surface energy are greatly in excess of those calculated on the basis of separating planes of atoms to form the fracture surface. This led Orowan and others to

propose that the surface-free energy may also include a term arising from the plastic work done in deformation adjacent to the fracture plane as the crack propagates.

Various extensions and improvements in fracture mechanics over the years have been made. Some of the important ones are the J-integral and the Crack Opening Displacement.

The J-integral uses a parameter, J, derived from non-linear elastic behavior which bears the same function as does G in linear elastic theory and a critical value for J culminates in the fracture of the solid.

The Crack Opening Displacement (COD) criterion is based on the consideration that a critical COD is needed to determine whether the fracture is brittle or ductile. A correlation of  $(COD)_{critical}$  to either  $G_{critical}$  or  $K_{Ic}$  values of fracture criteria is lacking.

An active research in the use of fracture mechanics for different materials is being pursued, but some polymeric materials do not conform to linear fracture mechanics and other approaches such as the J-integral or COD have not been successful either.

### 2.3 Viscoelastic Models

These models, based on the studies of Smith (2), Bueche and Halpin (3, 6) assume that for polymers (crosslinked rubber), the viscoelastic behavior could be reduced according to the time-temperature superposition principle for stress, strain-rate and temperature corresponding to their states. If the failure criterion refers to the unique molecular state (load-carrying capabilities), then the plot of reduced stress at break against the reduced strain at break should lead to a master curve, representing the failure envelope. Smith's results describe remarkably well the experimental behavior and the reduced shift factors obtained correspond to WLF equation for superposition of low strain linear viscoelastic behavior of the amorphous polymers. Bueche has theoretically derived such a failure envelope based on viscoelastic behavior for the polymers.

These models, however, do not allow the prediction of failure envelope or conversion of data

between different modes of excitation (uniaxial, biaxial, and multiaxial). They recognize the molecular origin of the viscoelastic behavior of a material, but do not refer to the discrete quantities, anisotropy of the molecular properties or distribution of molecular stress or strain, i.e., the solid is essentially treated as a continuum.

#### 2.4 Kinetic Rate Process Theories of Fracture

As opposed to continuum mechanical theories, molecular rate process theories of fracture recognize the presence of discrete elements forming the material body. The deformation and breakage of these elements determines the fracture of the structural material. The basic fracture events are controlled by the thermally and stress-activated primary or secondary bond rupture; the accumulation of these micro-events leading to formation of cracks, which upon reaching a critical value, cause specimen failure. Some of the rate process models have also taken into account the morphology of the material. A few of the characteristic aspects of these generalized, non-inmorphological rate process fracture theories are discussed here.

Tobolsky-Eyring Model: Tobolsky and Eyring (4) proposed that the breaking of polymer threads under uniaxial loads was due to the breaking of the secondary bonds at stress and temperature dependent rates. The rate of decrease of N number of such bonds per unit cross-sectional areas under constant stress  $f_0$  is given as

$$dN/Ndt = kT/h \exp\{-\Delta F/RT\} * 2 \sinh\{f_0/\lambda^2 NkT\}$$

$\lambda$  is the mean separation between the equilibrium positions of the minimum force potential.

Thread lifetime is obtained by integrating this equation from an initial value of N, namely  $N_0$ , to a final value of zero; that is, the thread breaks when the number of remaining bonds is zero. The above equation takes into consideration the possibility of a reverse reaction in which the bond would be

repaired. For large values of stresses, when the repair of bonds is insignificant, the equation is

$$dN/Ndt = kT/h \exp\{-\Delta F/RT\} * \exp\{f_0 \lambda/2NkT\}$$

According to this model, the logarithm of lifetime is related almost linearly to the applied stress.

This work laid the foundation for the kinetic theory of fracture which has been further worked on subsequently by a larger number of researchers.

Coleman Model: Coleman (5) applied a reaction rate model to the rupture of polymeric threads subjected to constant loads, to loads increasing linearly with time and to sinusoidal applied loads. His model differs from the Eyring approach in that Coleman assumes that bond slipping (not bond rupture) is the basic mechanism of failure and that the microstructure can tolerate maximum distortion of  $g = g_b$ . In keeping with this mechanism of bond slippage, the number of bonds stay constant at its initial value  $N_0$ . Coleman's differential equation is

$$dg/dt = kT/h \exp\{-\Delta F/RT\} * 2 \sinh \{\lambda/2N_0 kT\}$$

where  $g$  is the strain.

The solution in integrated form looks like

$$\tau * kT/h * \exp\{-\Delta F/RT\} = g_b / \exp\{-\lambda/2N_0 kT\}$$

Experimental rupture times obtained from Tobolsky-Eyring model and Coleman model give very similar values for the rupture time .

Bueche-Halpin Model: The limited viscoelastic extensibility of rubber strands, according to the theory proposed by Bueche and Halpin (6), determines the fracture of the elastomer. According to these authors, under a constant load the specimen elongates and small tears ( $10^{-5}$  cm. long) within the specimen are initiated. A very highly strained thin filament ( $10 - 100 \lambda^0$ ) exist at the tip of a tear. The

stress on filament is  $S^*K$  where  $S$  is applied stress and  $K$ , the stress intensity factor, is of the order of  $10^2 - 10^3$ . The filament creeps and ruptures on reaching a critical breaking elongation. On rupture of filament, the tear will propagate further through a distance the thickness of the filament. Idealizing the propagation process to be stepwise in nature, the new material at the tip takes a finite time to fracture. Thus, the rate of tear propagation is determined by the creep curve of the elastomer.

The sample as a whole ruptures when the tear has propagated through  $q$  filament lengths. Here  $q$  is of the order of  $10^4 - 10^7$ . If the sample as a whole breaks in time  $T_b$ , each filament requires only time  $T_b/q$  to break. The material at the tear tip is required to undergo a very rapid viscoelastic response in comparison to the response of the sample as whole. This theory does not take into consideration any change of stress distribution with growing crack length or the decrease of  $T_b/q$ , the time necessary to fracture one filament. According to Kausch, a group of  $q$  filaments, subject to the statistical condition that the fracture of one filament may start once the preceding filament was completed, has an average lifetime,  $\langle T_b \rangle$ , of  $qT_b$  and a Poisson distribution of  $T_b$ .

$$n(T_b) dT_b = dT_b / t(q-1) \{T_b/t\}^{q-1} * \exp(-T_b/t)$$

Zhurkov Model: Independently, Zhurkov (7) in USSR and Bueche (6) in US, expressed the idea that primary (chemical) bond breakage plays a significant role in the fracture of polymers. Zhurkov in 1965 showed that the lifetime  $T_b$  for 50 different solids (metals, polymers, alloys and non-metallic crystals) under constant load can be expressed by reaction rate equation of the form

$$T_b = T_0 \exp \{(U_0 - g\sigma)/RT\} \quad (1)$$

The three parameters in the above equation were associated as:  $T_0$  being  $10^{-13}$  per second, independent of the structure and chemical nature of the solid in question and equal to the reciprocal of

the natural oscillation frequency of the atoms in the solids;  $U_0$ , the activation energy for bond scission; and  $g$  the activation volume, a structure-sensitive parameter related to the internal stress distribution.

Zhurkov believed that this correlation was not fortuitous but rather an indication that stress-aided thermal bond dissociation is the controlling factor in the fracture, with such mechanisms as molecular flow playing secondary roles. This thermofluctuation model, as expressed by Zhurkov, involves the breakage of bonds under the influence of an applied stress at a rate which varies exponentially with the magnitude of the stress.

Of even greater importance, Zhurkov demonstrated the atomistic nature of polymer fracture by measurement of the radicals formed during bond rupture using ESR. Radical formation was found to increase exponentially with the magnitude of the applied stress, and furthermore, the stress coefficient for radical formation was identical with the stress coefficient measured for the time to break (i.e.,  $g/RT$ ). This bears out the assertion that the polymer bond rupture is some sort of thermally activated stress-aided process and the fact that the sample's lifetime under load obeys a similar relationship to the stress as the bond ruptures helps confirm the importance of the bond rupture process to macroscopic polymer fracture. This, however, did not explain the time-dependent nature of radical formation. Also, this interpretation did not take into account the distribution of molecular stresses which vary not only over the bond population, but also with time to account for morphological change occurring in the fiber, e.g., the rupture of a significant number of load-bearing tie chains during loading to fracture.

Also, Zhurkov found departure from equation (1) for low values of stress, noting that as the stress diminished, experimental lifetimes became infinitely large. The existence of a bond repair reaction was offered as the possible explanation for this behavior. An alternative explanation would be established by postulating a critical stress below which the deformation could be insufficient to have an effect on activation energy. The existence of such a critical stress has been established in fatigue studies of metals and many polymers.

Hsiao-Kausch Model: The polymeric materials studied by experimental methods like ESR were essentially highly drawn fibers and films which had a highly anisotropic structure. The fracture theory of Hsiao-Kausch (8, 9) takes into account the state of orientation of a polymeric solid. The theory combines the kinetic concept of Zhurkov or Bueche and the anisotropic nature of the solid.

The mathematical model for analysis is a matrix of identical rod-like oriented elastic elements. The fracture theory is based on the assumption that the mechanical properties of the solid are predominantly determined by the state of orientation and the properties of elastic elements. The kinetic aspects are introduced in this model through the assumption that the element can undergo breakage. Probability for failure is determined by the axial stress upon the element and that immediate redistribution of load occurs once the element has ruptured. The state of stress in the vicinity of a point in the solid may be represented by the time-dependent stress tensor  $s_{ij}$

$$s_{ij} = \int p(\theta, \phi, e) * f(\theta, \phi, t) * \psi(\theta, \phi, t) c_i c_j d\Omega \quad (2)$$

where  $\psi$  is the longitudinal stress acting along a group of parallel elements, a function of orientation  $(\theta, \phi)$  and time  $t$ ;  $f$ , the fraction of unbroken elements is function of orientation and time, and  $p$  is the density of probability distribution function of orientation.

The time-dependent nature of the fracture process can be formulated utilizing the statistical theory of reaction rate. The rate of change of  $f$  is given as

$$df/dt = k_r(1-f) - k_b f \quad (3)$$

where the rate of reformation of broken elements is

$$k_r = w_r \exp \{ -(U/RT) \cdot g_r \psi(t) \}$$

and the rate of bond rupture,  $k_b$ , is

$$k_b = w_b \exp \{ -(U/RT) + g_b \psi(t) \}$$

$w_f$  and  $w_b$  are respective frequencies for forming and breaking process. Eqs. (2) and (3) have been evaluated for a completely oriented and an unoriented network under constant uniaxial stress  $s_0$ . The time taken for the breakdown of the solid is given as (neglecting the term for reformation of broken elements)

$$k_b T_b = \{ -E_i(-g_b \psi_0 / RT) \} * C$$

where

$$-E_i(-y) = \int_y^{\infty} dz \exp(-z)/z$$

$\psi_0$  is the initial stress carried by elements of orientation  $\theta = 0$  and  $C$  is a slowly varying function the limits of which are expressed by

$$1 < C < 1 + 0.63g_b \psi_0 / RT$$

The lower limit refers to a completely oriented network, the upper one to a randomly oriented one.

Kausch (10) has calculated the effect of network orientation on defect accumulation and strength. It turns out that the range of orientation angels within which the elements break preferentially is narrow. The increase in strength resulting from improved uniaxial orientation is limited. This is illustrated in Figure 1 for a randomly oriented network where the initial distribution is independent of  $\theta$ . Elements oriented in the direction of uniaxial stress ( $\cos \theta = 1$ ) experience the largest initial stress and break preferentially. The angular distribution of  $f(\cos \theta, t)$  is shown for three different stages of defect development, namely, after  $f(1, t)$  had dropped to 0.5 and zero and for the point of impending failure

where the numerical calculations were terminated because breakage of the remaining elements occurs at a very high rate. The calculations as represented in Figure 1 show that almost one-half of the loading period has to pass before one-half of the most heavily stressed elements is broken. More than 90 % of the loading period has to elapse before all the elements within a small angular section are broken. At this stage the majority of the elements present are still unbroken. The step from the second to the third stage of defect accumulation is rather short (6% of the loading time) and from there to network failure, practically negligible.

Gotlib, Dobrodumov, El'yashevich and Svetlov Model: (11, 11a). The first ruptures in a large assembly of initially equally stressed solids will occur at random. The breakage and retraction of a particular element, however, leads to an increase in the axial stress of those elements to which it is coupled (through primary or secondary forces). As a result, the probability of rupture of stress-coupled elements will be higher than for others.

The rupture events will continue to occur at random for an initial period. With their growing number, chances are increasing that rupture events occur in an immediate vicinity of each other. This signals the end of the fracture initiation phase and the beginning of crack growth.

This process was numerically simulated by the above-mentioned authors for a set of elastically connected elements with different elastic constants in two perpendicular directions. At small load, a large number of isolated (random) defects appear until a crack forms through accidental accumulation of few defect points and starts growing. At higher loads, a small number of defect points initiate a crack and very little damage is done to the remainder of the specimen during fracture initiation. This is shown in Figure 2. This model deals with elastic elements and the only means for relieving local stress are through a rupture of bonds. Therefore, this model, as it stands, is only applicable to brittle glasses, where plastic deformation does not take place in fracture initiation.

Figure 1 : Decay Characteristics within a population of randomly oriented elements (9,10).

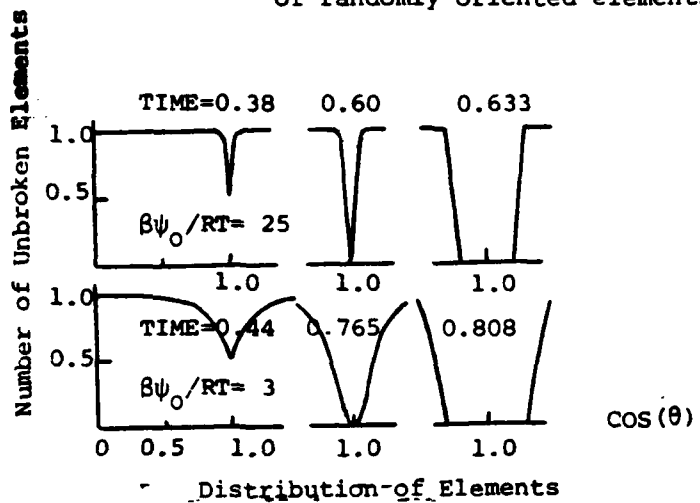
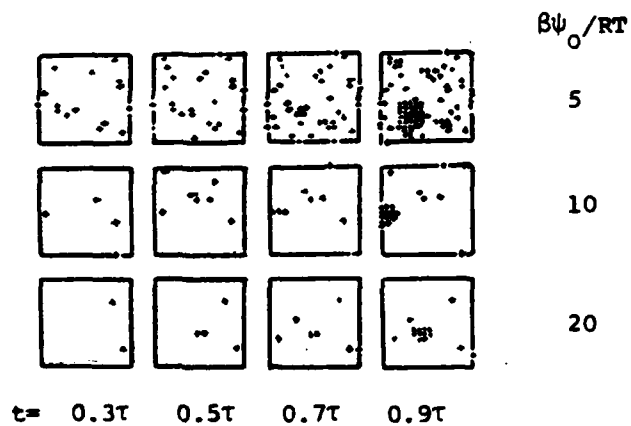


Figure 2 : Simulated brittle fracture events in x-y plane as a function of  $t/\tau$  ( $\tau$ =time to complete failure) ( ).



## 2.5 Molecular-Morphological Models of Fracture

Lloyd - DeVries Model: The ESR (12) and viscometry (13) evidence for bond rupture in nylon 6 shows a small fraction of the available tie chains breaking on fracture. One of the most interesting and intuitive experiments performed to study the molecular fracture processes is due to Kausch (14) and Lloyd (15). A full-length discussion of these and other experiments is available in Kausch's book (16); a short summary is presented here.

The experiment consisted in step-strain loading of the nylon 6 fiber specimens located in the microwave cavity of an ESR spectrometer. The concentration of free radicals after each increase in strain step was recorded, until the specimen was pulled out of the ESR cavity as a result of macroscopic fracture. The histograms of free radical concentrations as a function of the applied strain are shown in Figure 3. An analysis of these and other experimental results which formed a basis for mathematical interpretation of the results of Figure 3 are:

- stress relaxation or creep is not caused by slippage of fibrils or microfibrils.
- chain scission occurs in tie segments; generally tie segments interconnect adjacent crystal blocks within a microfibril, but more distant or interfibrillar ties also have to be considered.
- eventually, breaking tie segments are solidly held, most probably by the crystal blocks; although the clamping extends over 2 to 5 nm. in the crystal block, the tie segments are treated as if they had a well-defined end to end distance  $L_0$  and contour length  $L$ .
- chain scission occurs if the axial stress  $\sigma_a$  reaches chain strength.
- the large value of molecular stress concentration (ratio of  $\sigma_a$  to  $\sigma$  of the order of 50 or 80) (Ref.17, 18, 19) follows from the fact that individual (highly rigid and clearly extended) chains are subjected to comparatively large strains of intra- or interfibrillar amorphous regions they span.

Consider a fairly extended tie-segment of contour length  $L$ , end to end distance  $L_0$ , and elastic modulus  $E_k$ . Each segment spans an arbitrary number of amorphous regions  $n_{ci} = n_{ai} \cdot 1$  of crystalline

regions (thickness  $L_c$ ). The elastic stress experienced by the extended segment will be

$$\psi_i = (E_k/L_i) [L_a(1+s_a) + L_c(1+s)] \cdot E_k$$

$$\psi_i = E_k \{ [L_a(1+s_a)/L_i] \cdot 1 + \{ (L_o \cdot L_a)(1+s)/L_i \} \} \quad (4)$$

Equation (4) holds for tie segments connecting adjacent crystal blocks in a microfibril or intersubfibrillar tie molecules, with appropriate choice of values for  $L_a$  and  $L_o$ .

Lloyd's analysis of the histograms of Figure 3 is based on a direct correlation between the number of free radicals generated during a step-strain loading and number of tie molecules, of a given length, present in the amorphous region between two crystalline blocks. Thus the histograms of Figure 3 are converted to a distribution of tie chain lengths  $G_L\{L_{(i)}/L_o\}$  according to the following equation based on stress-aided first order rate process equation for fracture:

$$\{R\} = 2N_o \sum_i G_L\{L_{(i)}/L_o\} \{ 1 - \exp \{ \int_0^t w_b \exp(-U/Rt) dt \} \} \quad (5)$$

where  $\{R\}$  is the free radical concentration,  $N_o$  the total number of tie chains and  $w_b = w_0 \exp(-U_o/RT)$ .

A numerical iteration procedure is used to solve equation (5) for  $G_L\{L_{(i)}/L_o\}$  in such a way that concentration of free radicals  $\{R\}$  of histogram of Figure 3 is obeyed. The length distribution  $G_L\{L_{(i)}/L_o\}$  of the intrasubfibrillar tie-molecules as shown in Figure 4 varies from  $L/L_o$  of 1.06 to 1.18. If the same radical concentration were caused instead from the rupture of long intersubfibrillar molecules, the distribution of intersubfibrillar tie chain length lies in  $L/L_o$  range between 0.97 (?) and 1.05. (20). The distribution  $G_L\{L/L_o\}$  obtained, is called, by Lloyd-DeVries as the distribution of lengths of all the tie molecules present in the amorphous regions of the fiber structure. An exactly similar procedure has been repeated by Nagamura, et al. (21) on PEOB {Poly P-(2-hydroxyethoxy) benzoic acid} fibers.

The experiments cited in references 15 and 21 indicated that qualitatively the slopes of stress-strain and radical concentration-strain curves correspond. As a result, different variations of the four-phase

model as shown in Figure 5 have been used by Lloyd (15, 22), Nagamura, et al. (21) and Klinkenberg (23) to explain the stress-strain curves of fibers used. The tie chains in the amorphous regions were divided into three classes according to their contour lengths: Class I indicates tie chains already broken at macroscopic strain  $s$ ; Class II tie chains fully extended; Class III tie chains which are long and not fully extended; and the distribution of lengths of all the tie chains being given by function  $G_L\{L/L_0\}$ . Once the strain-dependent widths of the fractions are obtained from  $G_L\{L/L_0\}$  and appropriate moduli are assigned to individual phases, a stress-strain curve is obtained. A gaussian distribution  $G_L\{L/L_0\}$  for tie chain lengths was used.

A fit of observed and calculated stress-strain curves was obtained if the number of tie chains was taken to be larger than the observed number of free radicals by a factor  $f$  of 20 (Ref. 23) and 40 (Ref. 21). The possible explanations for such a discrepancy are: (1). The number of broken chains is systematically larger than the number of free radicals, e.g., due to a Zakrevskii mechanism (24) or a decay of the free radicals. (2). The breakage of  $N$  chains in a volume results in preferential unloading of  $fN$  extended chains. This could be explained on the basis of microfibrillar morphology (25, 26), or an unloading of chains due to temperature rise in the neighborhood of a broken chain or a group of chains (34, 35).

Some of the limitations of this model are:

- the observed amount of bond scission is too small to explain the observed stress-strain behavior.
- no attempt is made by the authors to explain how macroscopic fracture can result from scission of only 1% of the available tie chains.
- it is assumed that the distribution of free radicals observed also represents the distribution of the tie chain lengths.
- a mechanism for the formation of submicroscopic cracks is not proposed.

Peterlin's microfibrillar model attempts to take some of these factors into consideration.

Microfibril Model of Fracture: The microfibril model has been strongly advocated by Peterlin (25,

26) to explain the fracture and strength of the fibrous structure. A doubt has been cast on the model for drawing process as a result of new experimental evidence from neutron scattering of polyethylene lamella by Flory and others (27). An alternative explanation of the cold drawing process and the details of the resulting fibrous structure are still lacking, though many of the features of the drawing process and fibrous structure may still be very much similar to Peterlin's model.

According to the microfibrillar model of fibrous structure (25), the highly drawn crystalline polymer consists of densely packed, highly aligned, very long and thin microfibrils bound into long and somewhat skewed fibrils. These features are schematically shown in Figures 7 and 8. A typical dimension for the microfibril has been ascribed as  $10\mu$  in length and about  $100 \text{ \AA}^0$  wide. In each microfibril, looped (folded) chain crystalline blocks alternate in axial direction with amorphous layers, bridged by a large number of tie molecules. The fraction of tie molecules is between 10 and 30 % of the chains in the crystal lattice (28). The tie molecules connect not only subsequent blocks (intrafibrillar tie molecules) of the microfibril but also blocks farther away and blocks of adjacent microfibrils (intersubfibrillar tie molecules). The total fraction of 'taut chain molecules' determines the axial elastic modulus of fibrous material. This fraction is estimated to be of the order of 2 - 5 % of the total tie molecules.

The large surface-to-cross-section ratio means an easy lateral transfer of axial forces and hampers any large-scale local deformation of the microfibril. The dense packing of microfibrils prevents any large-scale lateral movement of the crystalline blocks, and the longitudinal connection by tie molecules prevents large axial displacements. If the stress cannot be relieved through sliding of microfibrils or fibrils (i.e., creep) or separation of adjacent structural elements, it may do so by crack jumping through an amorphous region of the microfibril structure rupturing all the tie chains in its path. Different possible mechanisms for microcrack nucleation and propagation are shown in Figure 8.

The formation of microcracks has been supported by observations of Zhurkov (31, 32) using SAXS. The size and density of microcracks obtained appear to be in close agreement with the expected values

for a microfibrillar model. Peterlin (33) has also hypothesized from similar results on various fibrous materials a critical volume fraction for the microcracks forming a criterion for macroscopic failure.

The effects of stress irregularities as proposed by Peterlin to explain the observed response of the fibrous structure is not adequate:

- the voids do not prevent the build-up of large elastic strains in the fibers, as evidenced by scissioning of chains and the appearance of deformed IR bands.
- if the chain scission in regions adjacent to the stress irregularities is the mechanism for failure and the stress-strain response, how is it possible that during second stressing (i.e., after the load has completely been relieved once) the stress-strain behavior is the same?
- if the chain scission would occur preferably adjacent to microfibril ends, further widening of these existing microcracks would then invariably accelerate chain scission.
- microfibril ends are free to undergo shear deformation.
- existence of microfibril ends in nylon 6 fibers has not been observed from TEM studies.
- drawing of semi-crystalline polymers is a matter of controversy at the present time.

Kausch's Model: Another approach to molecular fracture process, based on the energetic consideration of the stressed tie chains and their surroundings has been proposed by Kausch (34, 35). Earlier work along similar lines was done by Godovskii, et al. (36), who determined the mechanical work input and the heat evolved in a cyclical loading - unloading of nylon 6 of a draw ratio of 5.5. It was observed that the difference in mechanical work  $\Delta A$  and the heat evolved  $\Delta Q$  between the first cycle and the second or any subsequent cyclical stressing was the same.  $\Delta A$  and  $\Delta Q$  as functions of applied stress are shown in Figure 9. The difference in mechanical work performed  $\Delta A$  and the heat evolved  $\Delta Q$  between the first and the second cycle ( $\Delta A = \delta A - \delta A_2, \Delta Q = \delta Q - \delta Q_2$ ) was taken as the increase in internal energy ' $\Delta U$ '. The internal energy ' $\Delta U$ ' was ascribed to the energetic characteristics of those chain molecules stretched and ruptured during the first loading cycle. The

extension of these molecules involves the expenditure of work, stored as elastic potential energy; a part of it is used as chemical energy for bond breakage and a large part is evolved as heat due to dissipation of the mechanical energy by two 'halves' of the ruptured molecule. According to Godovskii, the energy characteristics were not affected by plastic effects (structural re-arrangements and conformational transitions of macromolecules) as evidenced by analogous experiments on nylon 6 of different degrees of orientation, though Kausch suggests the possibility of an internal energy due to local rearrangements triggered by chain scission.

A mathematical treatment due to Kausch is presented. The total elastic energy in a segment of length  $L$ , cross-section  $q$  and elastic modulus  $E_k$  amounts to

$$W_k = qL\psi^2/2E_k \quad (6)$$

For a nylon 6 segment of 5 nm. length with  $q = 0.189 \text{ nm}^2$ ,  $\psi_b = 21 \text{ GN/m}^2$  and  $E_k = 200 \text{ GN/m}^2$ , give a value of  $1.4 \cdot 10^{-18} \text{ J}$  per segment or 600 kJ/mole for the elastic energy stored in a chain at breakage. The contribution of elastic forces that hold the highly stressed tie-segment ends within the crystal lamellae is 190 kJ/mole for each segment at the rupture stress. Thus an energy of 870 kJ/mole liberated at the moment of chain scission has to be dissipated as heat. If this energy released were to be confined within the volume of the segment and its two ruptured ends, it would constitute an energy density of  $W_{\text{total}}/qL = 764 \text{ MJ/m}^3$ . Thus chain scission event is like a micro-explosion.

The local temperature rise  $\Delta T$  in the neighborhood of the broken segment will depend upon the number  $N$  of segments on which the energy of the breaking segment is distributed. Using the following values for nylon 6 (37) - a heat capacity  $c_p = 1.47 \text{ cal/gm.}^\circ\text{K}$  and a density of the amorphous region  $\rho = 1.084 \text{ gm./cm.}^3$ , one obtains

$$\Delta T = \{764/(N * \rho * c_p)\} * \text{MJ/m}^3 = (479/N)^\circ\text{K} \quad (7)$$

This temperature rise not only increases the mobility of the chains in the region but also results in a decrease  $\Psi_b$ , the strength of the  $N_c$  affected tie chains, which can be obtained by differentiating the equation

$$\Psi_b(T) = \{U_0 - RT \log_e(w_0 T_b)\}/\beta \quad (8)$$

$$\Delta\Psi_b = \{-R \log_e(w_0 T_b)\}\Delta T/\beta$$

Using  $\beta = 5.53 \times 10^{-6} \text{ m}^3$  and  $w_0 \tau_b = (10^{13} \text{ sec}^{-1} * 1 \text{ sec}) = 10^{13}$ ,

$$\Delta\Psi_b = (-48 * \Delta T) \text{ MN/m}^2 = (-23/N) \text{ GN/m}^2 \quad (9)$$

As mentioned earlier, a qualitative agreement is observed between the slopes of stress-strain curve and free radical-strain curve. A quantitative correspondence requires that 20 to 40 times as many tie chains experience breaking stress as are the number of free radicals observed. A local temperature rise due to breakage of a tie chain segment facilitates the extension of kinked chains due to annihilation of kinks and therefore the chain will be unloaded without breaking. Within this framework one would have to assume that the breakage of one amorphous segment at maximum load ( $\Psi_{break}$ ) leads to conformational changes in the surrounding segments of the same microfibrillar region, resulting in load decreases of 40  $\Psi_{break}$ . According to Kausch, there are more than 2000 surrounding segments (of 5 nm. length in any amorphous region  $400 \text{ nm}^2$  in cross-section) and the value of 40  $\Psi_{break}$  is thus reasonable.

Kausch's approach, though it presents an alternative explanation of Lloyd - DeVries result, is very speculative at this moment. Some experimental evidence in this direction is desired. Furthermore, Kausch mentions that there are 2000 segments per  $400 \text{ nm}^2$  cross-section. This is the number of segments in a crystalline block and not in the amorphous region where the number is generally expected to be smaller by an order of magnitude.

Figure 3 : Histograms of nylon 6 free radical concentration from step-strain data at room temperature:

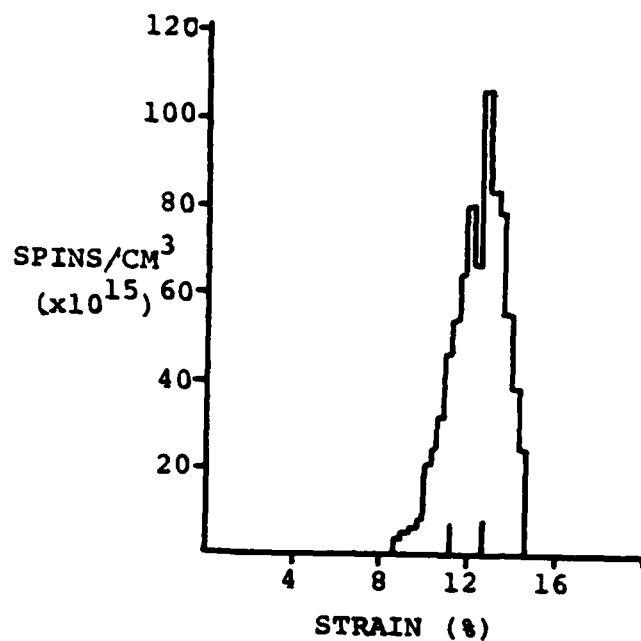
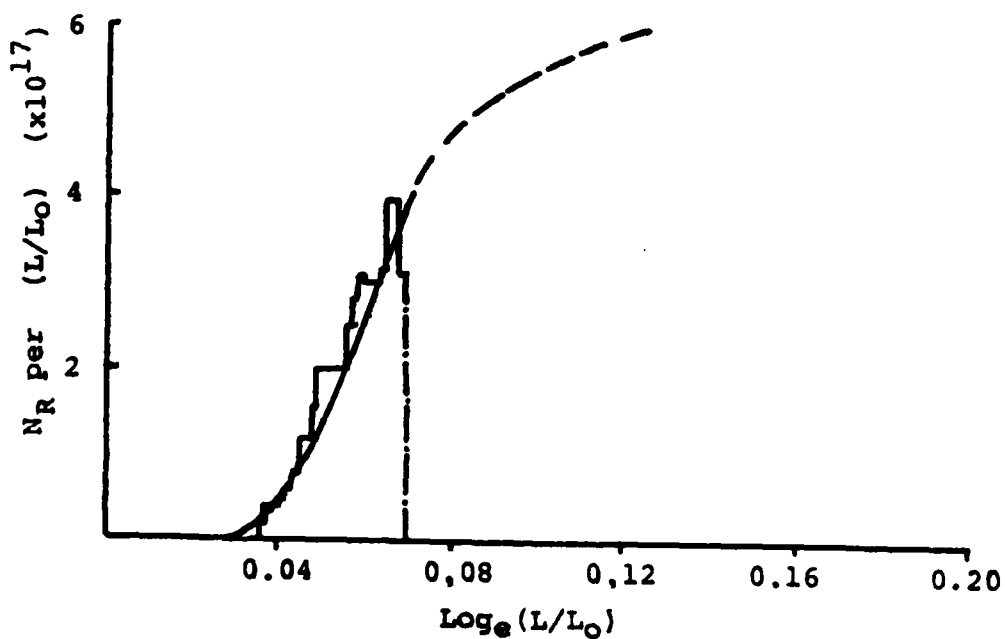
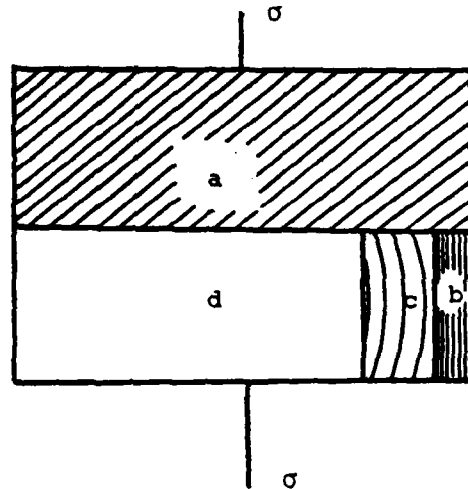


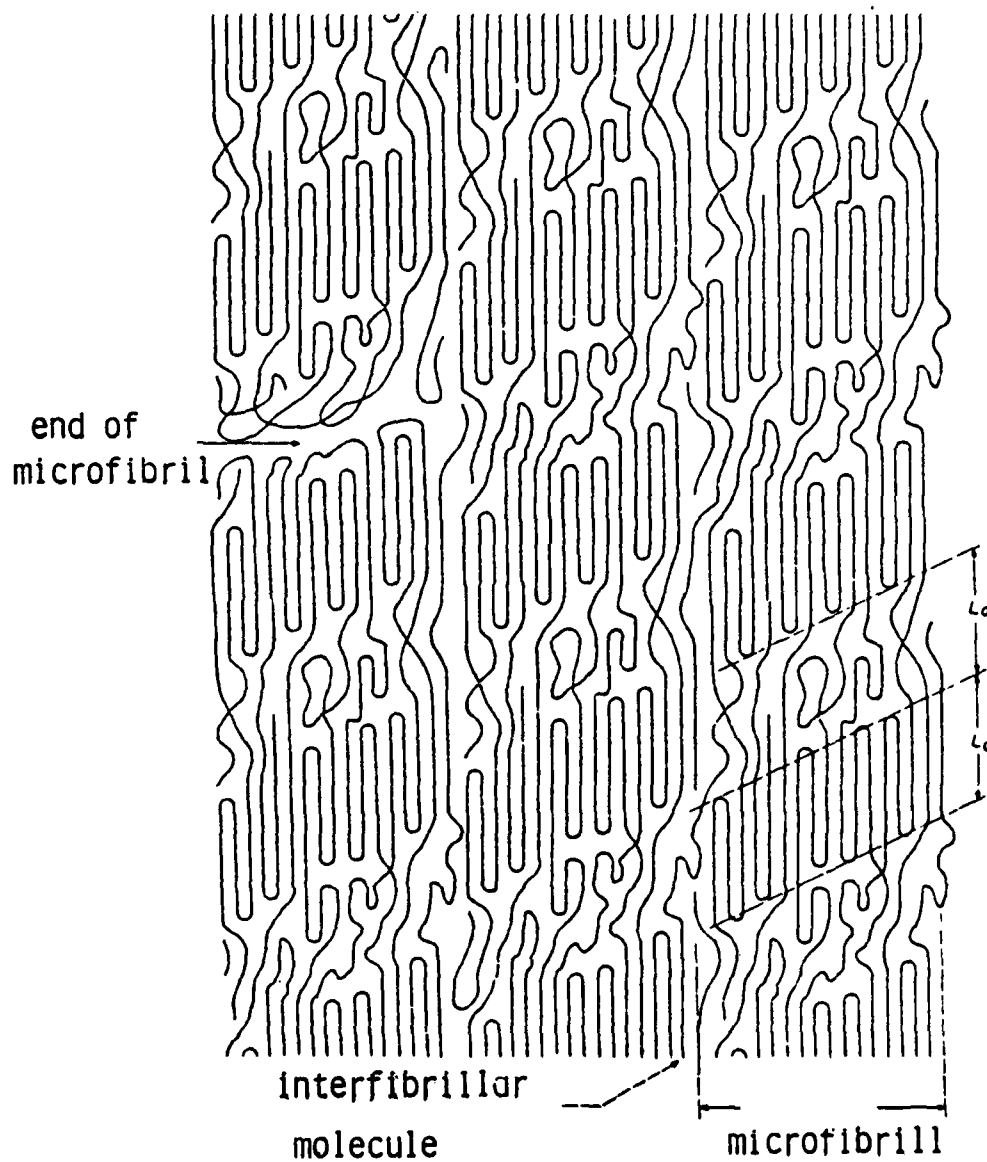
Figure 4 : Distribution of relative chain lengths of tie molecules ( $L/L_0$ ) of nylon 6 fibers from step-strain data using Lloyd-DeVries model.



**Figure 5 : Four phase model of fibrous structure**  
(a) crystalline phase (b) taut (extended)  
tie chains (c) non-extended tie chains  
(d) matrix (loops, cilia, chain ends).



**FIGURE 6**



Model of highly oriented, semicrystalline fiber.

**Figure 7 : Fibrillar model of the fibrous structure.**

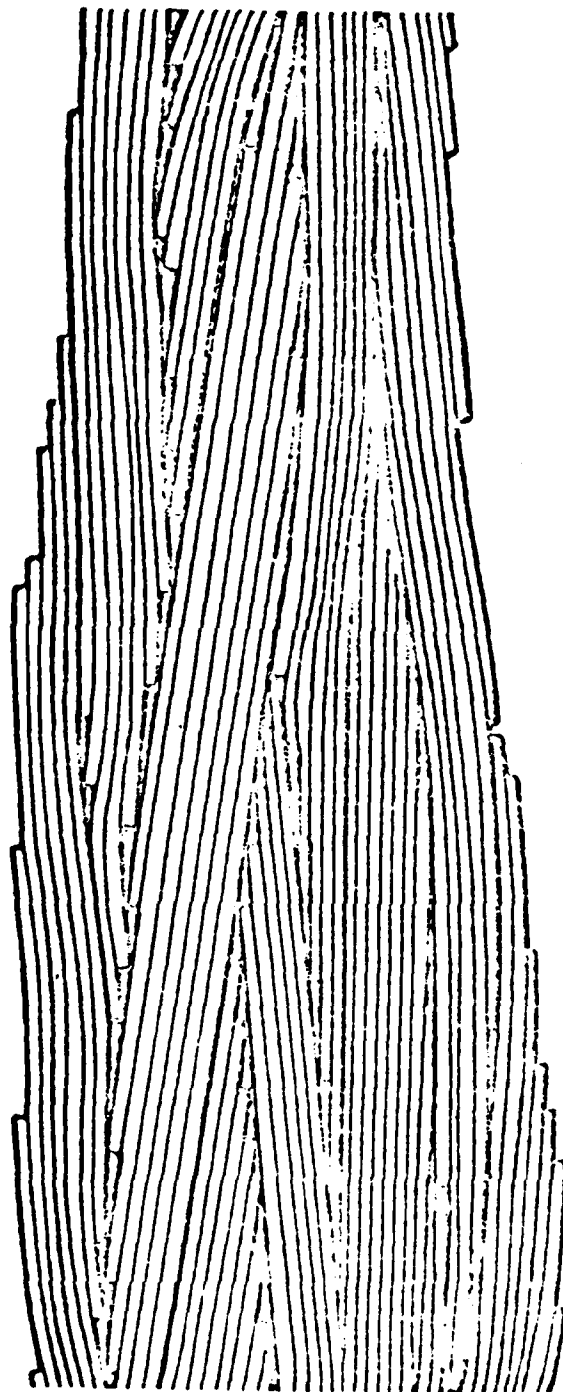


Figure 8 : Crack coalescence along (a) radial, (b) axial direction.  
 In the former case a microfibril is broken with all the tie molecules ruptured in at least one amorphous layer B, no or very few molecules (interfibrillar tie molecules are ruptured in the latter case( )).

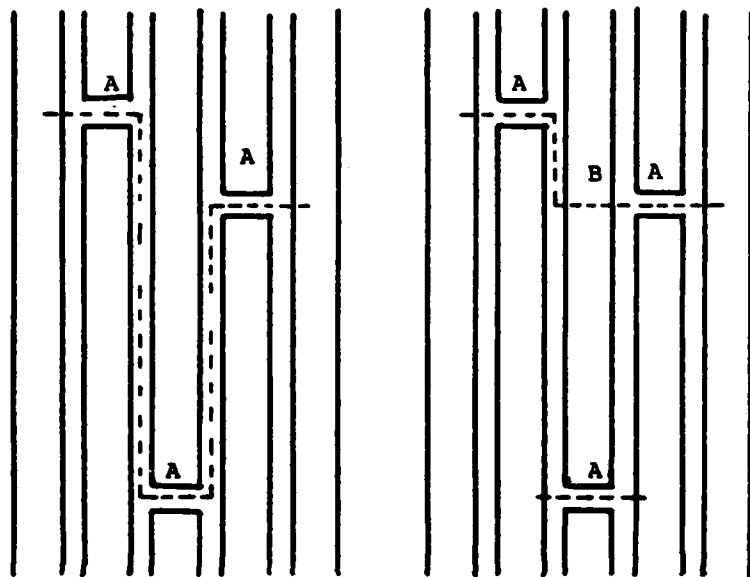
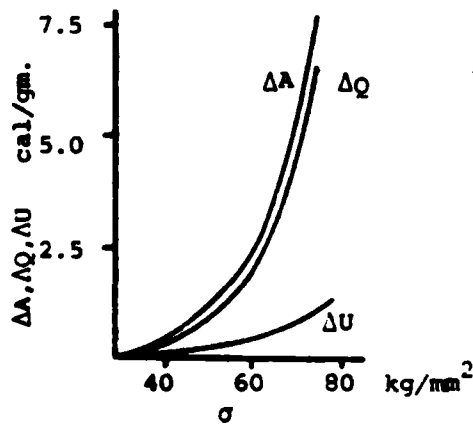


Figure 9 : Energetic characteristics due to rupture of molecules during loading of nylon 6. A) Mechanical work spent in elastic extension of macromolecules; Q) heat evolved after the rupture of the stressed molecules; U) energy expended directly on rupture of molecules (36).



### **3. Experimental Studies of Mechanochemical Degradation**

#### **3.1 Introduction**

The action of an applied uniaxial tension on a covalent bond R-R results in a decreased binding energy of the chemical bond and therefore the probability for bond scission increases. If the applied load is large, a covalent bond rupture would certainly occur generally in a homolytic manner; this being the energetically favored mode. Zhurkov, et al. (7), using ESR, observed such a homolytic bond scission in nylon fibers stretched to failure. This led Zhurkov (7) to propose a stress-aided thermo-fluctuation mechanism of fracture based on Tobolsky-Eyring (38) type kinetic rate processes. Zhurkov postulated that fracture accompanied by bond scission can be broken down into three phases:

- (1). Excitation of the bonds being broken
- (2). Breakage of excited bonds by thermal fluctuations
- (3). Accumulation of ruptured bonds resulting in the loss of stability in the body with its eventual breakdown.

The studies towards formulating a correlation mentioned in the last statement has been an active area for research ever since.

Verma (39), Becht and Fischer (40) demonstrated that the observed free radicals are formed in the amorphous regions of the fibrous material. The amount of bond rupture as observed by ESR (12) is of the order of  $5 \times 10^{17}/\text{cm}^3$  for the nylon fibers. Considering a chain of  $20\text{\AA}^2$  cross-section, there are  $5 \times 10^{14}$  molecular chains crossing a  $\text{cm}^2$  of the cross-sectional area. Therefore the number of scissions generated by a planar crack is much smaller than the observed number detected by ESR. This implies that a global bond scission occurs throughout the volume of the fibrous material. This has been experimentally verified by Crist (13) who determined the bond scission/ $\text{cm}^3$  for different portions along the length of a fractured fiber using viscosity average molecular weights and found it to be uniformly same all along the fractured fiber. It is generally believed that the crystallites in the fibrous morphology

act as crack stoppers and extensive hydrogen bonding in polyamides inhibits interchain separation, forcing the crack to pass through relatively weak tie chain regions and cause covalent bond scission. In other materials such as polyethylene where intermolecular forces are weaker, the crack propagation is easier along the fiber direction and fewer tie molecules are expected to break. This has been observed experimentally. A postulated crack propagation mechanism is schematically shown in Figure 8.

The observed free radical concentration of  $5 \times 10^{17}/\text{cm}^3$  in nylon 6 represents  $2.5 \times 10^{17}/\text{cm}^3$  of ruptured tie molecules. This is only 0.25 - 0.50 % of the  $1 \times 10^{20} - 5 \times 10^{19}/\text{cm}^3$  of the tie molecules estimated to be present in nylon 6. Therefore, in spite of the global nature of the bond scission process, as large as 99.5 % of the tie molecules are unaffected by macroscopic fracture. Prevorsek has shown that the strength of the two segments of the fractured specimen are the same as of the original specimen. This will be discussed further in a later section.

The nylon 6 fibers used for ESR and other studies are the same as used earlier by Roylance-DeVries, Lloyd-DeVries and Park-DeVries at the University of Utah. These fibers, supplied by Allied Chemical Company, were produced in a melt spun, hot draw process and were highly oriented as received. Their commercial application would have been for use as high-strength tire yarn. The nylon 6 used had a single filament diameter of 0.01118 inch with 136 filaments plied together in each yarn. The density of these fibers were determined by a density gradient column as 1.139 gm./ml. Crystallinity of 37.5 % was obtained using crystalline and amorphous density of 1.230 gm./ml. and 1.084 gm./ml. respectively. Crystallinity of 50 %, from X-ray diffraction, was obtained by Park. A differential scanning calorimetry analysis (DSC) indicated a melting temperature of  $496^\circ\text{K}$  for the fibers. Park (41) had determined a long period of approximately  $97 \text{ \AA}^0$  from small angle X-ray scattering data. Also, 'processing temperature' of  $155^\circ\text{C}$  was obtained by plotting long period, density, shrinkage and orientation angle as a function of annealing temperature. These parameters showed an abrupt change at  $155^\circ\text{C}$ .

Nylon properties can be significantly affected by moisture; preliminary investigations suggested a decrease in the mass of fiber specimens by 1 to 2 % upon dessicating for a minimum of 7 days. All the nylon specimens for the analyses in this study were dessicated for at least seven days.

A tensile specimen of nylon 6 fibers for obtaining fractured material and the stress-strain response was prepared by winding the fiber yarn on a solid bar to the desired number of yarn strands. The ends of fiber yarn were tied, the yarn removed from the bar, tied at four places and bonded between the ties with epoxy as shown in Figure 10. After the epoxy had cured, a pre-determined number (eight out of initial twenty) of strands were cut and removed from the center portion of the specimen. Such a tensile specimen behaves essentially like a notched solid tensile bar. The specimen so prepared was again dessicated for seven days and thereafter fractured on the instron testing machine at an extension rate of 0.127 cms. (0.05") per minute. This corresponds to an engineering strain rate, for a specimen of 10 cms. length, of 1.3 % per minute. The stress-strain (41) curve is shown in Figure 11.

Figure 10 : Nylon 6 fiber tensile specimen (dimensions and configuration).

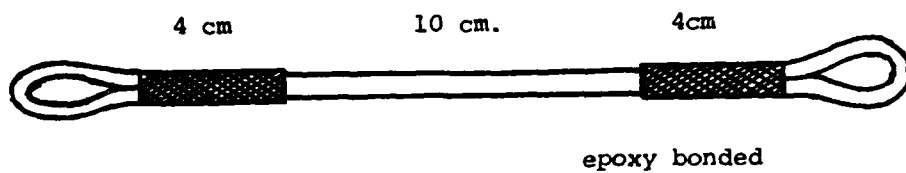
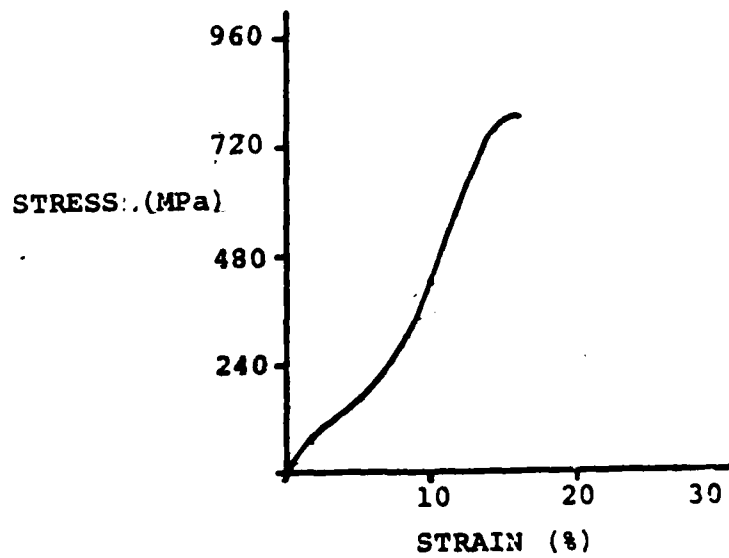


Figure 11 : Stress-strain curve for nylon 6 fiber tensile specimen at room temperature ( $25^{\circ}\text{C}$ ).



### 3.2 ESR Studies

Electron Spin Resonance (ESR) has been extensively used to study mechanical fracture in nylon 6 fibers and other materials by Zhurkov (42) at the Ioffe Physical Testing Center, DeVries (43) at the University of Utah and at a few other places. ESR, a very sensitive technique for the study of free radicals, has a major shortcoming regarding the count of free radicals observed versus the actual number of bond scissions incurred upon fracture. The ESR count of bond scissions is suspect on two grounds:

First, the free radicals decay with time. Therefore, the number of free radicals observed at any time is the number produced during the original scission event minus the number that has decayed since. The decay kinetics of free radicals have been used to obtain the actual number of scissions incurred (44) on fracture. The decay kinetics have been studied here to understand the nature of decay characteristics and obtain an activation energy for the decay process.

Second, the free radicals may undergo secondary radical reactions, as proposed by Zakrevskii (24a, 24b), to produce as many as a few hundred bond scissions without any increase in the radical concentration. These results are further discussed in the next two sections on Infra-red and GPC studies.

Free Radical Kinetics: The secondary free radicals of nylon 6, for which the ESR spectrum is shown in Figure 12, are obtained according to a mechanism proposed by Zakrevskii and others (46). The observed ESR spectrum at room temperature has been interpreted to result from two secondary free radicals: (I)  $\text{CH}_2 - \text{CO} - \text{NH} - \dot{\text{C}}\text{H} - \text{CH}_2^-$ , and (II)  $-\text{CH}_2 - \text{CH}\dot{\text{O}} - \text{NH} - \text{CH}_2^-$ . Radical II is less stable at higher temperatures as evidenced by comparing the spectra in Figures 12, 13, 14, and 15 which show a relatively decreasing intensity of the inner peak at higher temperatures. The kinetics of free radical (I) have been investigated here.

The free radical decay may be a second or first order process governed as to whether recombination of free radicals or reaction with the environment is the primary mode of transformation. Nylon 6 secondary radicals are observed to decay according to a first order rate process.

The concentration of free radicals is a double integral of the area under the ESR spectrum. A direct correlation exists between the concentration of free radicals and the peak height of the spectrum as shown in Figure 16. The rate of change of free radical concentration for a first order rate process is

$$\frac{dN}{dT} = -KN \quad (10)$$

$$\text{i.e., } \log_e N(t) = \log_e N_0 - Kt \quad (11)$$

$$\text{and, } \tau = 1/K \quad (12)$$

where  $\tau$  is the average lifetime of the free radical.

According to the theory of absolute reaction rate,

$$\tau = \tau_0 \exp(U_0/RT) \quad (13)$$

$$\text{i.e., } \log_e \tau = \log_e \tau_0 + U_0/RT \quad (14)$$

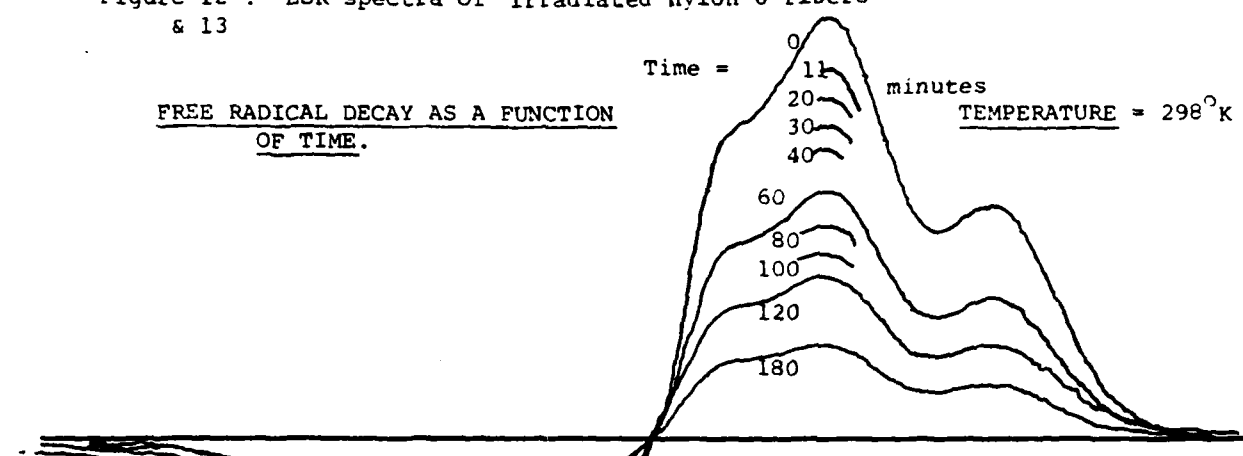
where  $U_0$  is the activation energy for the free radical decay mechanism.

Equation (11) provides  $K$ , the slope of a plot of  $\log_e N(t)$  against time  $t$  from Figure 17.  $K$  is evaluated at temperatures of  $298^0\text{K}$  and  $269^0\text{K}$ . Using equation (14), from the slope of the curve for  $\log_e \tau$  against  $1/T$ , the activation energy ' $U_0$ ' of 11 kcal/mole is obtained. This is obtained from the data available at two temperatures only, so some error in the value obtained is possible; but ' $U_0$ ' of 11 kcal/mole is in the range of activation energy values generally observed for a diffusion-controlled process.

A half-life of 260 and 33 minutes is observed for the free radical I at temperatures of  $269^0\text{K}$  and  $298^0\text{K}$ , respectively.

Figure 12 : ESR spectra of irradiated nylon 6 fibers  
& 13

FREE RADICAL DECAY AS A FUNCTION  
OF TIME.



TEMPERATURE = 269°K

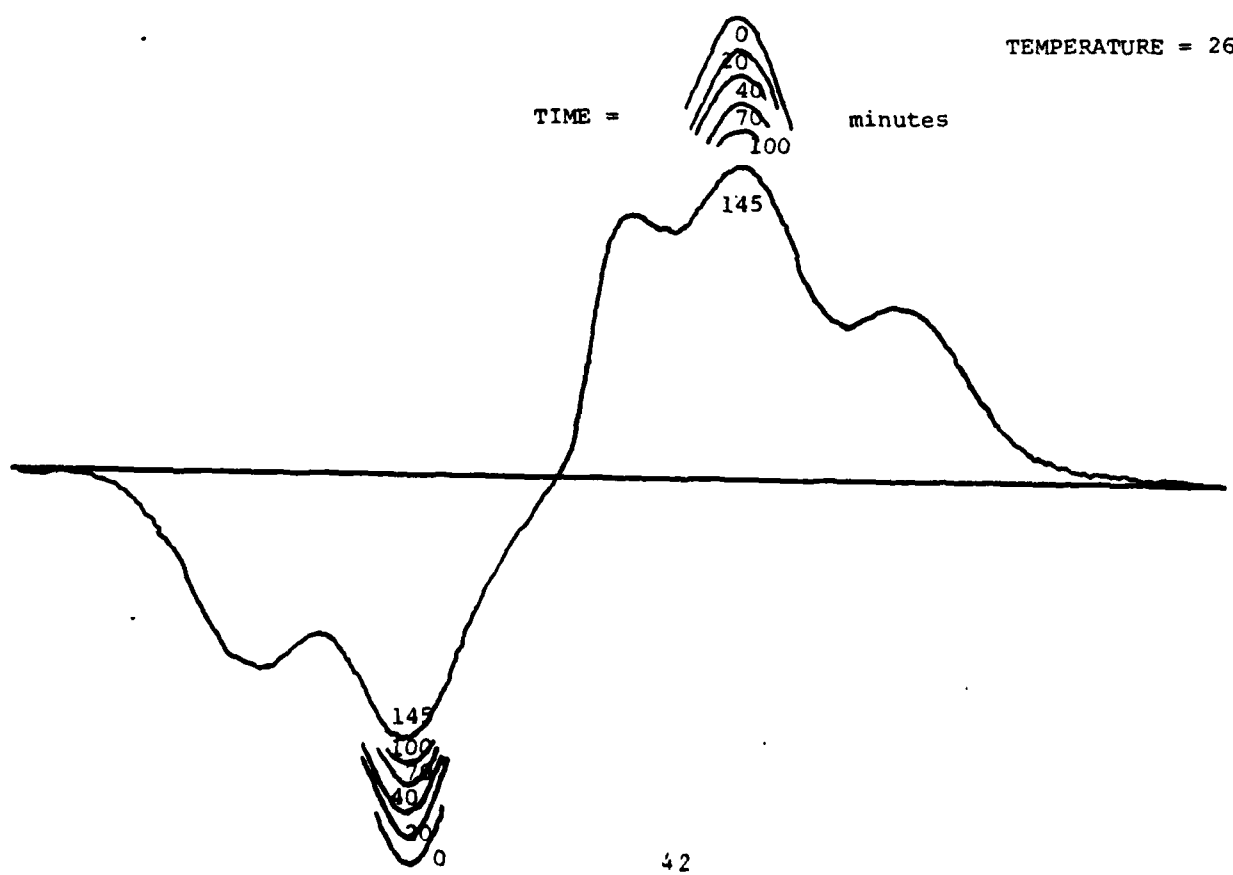


Figure 14 : ESR spectra of irradiated nylon 6 fibers

TEMPERATURE = 242°K

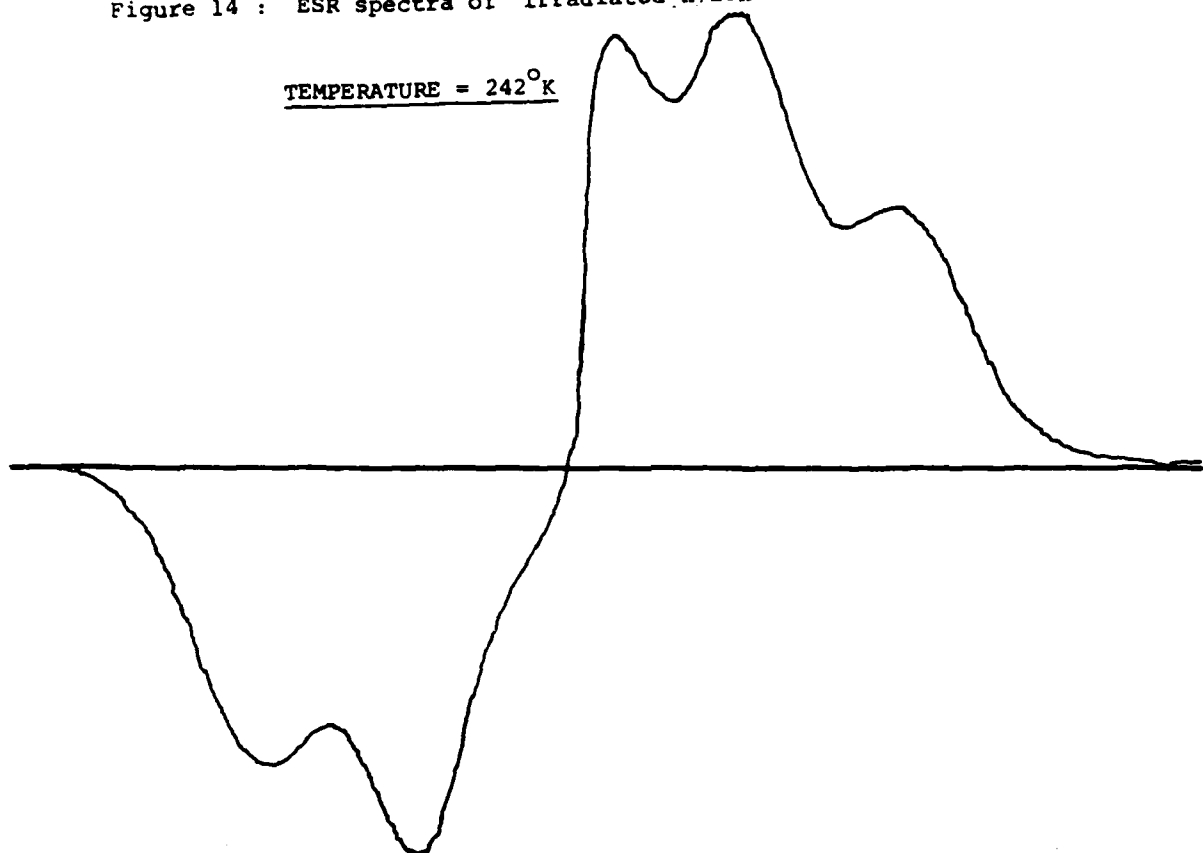


Figure 15 : ESR spectra of irradiated nylon 6 fibers

TEMPERATURE = 188°K

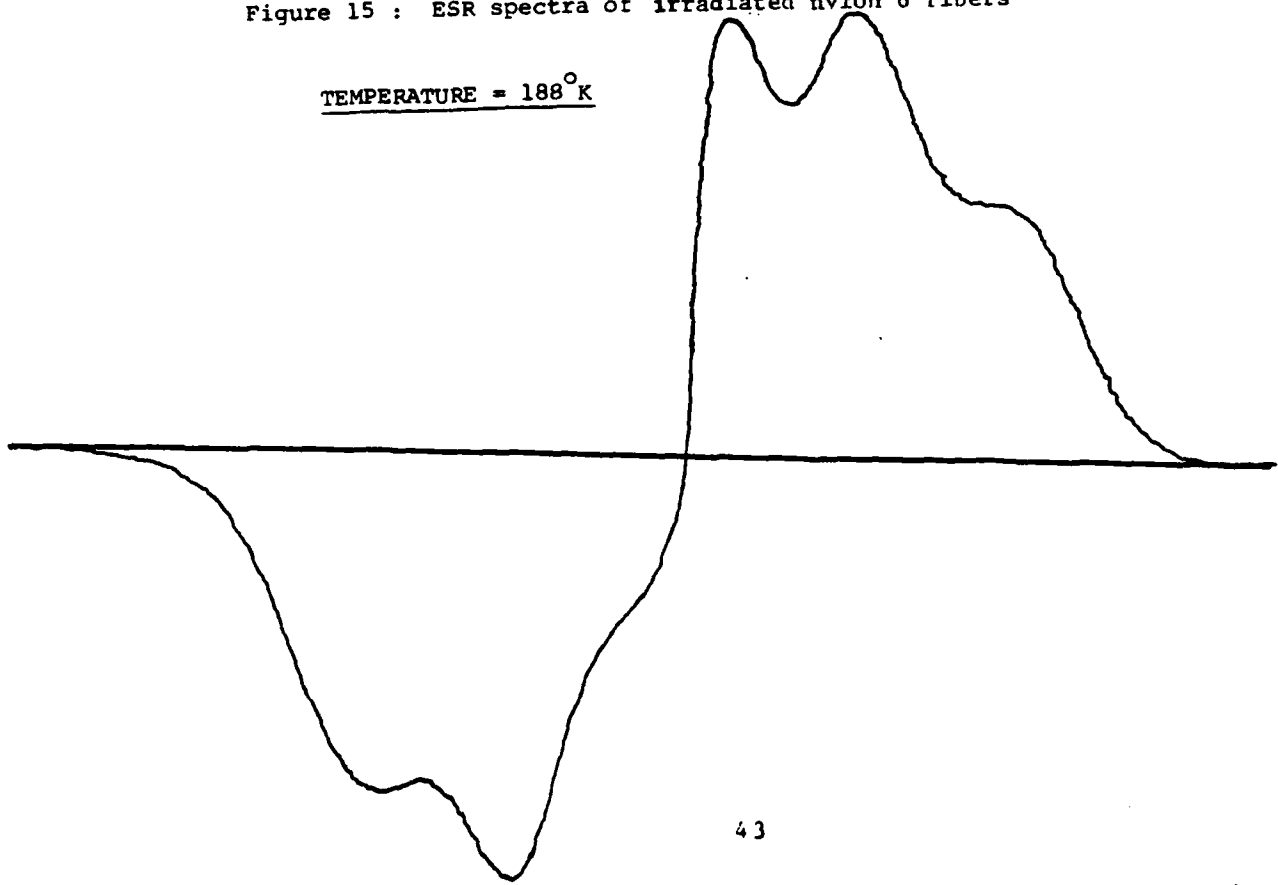


Figure 16 : Nylon 6 ESR calibration curve at 298°K.

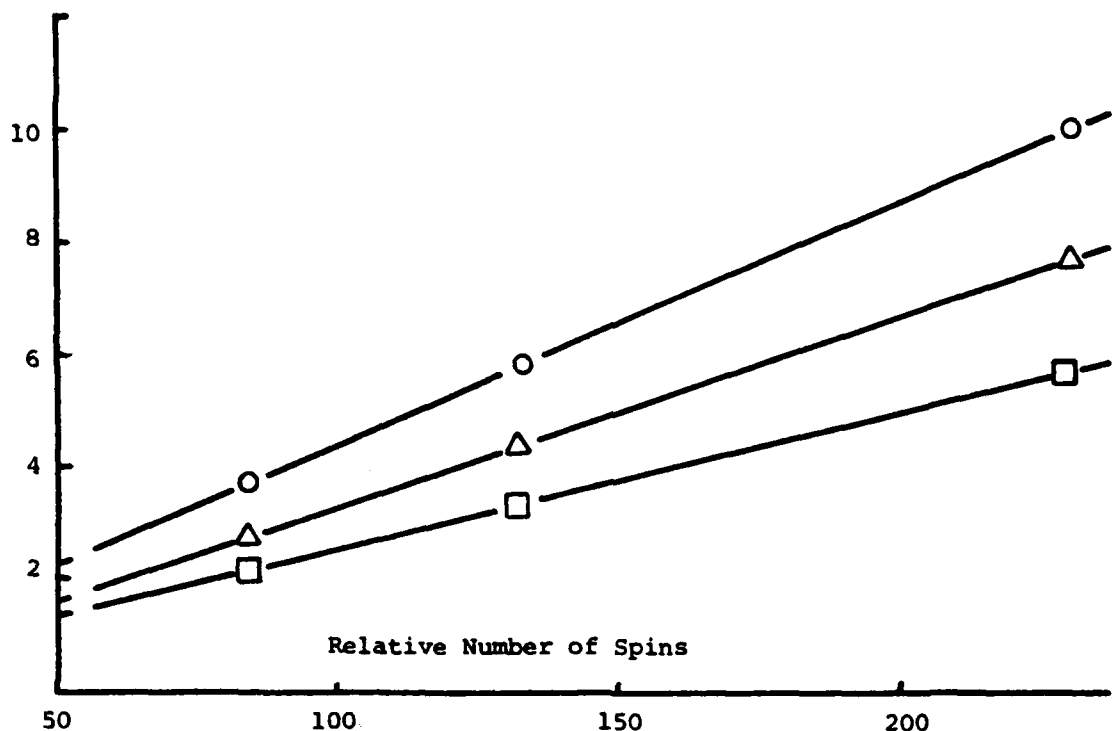
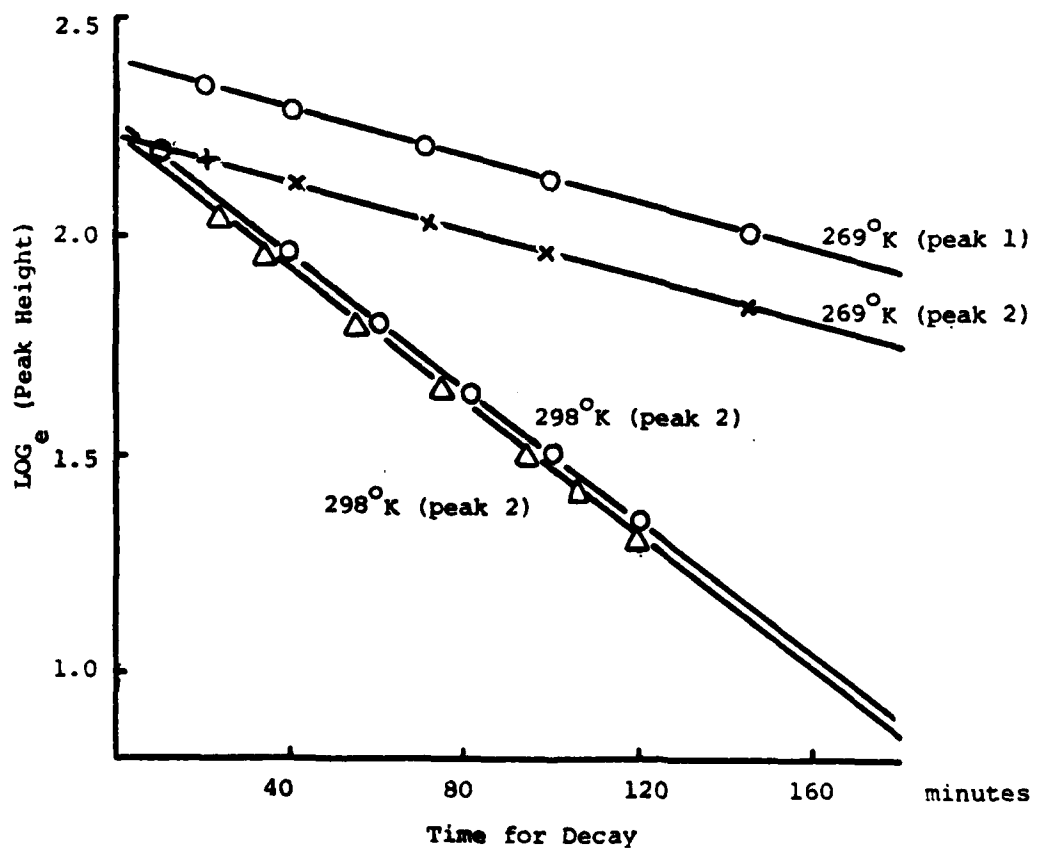


Figure 17 : Kinetics of free radical decay.



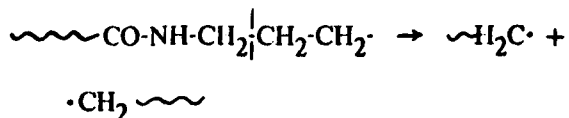
### 3.3 Infrared Spectroscopy of Nylon 6 and Polyethylene

The scission of molecular chains leads to free radicals and eventually free radicals upon decay form new stable molecules.

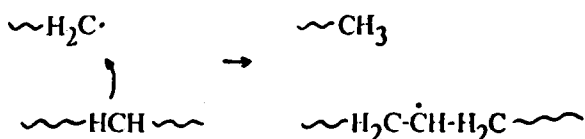
One of the possible mechanisms for free radical decay is suggested below.

#### SECONDARY RADICAL REACTIONS

##### SCISSION



##### ABSTRACTION FROM ADJOINING CHAIN



##### DISPROPORTIONATION - NEW SCISSION



The new end groups formed are mostly of the type: methyl, vinyl, aldehyde, carboxyl, ester, etc. These end groups generally have characteristic IR bands. Therefore an increase in the intensity of any of these bands or the formation of a new band may be detected provided the concentration of the newly formed end groups is large.

Assuming one-to-one correspondence between the free radicals and the resulting end groups formed, a concentration of  $5 \times 10^{17}$  /gm. is expected upon fracture in nylon 6. No new band in the IR

spectrum of fractured nylon 6 of Figure 19 specimen is observed, thereby implying that the end groups formed are similar to some of the existing end groups. One of the bands at wave number  $886\text{ cm}^{-1}$  in nylon 6 spectrum has been assigned to vinyl type of unsaturated end groups.

Nylon 6 has number average molecular weight of approximately 30,000; the number of end groups in such a specimen will be  $4 \times 10^{19}/\text{gm.}$  of the material. Considering for a moment that all the end groups present originally are of the same type and that bond rupture produces  $5 \times 10^{17}/\text{gm.}$  of new end groups of the same kind, the increase in intensity of the IR band for this end group will be approximately 1 %. The small change may be detected if a different spectrum between fractured and virgin specimen can be obtained; this calls for availability of an internal standard of intensity calibration, which is not available for nylon 6. Qualitative comparison of the intensities of the spectra in Figures 18 and 19 does indicate a small increase in the intensities of IR bands at wavenumbers of 845 and  $885\text{ cm}^{-1}$ . A quantitative evaluation of the change is not possible due to lack of absorption coefficients for these bands and the absence of an internal intensity standard in the IR spectra of nylon 6.

Thus it can be stated that the new end groups are formed upon fracture of nylon 6 fibers in uniaxial tension but their concentration is small. IR spectra have also been obtained after irradiating the nylon 6 fibers using electron radiation at 2.5 Mrad doze or grinding them in a vibration mill type of arrangement. These two processes have been observed to produce similar kind of free radicals (47, 48) as in mechanical failure, but at a much higher concentration. A qualitative comparison of the IR spectra of virgin, fractured, irradiated and ground nylon 6 specimens of Figures 18, 19, 20 and 21 respectively does show formation of new bands or increase in the intensity of some of the IR bands. In Table 1 the IR bands of virgin nylon 6 are assigned for various modes of vibrations. Table 2 and 3 indicate the changes observed in the IR bands upon irradiation and grinding of nylon 6 fibers.

Figure 18 : IR spectra of virgin nylon 6 fibers.

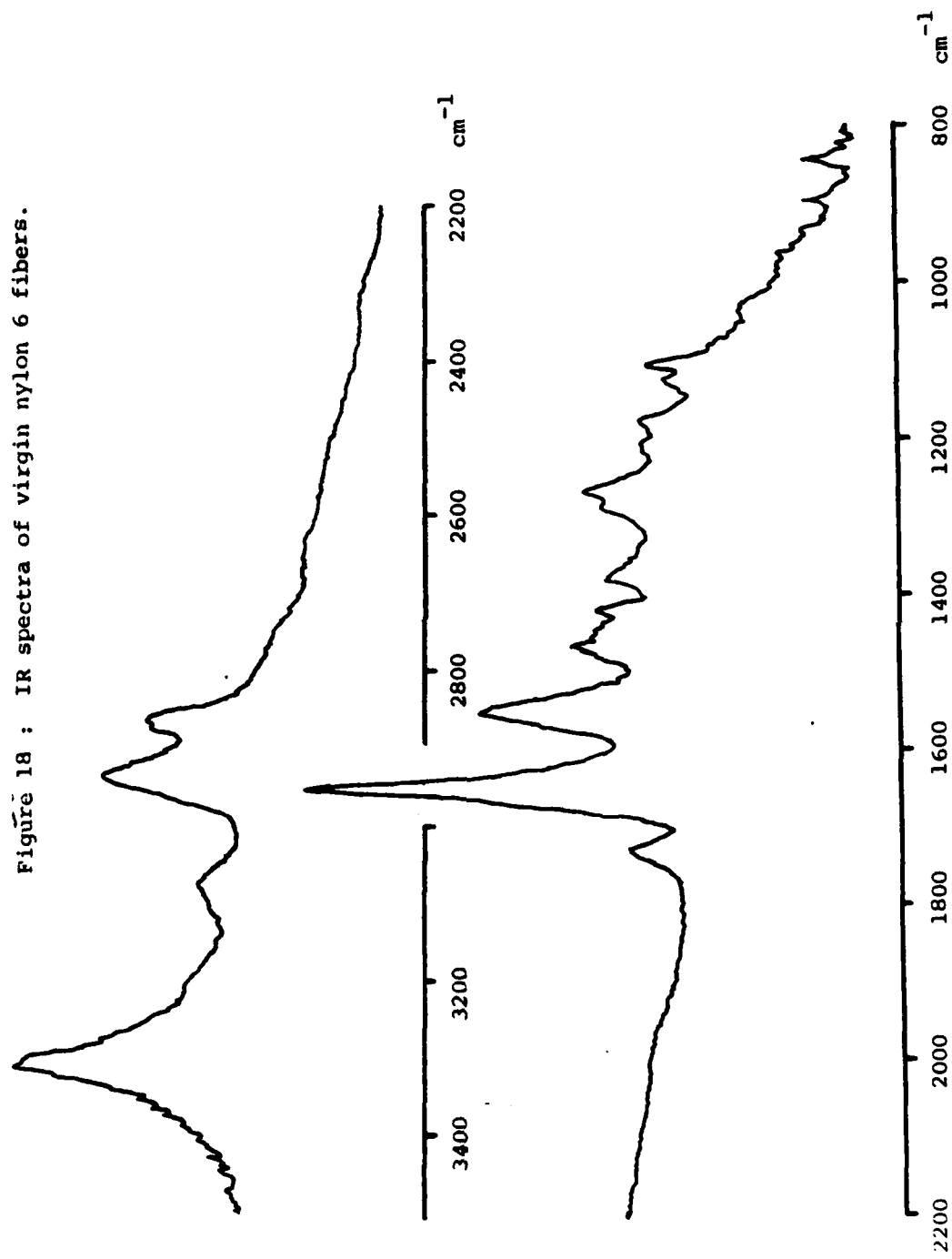


Figure 19 : IR spectra of fractured nylon 6 fibers.

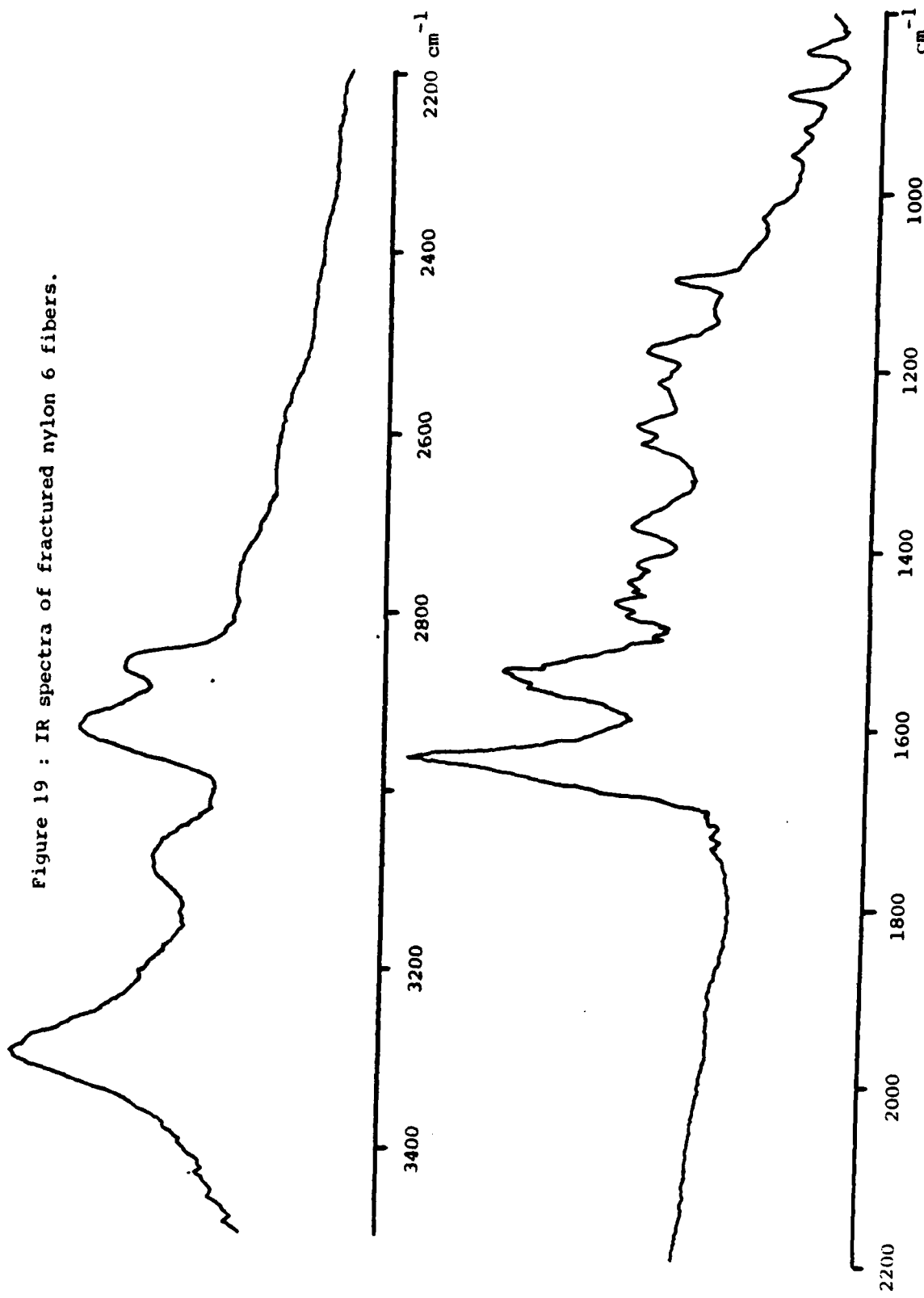


Figure 20 : IR spectra of grinded nylon 6 fibers.

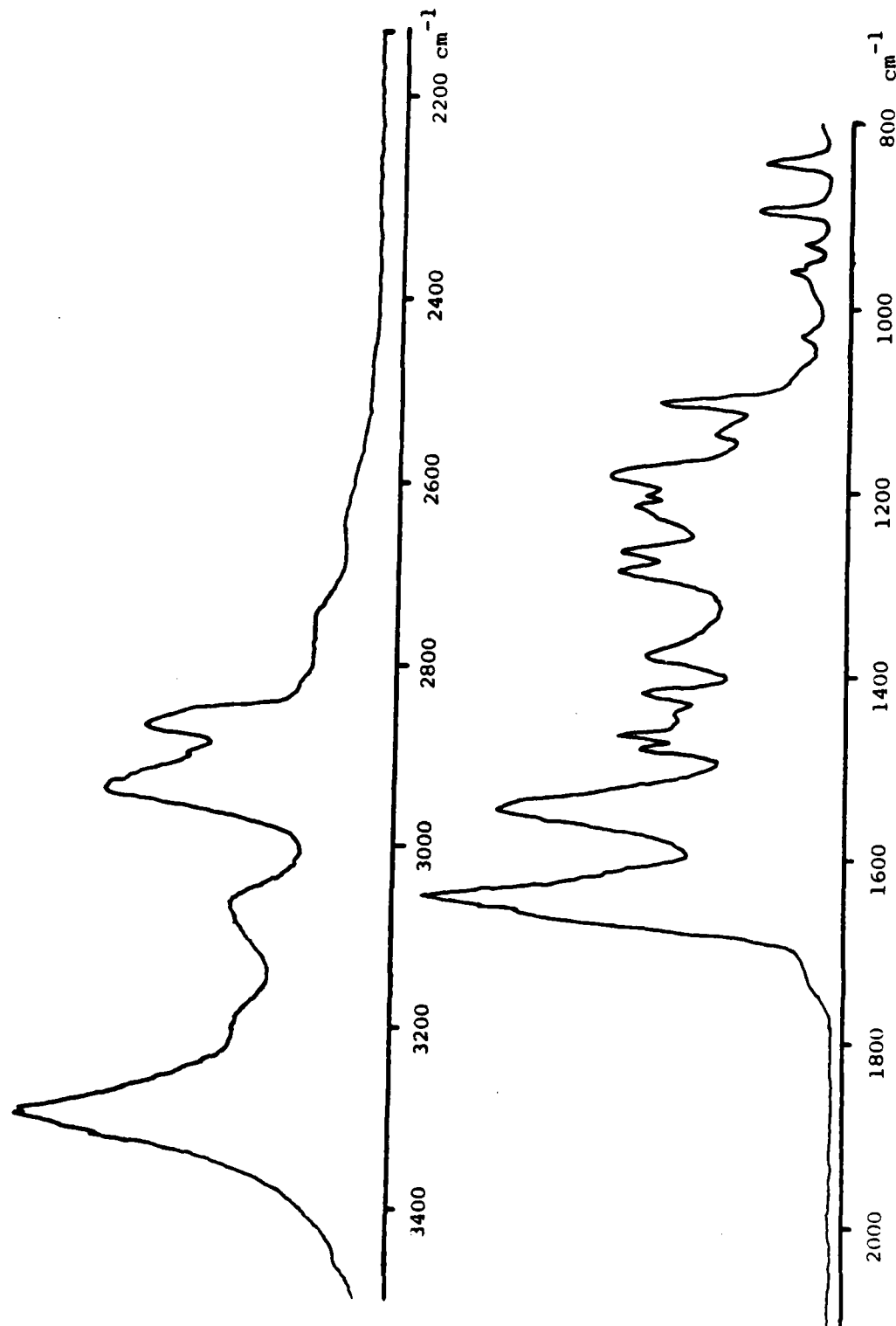


Figure 21 : IR spectra of irradiated nylon 6 fibers.

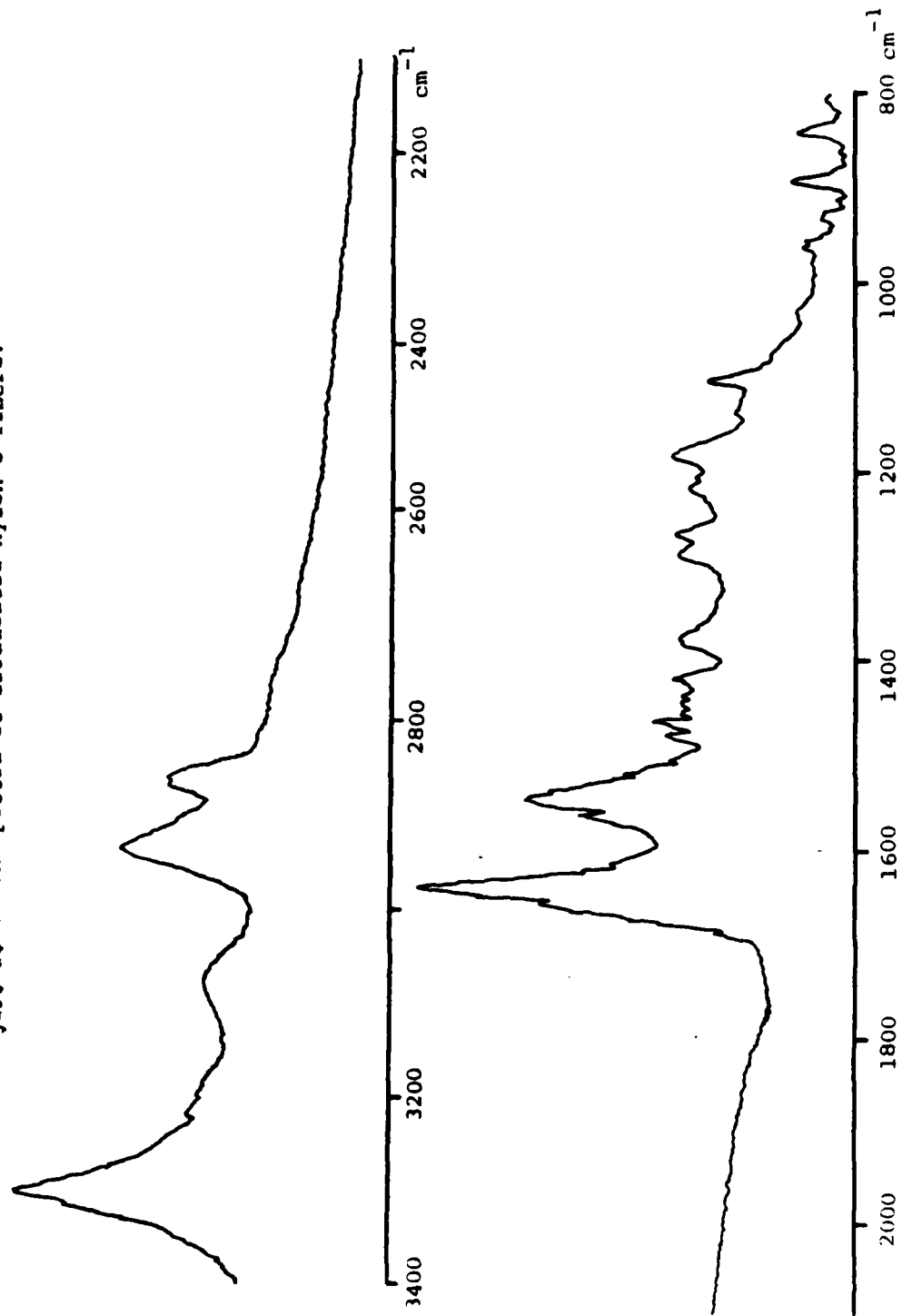


Table 1.

Nylon 6 Band Assignment for IR Spectroscopy

Wave Number	Characteristics	Assignment
3300	S, broad	N-H stretch
3185	sh	
3070	W, broad	free N-H stretch (also could be due to unsaturation)
2965	sh	assym. $\text{CH}_3$ stretching (PE)
2935	S	assym. $\text{CH}_2$ stretching
2900	sh	symm. $\text{CH}_3$ stretching (PE)
2867	M	symm. $\text{CH}_2$ stretching or sum $\text{CH}_3$ stretching
2850	sh	sym. stretching in methylene
1655	sh	
1640	S	amide I - $-\text{C=O}$ stretching
1545	S	amide II, NH def.
1478	W	
1464	W	$\text{CH}_2$ bending (PE)
1417	W	
1375	M & broad	Ch def., $\text{CH}_2$ twisting- Also sym.
1335	VWW sh	def. of methyl groups
1285	W	def. of methylene groups
1262	M	
1215	W	
1202	W	
1179	M & Broad	skeletal motion inv. CONH group
1125	sh broad	
1103	M	
1025	W broad	CONH in plane?
950-970	VW	CONH in plane
928	VW	CONH in plane vibs.
890		$\text{CH}_3$ rocking
888		$\text{RR}'\text{C}=\text{CH}_2$
908		$\text{RCH}=\text{CH}_2$ (PE)

Note: S strong    W weak    VW very weak    sh shoulder    M medium  
 VWW very, very weak

Table 2

Changes in nylon 6 bands on irradiation

Wave Number ( $\text{cm}^{-1}$ )	Remarks
3190	shoulder more pronounced.
2900	
2820	
2750	shoulder more pronounced.
2645	
1464 & 1478	relative increase in the intensity of 1478 band.
1375	
1335	
1215 & 1262	relative increase in the intensity of 1285 band.
1215 & 1202	relative increase in the intensity of 1215 band.
1179	increased intensity.
1135	a band in place of the shoulder is observed.
1075	shoulder changes to a weak band.
1025	band is sharper.
893	considerable increase in the inten- sity of the band.
849	considerable increase in the inten- sity of the band.

Table 3.  
Changes in Nylon 6 Bands on Grinding

<u>Wave Number (cm<sup>-1</sup>)</u>	<u>Remarks</u>
3190	shoulder in fractured nylon is more pronounced
2900	slight increase in intensity
2820	new development of a shoulder
2750	increase in intensity of the shoulder
2645	new shoulder development
1735	?
1464 & 1478	change in relative intensity of bands increase in intensity of 1478
1375	intensity of 1375 band (?)
1335	disappearance of shoulder
1285 & 1262	increase in intensity of 1285 band relative to 1261
1215 & 1202	increase in relative intensity of 1215 band
1179	seems the intensity has increased
1135	a band is seen in place of a shoulder
1025	band is much sharper
893	intensity of band has increased
849	intensity of band has increased

Similar experiments were performed to observe the accumulation of end groups on fracture of drawn PE films. IR bands at wavenumbers of  $1303\text{ cm}^{-1}$  and  $1894\text{ cm}^{-1}$  due to  $-\text{CH}_2-$  vibrations in amorphous (49) and crystalline phase respectively have been used as internal intensity standard. PE used has a number average molecular weight of 20,000 and weight average molecular weight of 80,000. This corresponds to approximately  $3 \times 10^{19}$  end groups per gram of PE material. If a bond scission of approximately  $9.9 \times 10^{18}/\text{cm}^3$ , as proposed by Zhurkov, Zakrevskii (24a, 24b) were to take place, the intensity of IR bands corresponding to various end groups will increase by 30 %. Such a change in the intensity should be easily observable, but the experiments performed by the author here to obtain the difference spectrum between fractured and drawn PE films, using both  $1303\text{ cm}^{-1}$  or  $1894\text{ cm}^{-1}$  bands as internal standards, failed to indicate any changes in the end group concentration. Similar observations have been made by DeVries (50) at the University of Utah.

Assuming that a 1 % change in the intensity of IR bands due to end groups is the minimum detectable limit for the IR technique, these negative results would mean that the number of end groups formed on fracture in PE is less than  $3 \times 10^{17}/\text{gm}$ . Therefore, a secondary radical reaction as proposed by Zhurkov and Zakrevskii (24a, 24b), leading to the formation of the submicroscopic cracks is not feasible, since it requires that each free radical must rupture 4000 or so additional covalent bonds before it decays.

A comparison of the vinyl end groups ( $\text{R}-\text{CH}=\text{CH}_2$ ) intensities of undrawn and drawn (draw ratio = 15) was performed and the results are shown in Table 4. The intensity of the vinyl end group showed an increase in concentration of the order of 3 %, which corresponds to approximately  $9 \times 10^{17}$  scissions per gram occurring in the draw process. These results lend support to Flory's (51) suggestion regarding bond scission accompanying drawing of the semicrystalline polymer lamella.

Table 4.

Changes in intensity of IR end-group bands on drawing of polyethylene

Polyethylene Specimen	Absorbance of $908\text{ cm}^{-1}$ band Absorbance of $1894\text{ cm}^{-1}$ band	Absorbance of $990\text{ cm}^{-1}$ band Absorbance of $1894\text{ cm}^{-1}$ band
Undrawn	2.62	0.69
Drawn	2.70	0.72

Percentage increase in the intensity of  $\text{RCH}=\text{CH}_2$  groups on drawing $908\text{ cm}^{-1}$        $990\text{ cm}^{-1}$ 

3.1%      4.3%

## **3.4 Gel Permeation Chromatography**

### **3.4.1 Introduction**

A major effort of this study as stated in the thesis proposal, was to be devoted to monitoring the effects of fracture on molecular weight distribution (MWD) using Gel Permeation Chromatography (GPC). Fracture, being a criticality phenomenon, is determined by the largest flaw present in the material and generally affects the material in a local region near the fracture surface without affecting in any significant manner the overall state of the material. An exception to this behavior is the fracture in a highly drawn fibrous morphology. As a result, the expected change in MWD for most materials will be insignificantly small to be observed by GPC, but a repeated fracture or extensive crazing (cracking) of the material by some means might produce a detectable shift in MWD.

Nylon 6 fibers, where a significant bond scission has been reported from ESR studies, was the major case for the investigation of MWDs. This being the first reported study of the kind investigating the fracture in nylon fibers using GPC, a major effort has gone into developing the details of the technique. Furthermore, it was also shown during preliminary work that a change in MWD in glassy polymers like polystyrene can be observed, provided an extensive damage is done by producing a high craze (crack) density. The polystyrene work is presented in the 'Preliminary Work' subsection.

### **3.4.2 Principles of GPC**

Gel Permeation, or size separation, is a form of liquid chromatography in which the solute molecules are separated as a result of their permeation into a solvent-filled matrix in the column packing. Large molecules may be excluded from some or all of the porous matrices of the packing by virtue of their physical size. They elute from the column before smaller molecules which have the opportunity to permeate into a greater percentage of the solvent-filled matrix. In  $\mu$ styragel ( $10^6$  to  $10^3 \text{ \AA}^0$  pore size) or

any other system of columns, there are experimentally determined size limits between which the separation occurs. Those molecules with molecular size equal to or larger than the largest pore size will elute at the same point, known as the Void Volume  $V_0$  in GPC. Also, there exists a point of total permeation, i.e., a volume where all molecules of a given size and smaller will elute at exactly the same place. This is known as the total permeation volume or  $V_t$ . The difference between  $V_0$  and  $V_t$  is called  $V_i$ , the interstitial distance volume, and is the volume where separation takes place. For a given set of columns  $V_0$  and  $V_t$  are fixed quantities; therefore, the total volume, and hence the total time required for an analysis are fixed. The separation process,  $V_0$ ,  $V_i$ , and  $V_t$  are depicted in Figure 22. Figure 23 is a schematic diagram of the GPC instrument.

Figure 22 : Principles of Gel Permeation Chromatography.

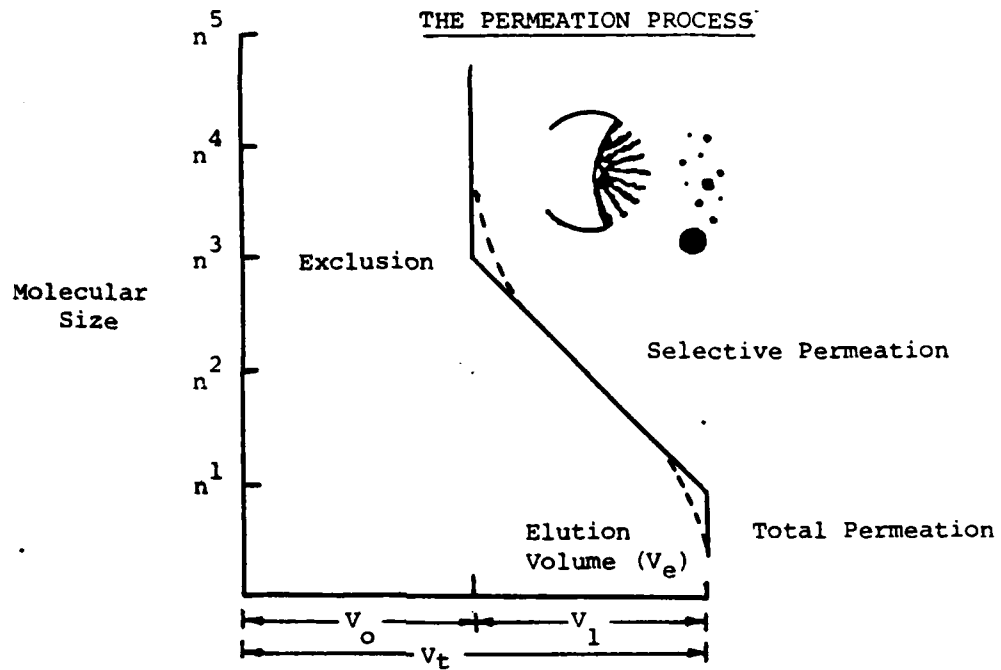
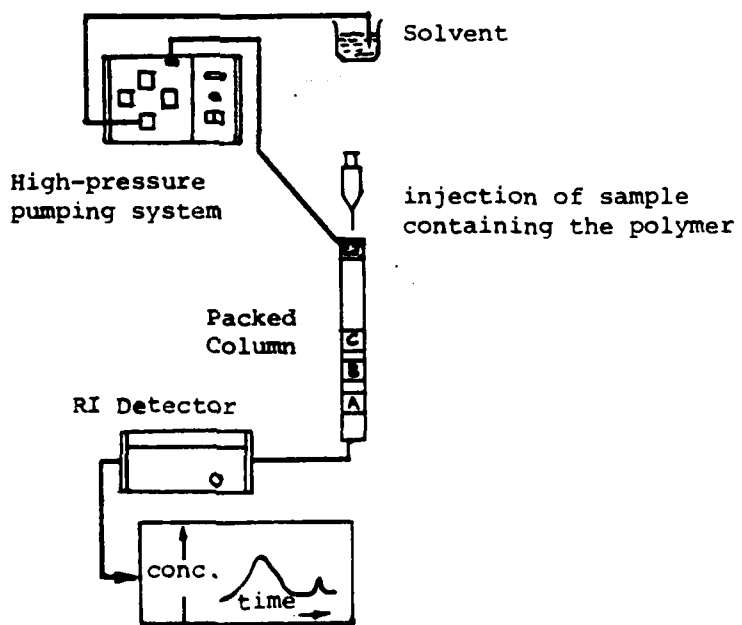


Figure 23 : Schematic of GPC instrument.



### 3.4.3 Preliminary Work

Fracture in glassy polymers is believed to occur through secondary bond rupture such as sliding of molecules past each other. The role of primary covalent bond has never been too clear and only a small amount of bond scission, if any, is expected.

A high density of cracks in a thin polystyrene specimen was obtained by bending it back and forth. The virgin and highly crazed (cracked) specimens and polystyrene standards of narrow molecular weight distribution ( $\bar{M}_w/\bar{M}_n < 1.1$ ) dissolved in chloroform to prepare approximately 0.125 % concentration solution for GPC analysis. GPC analysis of polystyrene standards is performed and the elution volumes plotted against the molecular weights to obtain a calibration curve for polystyrene as shown in Figure 24. (More details of calibration procedures are discussed in Appendix IV.)

Nine molecular weight distributions (MWDs) for the virgin and crazed (cracked) polystyrene specimens are obtained and the data stored in digital form on the computer. These data are then used to obtain the number and weight average molecular weights as shown in Table 5 for the virgin and fractured specimen. Also, averaged virgin and crazed MWDs from these data are obtained and plotted in Figure 25.

Figure 25 clearly shows that MWD shifts towards lower values on fracture. Number and weight average molecular weight data in Table 5 are further analyzed for changes according to median rank plotting in Figures 26 and 27. Median rank plotting t-statistics procedures are described in Appendix V.

Furthermore, a t-statistic test of the  $\bar{M}_w$  and  $\bar{M}_n$  values of Table 5 indicated that one can state with 95 % confidence that  $\bar{M}_w$  has decreased upon crazing and failure. A similar statement for  $\bar{M}_n$  is not possible due to the higher scatter in the  $\bar{M}_n$  measurements.

These observations can only be explained on the basis of covalent bond rupture of higher molecular weight (longer) molecules which will affect  $\bar{M}_w$  much more strongly than  $\bar{M}_n$ . Some error in the determination of  $\bar{M}_n$  may also have resulted from the presence of a low molecular weight component

(some kind of processing aid in the specimen and not part of the MWD shown). This does interfere with a precise measurement of the concentration for low molecular weight part of the distribution, which will have strong influence on the calculated  $\bar{M}_n$ .

Figure 24 : GPC calibration curve for polystyrene at 25°C.

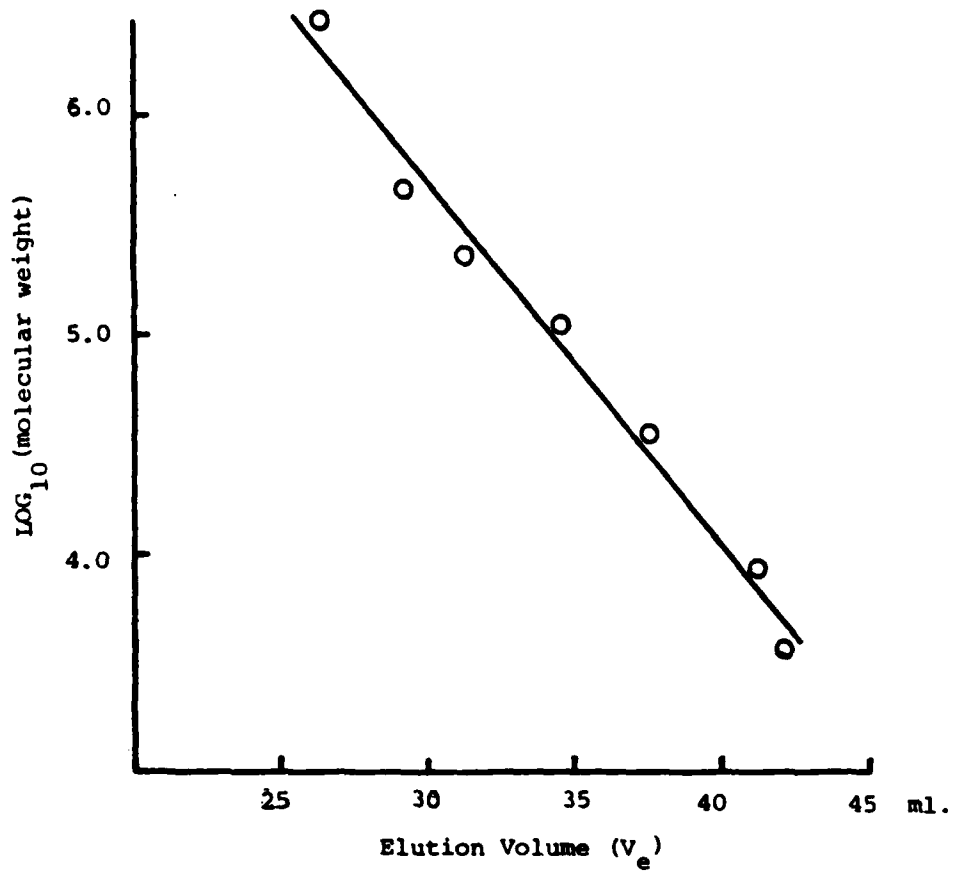
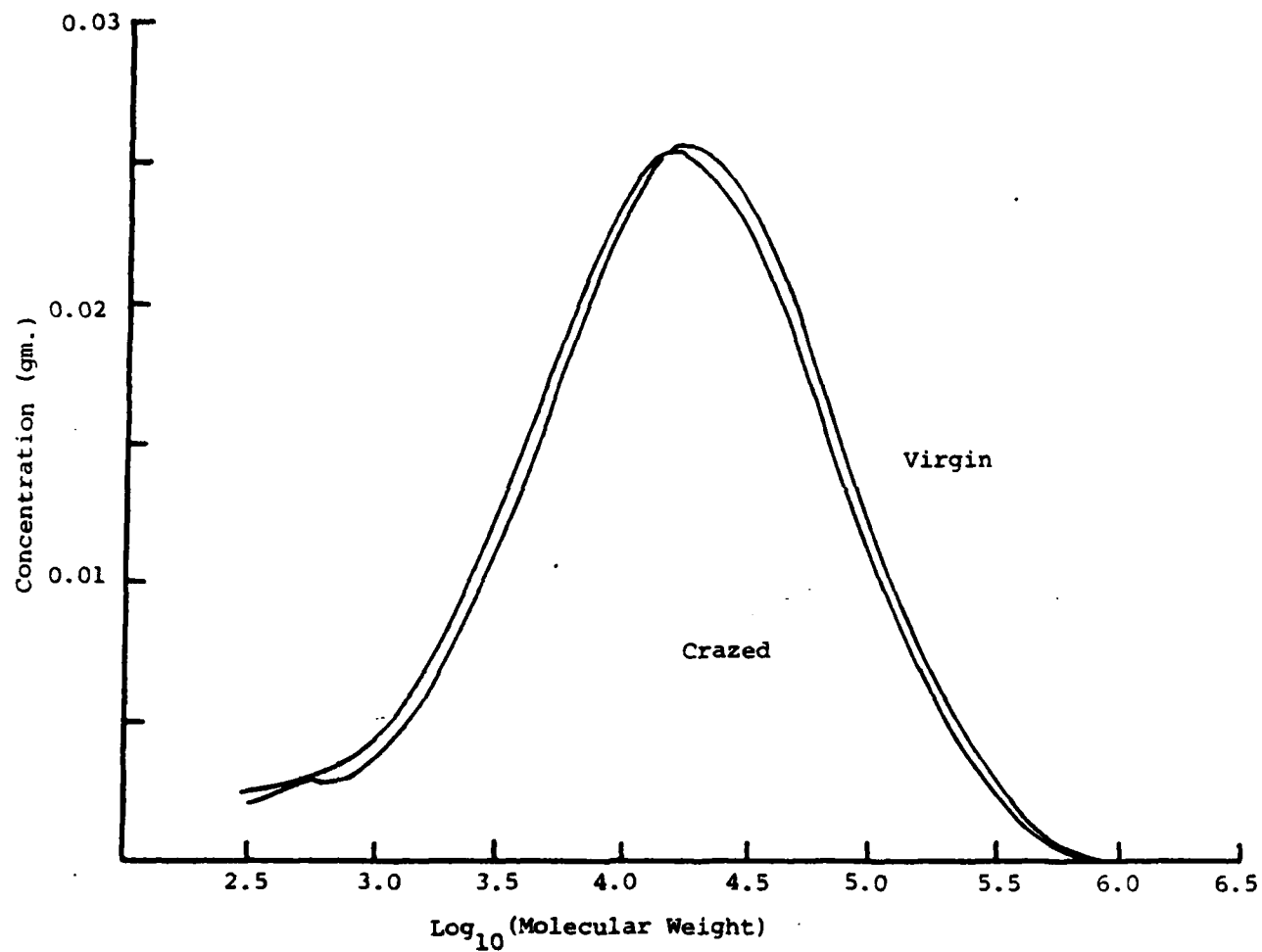


Figure 25 : Averaged molecular weight distribution (MWD) of virgin and crazed (fractured) polystyrene at 25°C.



Note : Total concentration for each of the MWD is 1.0 gm.

TABLE 5

VIRGIN POLYSTYRENE			CRAZED (AND FRACTURED) POLYSTYRENE		
Weight Average Molecular Weight $\times 10^4$	Number Average Molecular Weight $\times 10^3$	Dispersity	Weight Average Molecular Weight $\times 10^4$	Number Average Molecular Weight $\times 10^3$	Dispersity
3.402	4.369	7.8	3.081	3.465	8.9
3.630	4.773	7.6	3.192	5.902	5.4
3.633	4.330	8.4	3.403	4.045	8.4
3.909	4.865	8.0	3.483	4.091	8.5
4.026	5.885	6.8	3.611	4.829	7.5
4.135	5.069	8.2	3.760	6.580	5.7
4.226	6.192	6.8	3.921	6.674	5.9
4.315	7.198	6.0	4.083	6.640	6.1
4.402	7.141	6.2	4.260	7.439	5.7

Figure 26 : Median rank plot for weight average molecular weight ( $\bar{M}_w$ ) of polystyrene.

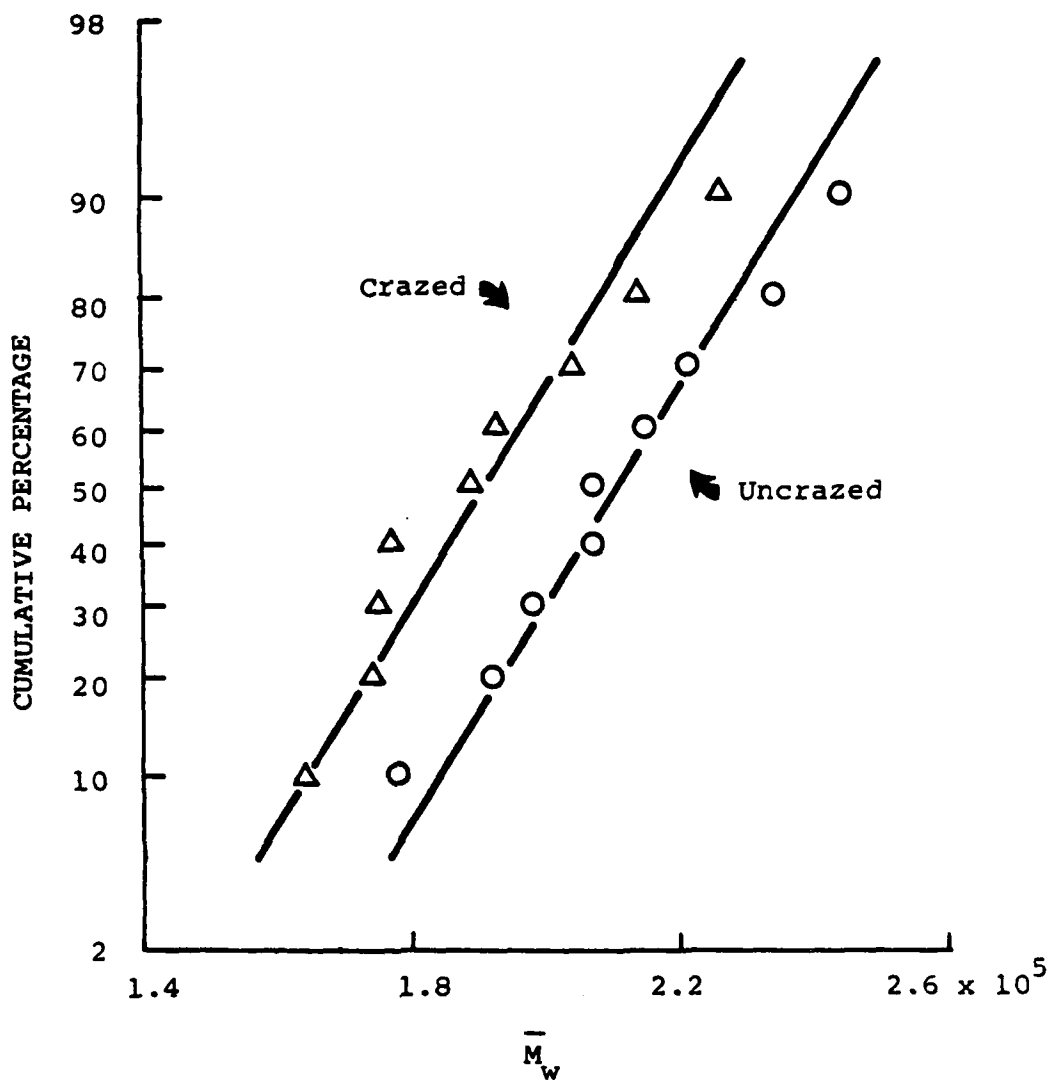
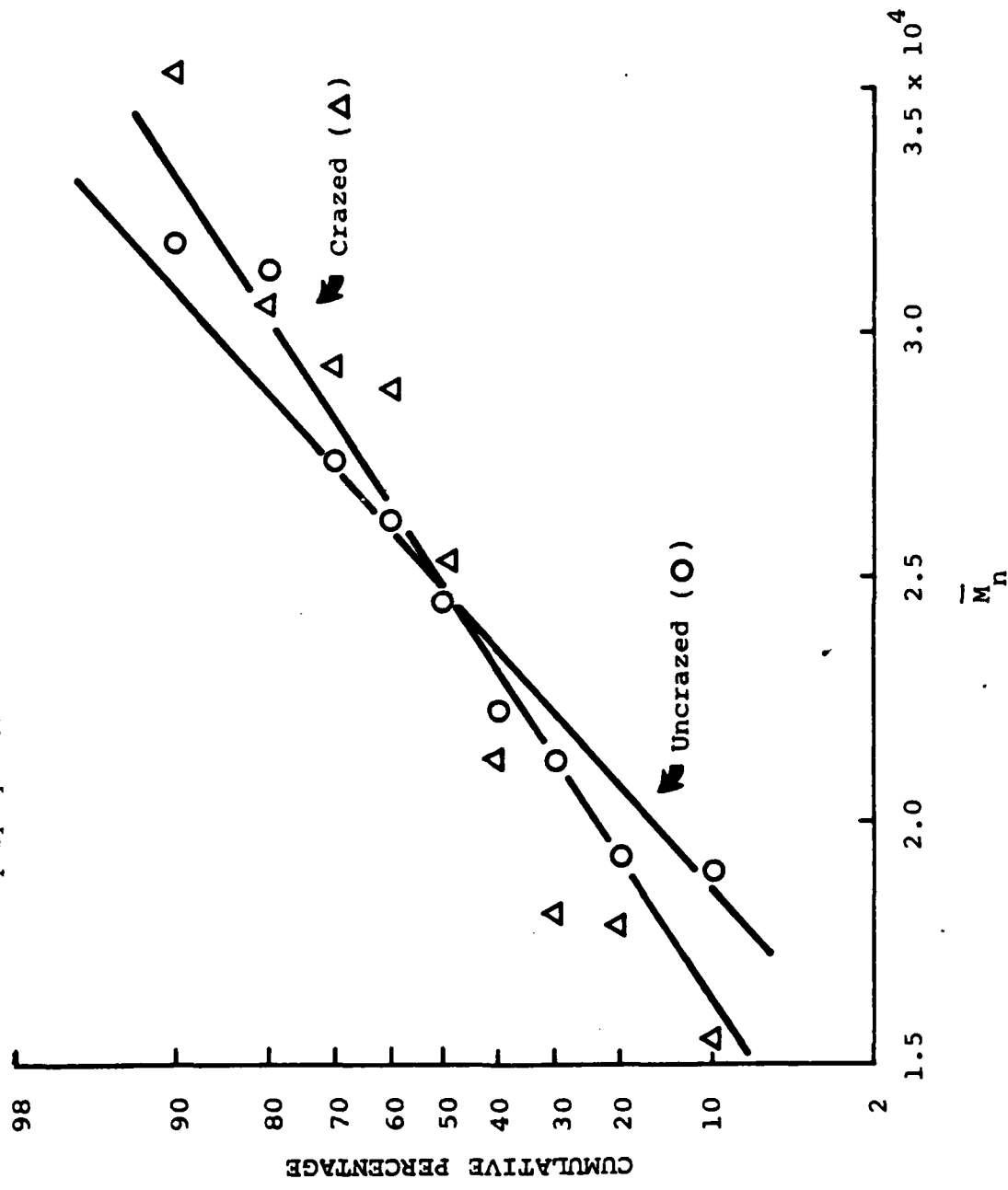


Figure 27 : Median rank plot for number average molecular weight ( $\bar{M}_n$ ) of polystyrene.



### 3.4.4 GPC of Nylon 6 Fibers

The nylon 6 specimens used for GPC analysis are virgin and fractured nylon 6 fibers. The fractured specimen is obtained by breaking a tensile nylon 6 fiber specimen of the kind in Figure 10, in a uniaxial tension mode. Hexafluoro iso-propanol is the only solvent for nylon 6 at room temperature and which is also compatible with  $\mu$ -styrigel GPC columns, but nylon 6 exhibits a polyelectrolyte behavior for dilute solutions in HFIP. Such a behavior has to be suppressed for a meaningful analysis of the MWD from GPC. This is done through the use of a 0.1 molar solution of sodium trifluoroacetate in HFIP as the mobile phase replacing pure HFIP. This mobile phase will be called as 'S-HFIP' for future reference. The nature of polyelectrolyte behavior, its effect on size separation by GPC and suppression of polyelectrolyte effect through the use of S-HFIP, and other data are presented in much greater detail in Appendix VI.

The calibration curve of Figure 24 for narrow ( $\bar{M}_w/\bar{M}_n < 1.1$ ) polystyrene standards cannot be used to obtain MWD of nylon specimens. Narrow molecular weight standards for nylon are not available and neither are polystyrene standards soluble in S-HFIP for getting a universal calibration curve. In absence of these commonly used means of calibration, a third approach in which known number and weight average molecular weight of a broad nylon 6 specimen are used to fit a linear calibration curve is adopted here. This and other calibration procedures are described in detail in Appendix IV.

The shift in the MWD upon fracture in nylon 6 is expected to be small, similar to the polystyrene behavior; therefore, repeated analysis of the same specimen were performed. In this case six MWDs for each of the virgin and fractured nylon 6 specimens are obtained. The data are then analyzed in the same manner as of polystyrene described in the previous section. Averaged MWDs of virgin and fractured nylon 6 specimens are plotted together in Figure 28 for comparison. The number, weight average molecular weights and polydispersity for virgin and fractured MWDs are tabulated in Table 6. These are plotted according to median rank plotting in Figures 29, 30 and 31. The plots of Figures 28, 29 and 30

clearly show the decrease in molecular weight averages and the shift in MWID towards lower molecular weights on fracture. The rupture of large molecules on fracture suggests that the decrease in weight average molecular weight  $\bar{M}_w$  will be greater than the decrease in number average molecular weight  $\bar{M}_n$ . Therefore, polydispersity =  $\bar{M}_w/\bar{M}_n$  will also decrease on fracture. The changes in  $\bar{M}_w$  and  $\bar{M}_n$  being small, a large shift in polydispersity is not expected as is also evident from Figure 31. Figure 33 plots the difference between averaged MWDs of virgin and fractured specimens of Figure 28 and shows that the molecules belonging to higher molecular weight component rupture during fracture. This presents a positive proof of the assumption made in calculating the amount of bond rupture from decrease in viscosity average molecular weight by Crist (13), and Becht and Fischer (40).

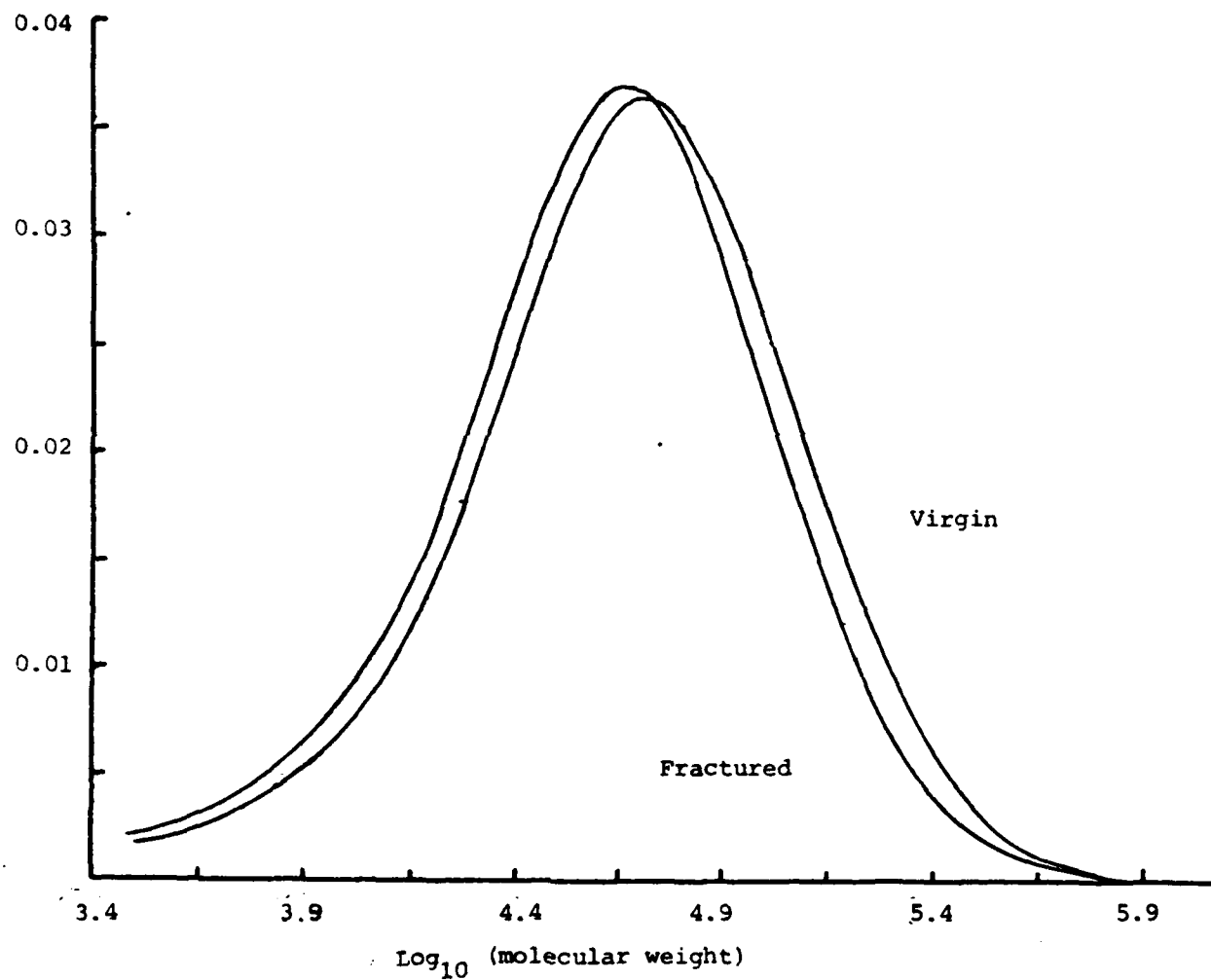
Figure 32 shows the number and weight average molecular weights for the averaged virgin and fractured chromatograms of Figure 28. It shows that the approximate number for bond scission per gram ( $\beta_{gpc}$ ) is  $2.8 \times 10^{18}$ . A more accurate number for  $\beta_{gpc}$  is obtained from a calculation of the number of molecules per gram in virgin and fractured specimens as shown next.

Figures 33 and 34 are obtained, according to the following equation, from average MWID of virgin and fractured specimens and present  $N(i)$ , the number of molecules per gram of nylon 6 versus molecular weights MWDs of virgin and fractured specimens.

$$N(i) = [w(i) * 6.023 \times 10^{23}] / MW(i) \quad (15)$$

where  $w(i)$  is the concentration of molecular weight  $MW(i)$  in one gram of nylon 6. The total number of molecules per gram for virgin and fractured nylon 6 fibers are calculated to be  $19.8 \times 10^{18}$  and  $22.4 \times 10^{18}$ , respectively. Thus the number of chains scissions per gram ( $\beta_{gpc}$ ) in nylon 6 is  $2.6 \times 10^{18}$  per gram. Considering the density of 1.14 per gram, this will give bond scission per  $\text{cm}^3$  ( $\beta'_{gpc}$ ) of  $2.3 \times 10^{18}$  for nylon 6.

Figure 28 : Averaged molecular weight distribution (MWD) of virgin and fractured nylon 6 fibers.



Note : Total concentration for each MWD is 1.0 gm.

Table 6.

	Number	Average Molecular Weight	Weight Average Molecular Weight		Polydispersity	
			Virgin	Fractured	Virgin	Fractured
1	29,570	25,440	65,190	56,850	2.14	2.16
2	29,980	26,040	65,480	58,890	2.20	2.18
3	30,580	26,180	67,640	59,000	2.21	2.20
4	30,650	26,850	68,630	59,430	2.28	2.23
5	30,680	27,350	72,780	63,720	2.29	2.28
6	31,180	29,220	73,510	64,740	2.40	2.41

Figure 29 : Median rank plot for number average molecular weight.

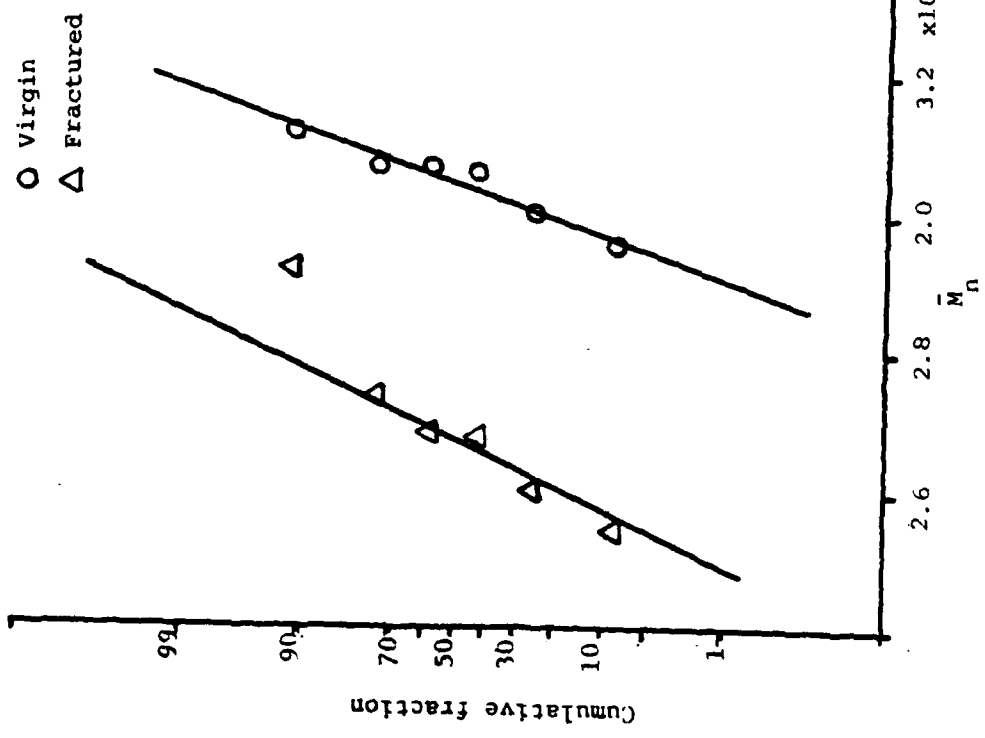


Figure 30 : Median rank plot for weight average molecular weight.

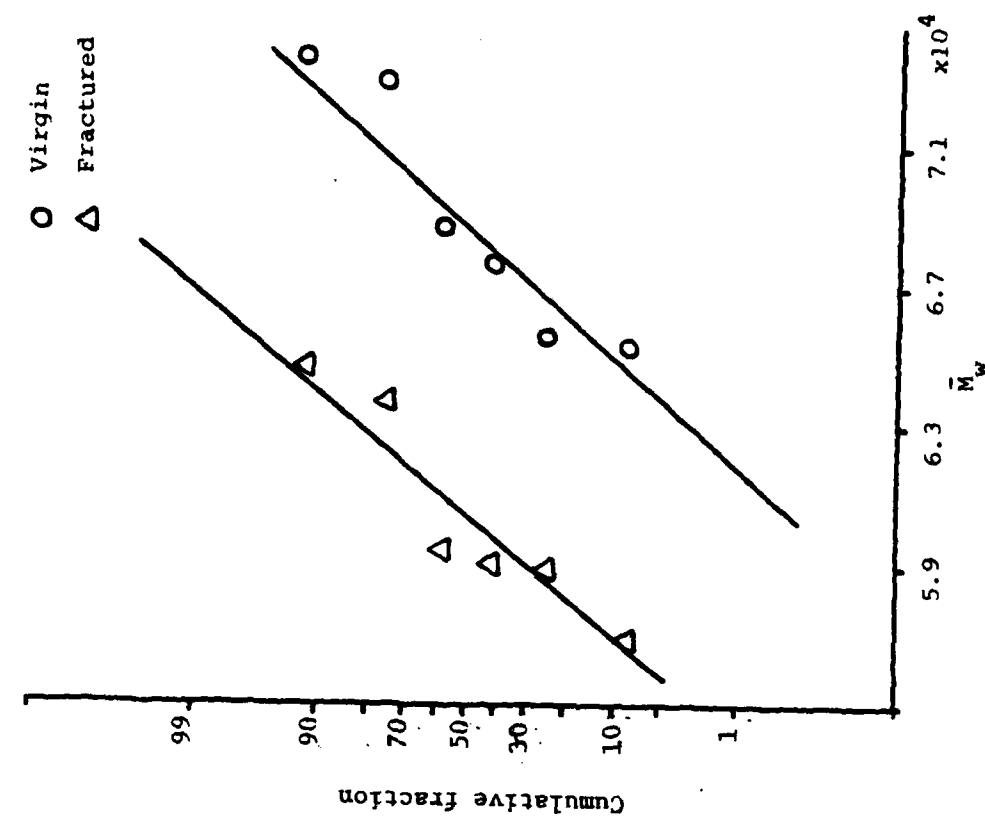


Figure 31 : Median rank plot for polydispersity.

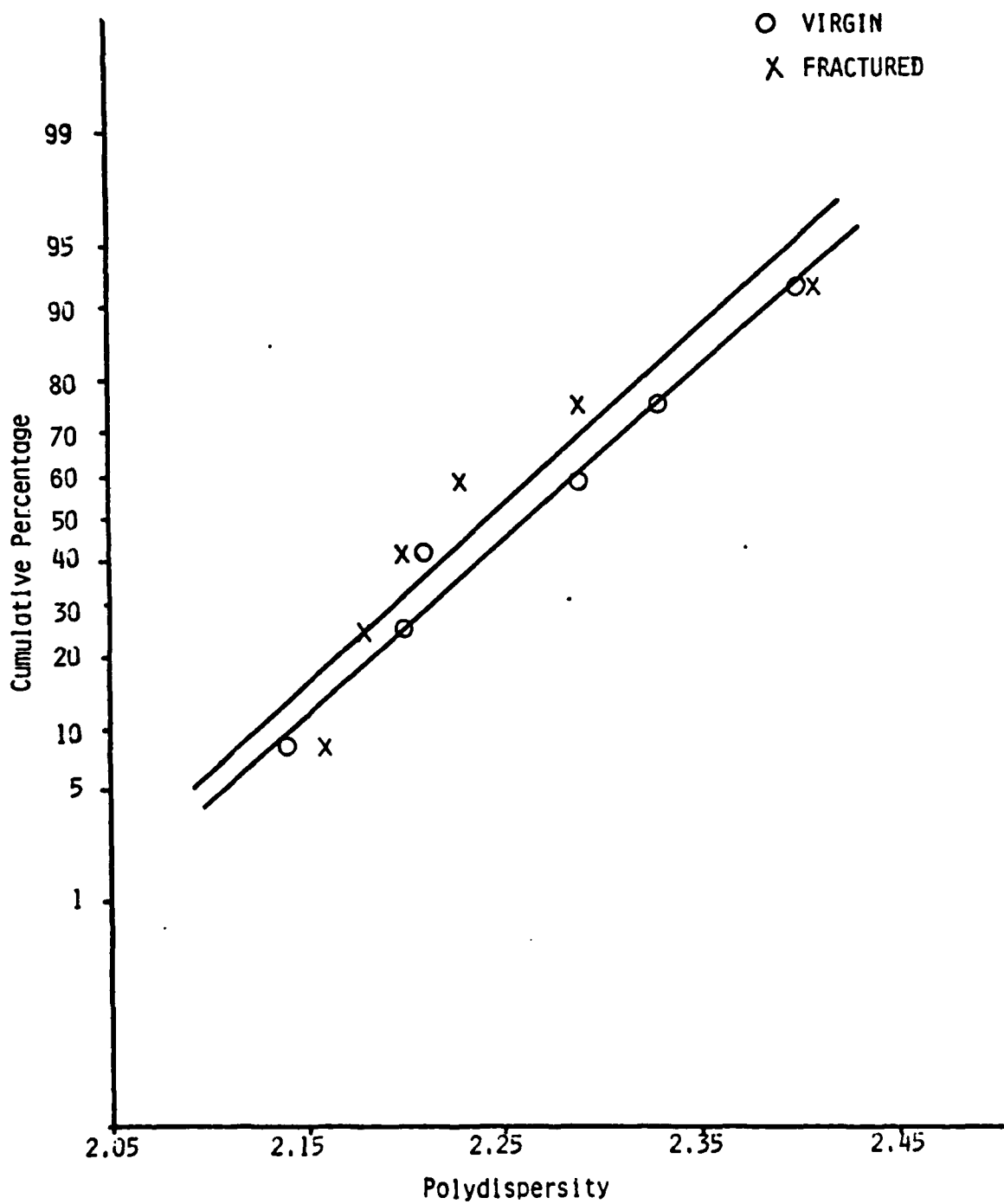


Figure 32 : Calculation of the number of molecules ruptured per gram of nylon 6 fibers on fracture.

Specimen	Number Average Molecular Weight	Weight Average Molecular Weight	Polydispersity
Virgin nylon 6 fiber	30,500	69,200	2.27
Fractured nylon 6 fiber	26,700	60,600	2.27

Number of molecules ruptured/gram in nylon 6 fibers on fracture ( $\beta_{GPC}$ )

$$\begin{aligned}
 &= 6.023 \times 10^{23} \left( \frac{1}{\bar{M}_n} \right) \text{ fractured} - \left( \frac{1}{\bar{M}_n} \right) \text{ virgin} \\
 &= 2.8 \times 10^{18} / \text{ gram}
 \end{aligned}$$

Figure 33 : Distribution of number of molecules/gm. in virgin and fractured nylon 6 fibers.

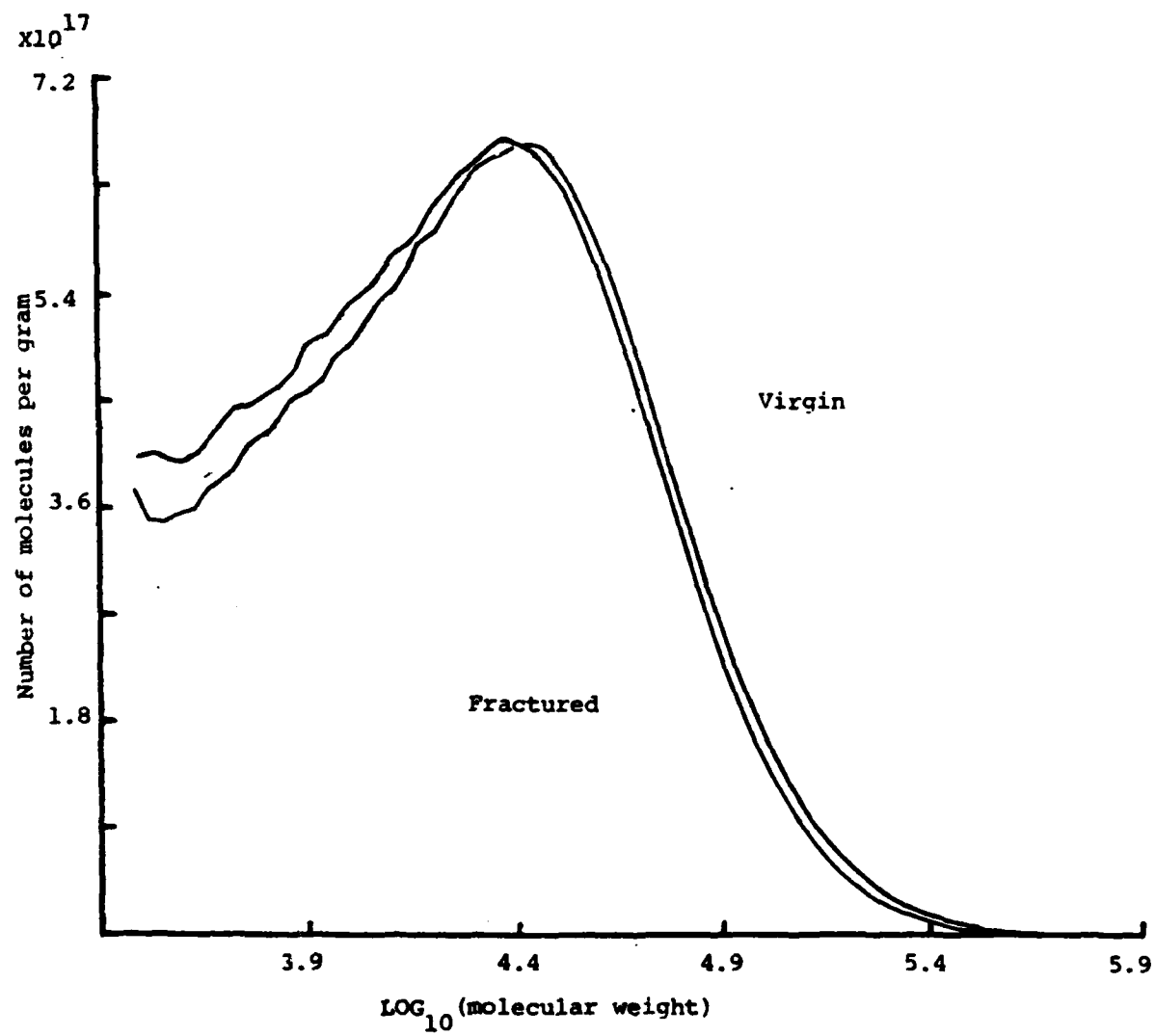


Figure 34 : Difference MWD = MWD of fractured nylon 6 fiber  
- MWD of virgin nylon 6 fiber

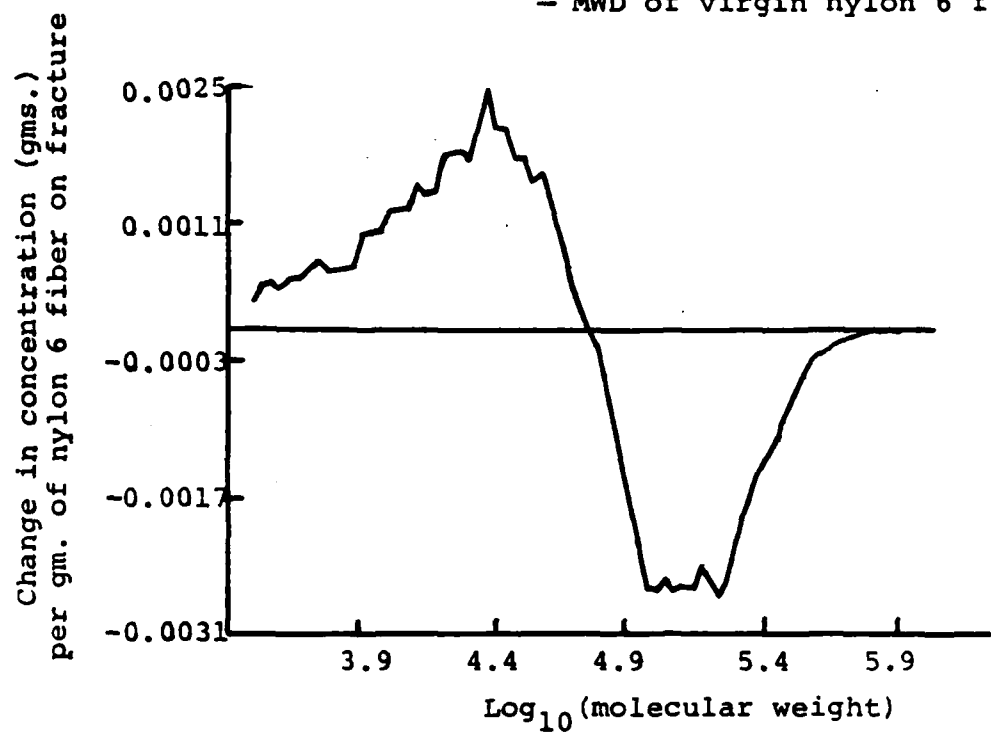
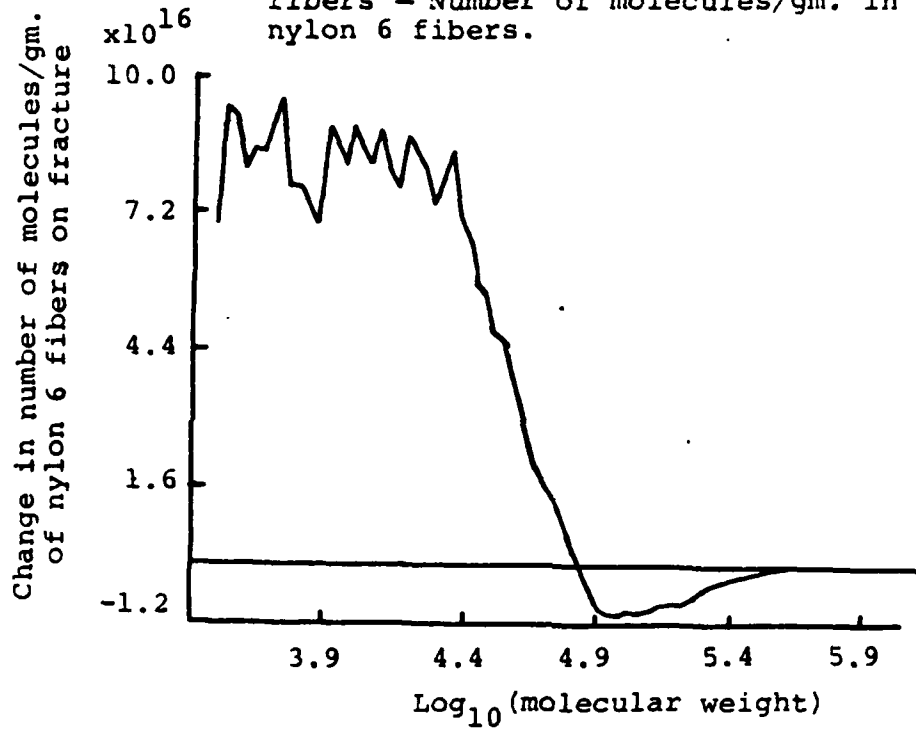


Figure 35 : Difference distribution =  
Number of molecules/gm. in fractured nylon 6  
fibers - Number of molecules/gm. in virgin  
nylon 6 fibers.



## **4. Analysis of Tie Chain Scission**

### **4.1 Model for Tie Chain Length Distribution**

The microstructure of highly drawn polymers, different in details from one polymer to another, consists essentially of alternating crystalline and amorphous regions. The amorphous regions consist of chain loops or folds at the interphase between crystalline and amorphous block, tie chains bridging the amorphous region connect adjacent crystalline blocks, chain ends and cilia. The tie molecules have different lengths which is a factor determining the mechanical properties of these materials. The tie molecules in the amorphous regions (15, 52) bear the load and as a result rupture under stress.

A model to obtain the density distribution function for tie chain lengths has been developed. The model calculations are performed for a basic element of semi-crystalline polymer consisting of two crystalline blocks and an amorphous region separating them, as shown in Figure 36. As an approximation, the real polymer chain is replaced by an equivalent model chain on a cubic lattice. The free energy  $F$  of the element under consideration consists of the energy contribution from crystalline blocks, the amorphous regions, and the interfacial zone between them. The energy  $F$  is given as

$$F = \{M - \sum_{N} v_N^* N\} F_c^0 + \sum_{N} v_N F_L(N) + kT \sum_{N} v_N \log_e(v_N/v) + 2v\gamma + \gamma'' \quad (16)$$

where

$M$  : Total number of model chain units present in the element.

$N$  : Number of tie chains of  $N$  units.

$F_c^0$  : Free energy per unit of the chain in the crystalline block.

$F_L(N)$  : Energy of a tie chain of  $N$  units.

$v$  : Total number of tie chains present in an amorphous regions.

$\gamma$  : Surface energy per tie chain coming off the crystal surface.

$\Upsilon''$ : Total surface energy of chain folds or loop.

The first term in equation (16) is the energy of crystalline blocks, the second term energy of tie chains and third the configurational energy of the tie chains, and the last two terms are the surface energy of the interfacial zone.

Figure 36 : A typical crystalline and amorphous region of the fibrous structure.

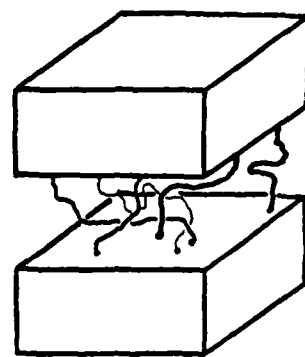


Figure 37 : Schematic drawing of a tie chain and the interfacial zone in an amorphous region.

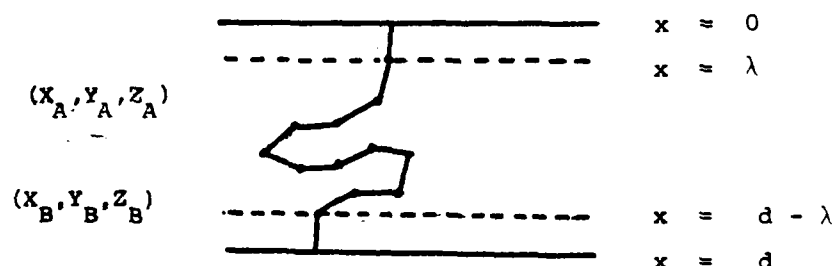


Figure 38 : A representatice chain configuration not allowed in the amorphous region of a semi-crystalline polymer.

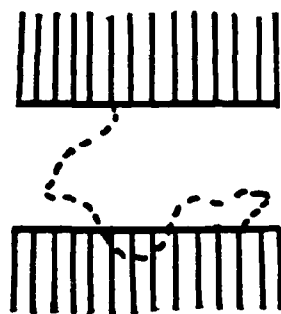


Figure 39 : Three-dimensional view of of alternating crystalline and amorphous blocks in the fibrous structure.

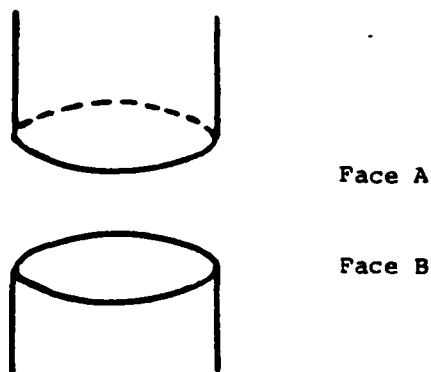
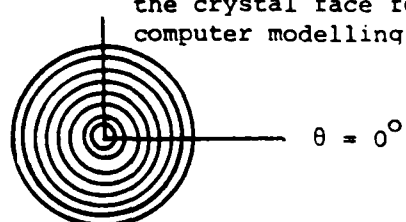


Figure 39A : Crossectional view of the crystal face for computer modelling.



The tie chain length distribution is obtained from the consideration that free energy  $F$  is minimum subject to the condition that

$$v = \sum v_N = \text{constant} \quad (17)$$

Therefore, the equation to be solved using Lagrange multipliers is:

$$\delta F = 0 \quad (18)$$

subject to the condition

$$\delta v = \delta \sum v_N = 0 \quad (19)$$

Solving these, one obtains

$$G(N) = v_N/v = \exp \{-\Delta F_L(N)/kT\} / \sum_N \exp \{-\Delta F_L(N)/kT\} \quad (20)$$

$$\text{where } \Delta F_L(N) = F_L(N) - N F_c^0 \quad (21)$$

Free energy  $\Delta F_L(N)$  consists of an enthalpy and an entropy term.

$$\Delta F_L(N) = \Delta H_L(N) - T \Delta S_L(N) \quad (22)$$

Enthalpy Term: The enthalpy term  $\Delta H_L(N)$  is the enthalpy of melting  $N$  crystalline units and a term due to chains in the interfacial zone (53, 27), which have both trans and gauche conformations.

Therefore,

$$\Delta H_L(N) = N \langle \Delta H_0 \rangle + Y(N) \quad (23)$$

where  $\langle \Delta H_0 \rangle$  is the melt enthalpy per unit of the model chain in the crystalline phase.

It is expected that the chains emerging from crystal blocks as tie chains will be somewhat more constrained in the interfacial zone than in a perfectly amorphous state (and will probably have more trans

conformations than in the melt or amorphous state). As a simplification procedure, we assume that all the tie chain constraints are confined to a small interfacial zone as shown in the Figure 37. It is also assumed that the interfacial energy  $\Upsilon^0(N)$  is independent of the length of the tie chain; in other words,  $\Upsilon^0(N) = \Upsilon$ .

Therefore,

$$\Delta H_L(N) = N \langle \Delta H_0 \rangle + \Upsilon \quad (24)$$

Entropy Term:  $S_L(N)$ , the entropy, for a chain of length L and number of units N, forming a tie molecule is different from a chain of N units in the melt, since the ends of the chains are fixed to the crystal and the volume available to the chains is limited to the volume confined between the two crystalline blocks.  $S_L(N)$  is solved for by arranging the model chain on a primitive cubic lattice of lattice constant 'a' subject to the above conditions. The entropy of a chain of N units having end to end distance r is given by

$$S_L(N,r) = S_t^*(N) + k \log_e \{Z^*(N,r)\} \quad (25)$$

where  $S_t^*(N)$  is the entropy contribution arising from inner vibrations of the chain and  $Z^*(N,r)$  is the number of configurations available to the chain in the presence of other chains. The quantity  $S_t^*(N)$  for a chain of N units in the present situation (amorphous phase) is the same as in the melt, but  $Z^*(N,r)$  is different.

According to Zachman and Peterlin (54), for a chain fixed at two ends,

$$Z^*(N,r) = W(N+1,r) * Z(N+1) * a^3 \quad (26)$$

where  $W(N+1,r) * a^3$  is the probability that the end of the model chain lies within the volume  $a^3$  at a distance r from the other end.  $Z(N+1)$  is the number of configurations of a chain of N + 1 units with

both ends free and in infinite space.

According to Chandrasekhar (55), the number of conformations of the shortened chain in the volume limited by crystal faces is given by the number of conformations in the infinite space minus the number of conformations of the chain which partly touch or cross either or both of the crystal faces. In other words, the conformations subtracted will be the ones for which the chain will cross from amorphous into at least one of the crystalline regions for a short hop before returning to the amorphous region. Such a representative chain configuration is shown by the dotted line in Figure 38.

The mathematical formulation for this is due to Gaylord (56). The probability of a chain of end to end distance  $r$  between two perfectly reflecting infinite walls (an approximation to the real finite size of crystal face) separated by a distance  $d$  is given as

$$W(|l|, r) = \sum_{m=-\infty}^{\infty} [W(x_1 - x_2 - 2md, y, z) - W(x_1 + x_2 - 2md, y, z)] \quad (27)$$

where  $(x_1, y_1, z_1)$  and  $(x_2, y_2, z_2)$  are the coordinates of the chain ends and

$$y = y_1 - y_2; z = z_1 - z_2.$$

Such a representative chain is shown in Figure 37.

Since the chain in the interfacial zone has only one conformation, the shortened chain of  $(N - 2)$  unit lengths connecting points 1 and 2 has the same number of conformations as the whole chain of  $N + 2$  units. For calculation purposes, the interfacial zone has been chosen to be of length  $2a$ , i.e.,  $\lambda = 2a$  (about  $4.9 \text{ \AA}^0$ ). Therefore, a tie molecule of  $N + 2$  units will effectively act, for the purposes of conformation calculation act, as a model chain of  $N - 2$  units.

From equations (26) and (27)

$$\begin{aligned} Z^*(N+2, r) &= \sum_{m=-\infty}^{\infty} Z(N-1) \{W(N-1, r(m)) - W(N-1, r'(m))\} * a^3 \\ &= Z(N-1)^* P(N, r) \end{aligned} \quad (28)$$

where

$$P(N,r) = \sum_{m=-\infty}^{\infty} \{W(n-1,r(m)) - W(N-1,r(m))\} * a^3 \quad (29)$$

From equations (25), (26), (27), (28), and (29), it follows that,

$$\begin{aligned} S_L(N+2,r) &= S_t(N+2) + k \log_e \{Z^*(N+2,r)\} \\ &= S_t(N+2) + k \log_e \{Z'(N-1)\} + k \log_e \{P(N,r)\} \end{aligned}$$

According to Flory (57), for a chain of N units on a cubic lattice,

$$Z(N) = 6^N$$

Thus,

$$S_L(N+2,r) = S_t(N+2) + k \log_e \{Z'(N+2)\} - 3k \log_e 6 + k \log_e \{P(N,r)\} \quad (30)$$

The entropy of a chain of N + 2 units in the melt is given by

$$S_m(N+2) = S_t(N+2) + k \log_e \{Z'(N+2)\} \quad (31)$$

Therefore,

$$S_L(N+2,r) = S_m(N+2) - 3k \log_e 6 + k \log_e \{P(N,r)\}$$

Let the entropy of a chain of N + 2 units in the crystal be  $S_c(N+2)$  and

$$S_m(N+2) - S_c(N+2) = (N+2) \langle \Delta S_0 \rangle$$

$\langle \Delta S_0 \rangle$  is the entropy of melting a unit length of chain of the crystalline block.

$$S_L(N+2,r) - S_c(N+2) = \Delta S_L(N+2)$$

$$= (N+2)\langle \Delta S_0 \rangle + k \log_e \{P(N,r)\} - 3k \log_e 6 \quad (32)$$

Therefore,

$$\begin{aligned} \Delta F_L(N+2) &= \Delta H_L(N+2) - T \Delta S_L(N+2) \\ &= (N+2)\langle \Delta H_0 \rangle (T_m^0 - T) / T_m^0 - kT \log_e \{P(N,r)\} + 3kT \log_e 6 \quad (33) \end{aligned}$$

The calculations for the function  $P(N,r)$  based on Gaussian probability function  $W$  are given in Appendix I.

Thus,

$$G(N+2) = v_N/v = \{\exp(-\Delta F_L(N+2)/kT)\} / \sum_N \{\exp(-\Delta F_L(N+2)/kT)\} \quad (34)$$

where

$$\begin{aligned} \Delta F_L(N+2)/kT &= \{(N+2)\langle \Delta H_0 \rangle\} * \{(T_m^0 - T) / T_m^0 * kT\} \\ &\quad - \log_e \{P(N,r)\} + 3 \log_e 6 \quad (35) \end{aligned}$$

and, to a first approximation as shown in Appendix I,  $\log_e P(N,r)$  is given as

$$\begin{aligned} \log_e \{P(N,r)\} &= -0.4158 - 1.5 \log_e (N-1) - \{1.5/a^2\}[(RSQR + 4a^2)/(N-1)] + \\ &\quad \log_e [\sinh \{6(d-2a)/(N-1)a\} * \exp \{-3(d-2a)^2/2(N-1)a^2\}] \\ &\quad \sinh \{6(d+2a)/(N-1)a\} * \exp \{-3(d+2a)^2/2(N-1)a^2\}] \quad (36) \end{aligned}$$

where

$$RSQR = y^2 + z^2 \quad (37)$$

The probability  $G(N)$  for a tie chain of length  $N$  units, according to equations (34), (35), and (36) is a function of the material parameters  $\langle \Delta H_0 \rangle$ ,  $T_m^0$ ,  $T$ ,  $d$  and other parameters  $\lambda$ , RSQR, a characteristic of the model.  $\lambda$  has been assigned value of  $2a$ , based on expected length and the used values for the size

of interfacial zone by other researchers (27). The length 'a' of the unit model chain is calculated from comparison of the melt entropy of the model chain with that of real chain. This calculation is described in a later section on parameters.

In order to evaluate the density function  $G(N)$  from equation (34), one needs to obtain  $\Delta F_L(N)$  as given by equation (35). The  $\log_e P(N,r)$  term in equation (36), as the argument of  $P(N,r)$  suggests, is a function of  $N$ , the number of model chain units and the distance  $r$  between chain ends of the tie molecule.  $r$  is given as

$$r^2 = RSQR + (d - 4a)^2 \quad (38)$$

where RSQR defined here is used for evaluation of  $\log_e [P(N,r)]$ .

A tie molecule in the amorphous region of an element of polymer structure as shown in Figure 39 can have an infinite possible values for  $r$  depending upon the location of end points of A and B in the surfaces 1 and 2 respectively. For the present purposes of calculation of  $G(N)$ , each of the crystalline/amorphous boundary surface has been divided into 100 elements. Since the microfibril has cylindrical cross-section, the element in Figure 39 is assumed to be cylindrical (the diameter of the cylinder is taken to be  $80 \text{ \AA}^0$ ); (20, 21). Each of the cylinder surface is divided into 8 rings of width  $5 \text{ \AA}^0$  each as shown in the Figure 39a.

Each ring is subdivided into elements of equal areas, such that areas of elements in different rings are very nearly the same. Each of these elements are assigned co-ordinates  $R$  and  $\theta$ .  $R$  for an element is the average of the outer and inner radii of the ring to which the element belongs. Considering a ring of  $N$  elements, the  $\theta$  co-ordinate of the  $j^{\text{th}}$  element in the ring will be  $[j \times 360/N]$  where  $j = 1, 2, \dots, N$ .  $\theta = 0^0$  co-ordinate for each ring lies on the same radius line of the circular cross-section. The  $\theta$  value increases anti-clockwise. The  $N$  values for the eight rings, starting from the outermost, were chosen as 24, 20, 18, 14, 10, 8, 4, and 2, respectively.

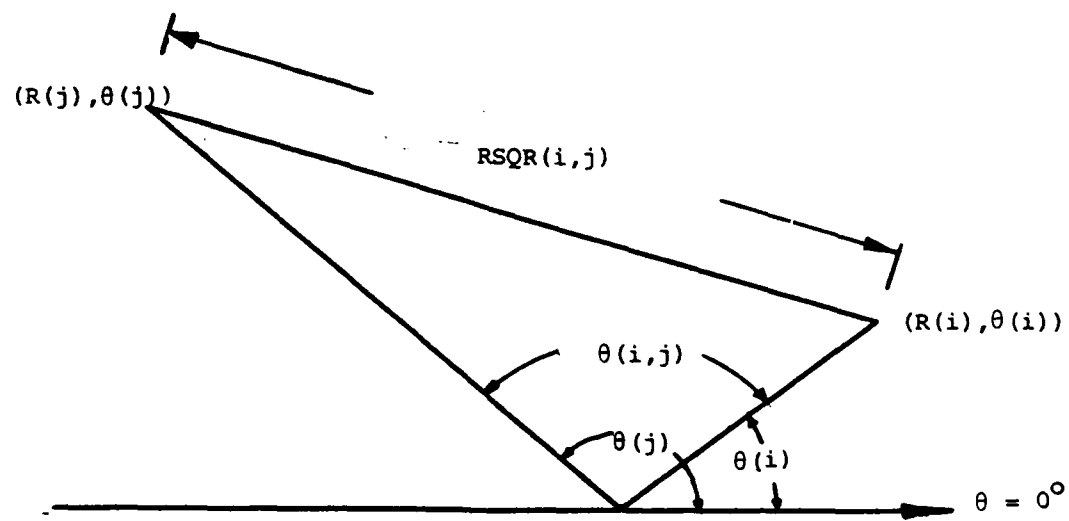
Having assigned  $(R,\theta)$  co-ordinates to each element on both faces 1 and 2 of the crystalline block,

consider a tie molecule connecting the  $i$ th element on the face 1 with  $j$ th element on face 2. In order to evaluate  $\log_e P(N,r)$  from equation (16), the RSQR for this tie molecule has to be obtained.

The RSQR ( $i,j$ ) from the law of cosines and Figure 40 is given as

$$\text{RSQR}(i,j) = \{R_1(i)\}^2 + \{R_2(j)\}^2 - 2\{R_1(i)*R_2(j)*\cos|\theta_1(i) - \theta_2(j)|\} \quad (39)$$

Figure 40 : A drawing for calcualtion of  $RSQR(i,j)$  in the model for tie chain length distribution.



#### 4.1.1 Model Parameters

The chosen values for the parameters of the model for the nylon 6 fiber materials are:

Crystallinity: The crystallinity of 37.5 % for nylon fiber is obtained from density measurements using

$$\text{Amorphous Density (34)} = 1.084 \text{ gm./cm}^3 = P_{\text{am}}$$

$$\text{Crystalline Density (34a)} = 1.230 \text{ gm./cm}^3 = P_{\text{cr}}$$

$$\text{Crystallinity } X_c = 100 * (P - P_{\text{am}}) / (P_{\text{cr}} - P_{\text{am}})$$

$$\text{Density of nylon 6 fiber } P = 1.139 \text{ gm./cm}^3$$

Crystallinity of 50 % is obtained from X-ray data.

Length of Crystalline and Amorphous Blocks: The length of crystalline ( $L_c$ ) and amorphous ( $L_a$ ) blocks of  $60 \text{ \AA}^0$  and  $30 \text{ \AA}^0$  were determined by Prevorsek (20) and Park (32) using WAXS and SAXS.

Melting Temperature: Melting temperature ( $T_m^0$ ) of  $496^0\text{K}$  for the nylon 6 fiber specimen is determined using Differential Scanning Calorimetry (DSC).

Processing Temperature: This was determined by Park (32) in his thesis work for these materials by annealing the nylon 6 fiber at different temperatures. The processing temperature is taken as the minimum annealing temperature at which the morphology, i.e., long period and orientation angle, show a sudden change. This was found to be  $428^0\text{K}$ .

Diameter of the Microfibril: This diameter was determined by Prevorsek (21) from his study of WAXS to be  $80 \text{ \AA}^0$ .

Enthalpy of Fusion: Enthalpy of fusion per mole of monomer for nylon 6 is 5400 calories. (34b).

Lattice Model Unit Length: The model unit length 'a' is obtained by comparing the melt entropy of a model unit with the melt entropy per covalent length linkage in nylon 6.

Melt entropy per model unit, according to equation (11) for a cubic lattice is  $= k * \log_6 6 = 1.79 \text{ k/unit}^0\text{K}$ . Nylon 6 monomer is of length  $8.62 \text{ \AA}^0$  and has 7 covalent linkages. Therefore, average

covalent linkage length is  $1.23 \text{ \AA}^0$ . Melt entropy per linkage is obtained using 5400 calories per mole as the enthalpy of the monomer and  $496^\circ \text{ K}$  as the melting temperature. This gives a value of  $0.78 \text{ k}^\circ \text{ K}$  for melt entropy per linkage.

The melt entropy per model unit is less if one takes into account the close packing of the macromolecules and therefore the competition for space in reducing the number of conformations. Hence, as a first approximation, one model unit is equivalent to two covalent linkages in the real chain. Thus the length of a model unit length 'a' is chosen as  $2.46 \text{ \AA}^0$ .

#### 4.1.2 Calculation of $G(N)$

RSQR (i,j) is evaluated according to the eq. (39) for:  $i = 1, 2, 3, \dots, 100$ , and  $j = 1, 2, 3, \dots, 100$ . For each RSQR (i,j),  $\log_e P(N,r)$  from equation (36) is used to obtain  $\Delta F_L(N)$  and  $G_{i,j}(N)$  for the relevant range of N values using equations (35) and (34) respectively. The  $G_{i,j}(N)$  for all possible i and j is then averaged to obtain the density distribution function  $G(N)$  for the tie molecule population of the element of Figure 32.

(Note: In actual computation on the computer, only a half of the elements for one of the surfaces corresponding to those with  $\theta$  co-ordinates between  $0^\circ$  and  $180^\circ$  have been used. This reduction in computation is possible since the two halves of this surface are identically symmetric with respect to the other surface.)

A plot of  $G(L)$  against the length  $L/L_0$  is shown in Figure 41 for a crystallization temperature T of  $428^\circ \text{K}$  or  $155^\circ \text{C}$ .  $L_0$  is the minimum tie chain length possible and will be equal to the width of the amorphous region in semi-crystalline nylon structure. Figure 42 shows cumulative  $G(L)$  against  $L/L_0$ , plotted on a normal probability paper. The latter half of this curve is a straight line, indicating that these tie chain lengths obey Gaussian statistics. Figure 42 also indicates that short tie chains, generally referred to as 'taut tie chains' have a concentration of 2 - 5 % of the total tie chains. This fractional number for

taut tie chains is in reasonably good agreement with the expected number of taut tie molecules.

Figure 41: Fraction of tie molecules versus ratio of tie chain length to minimum tie chain length ( $L/L_0$ ).

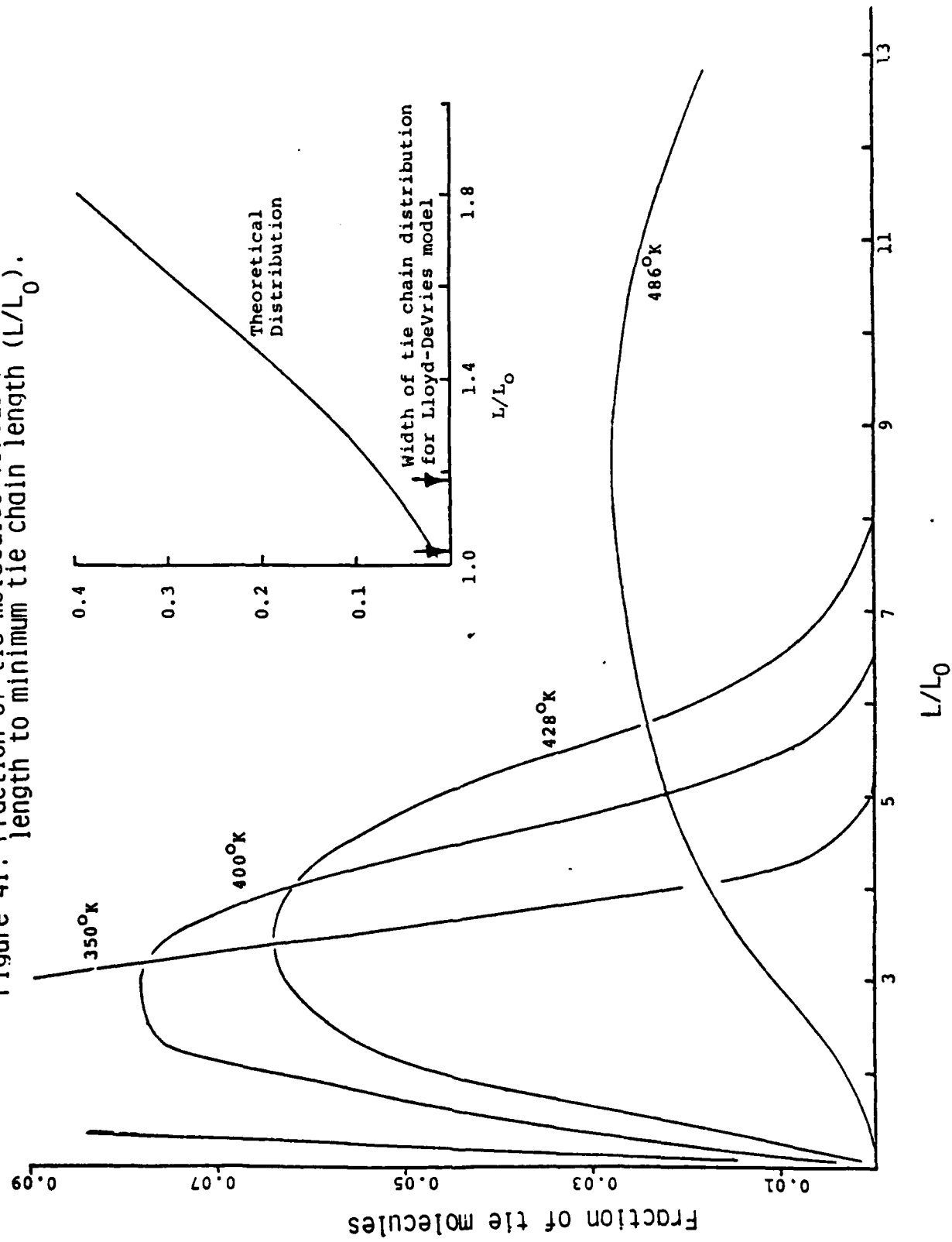
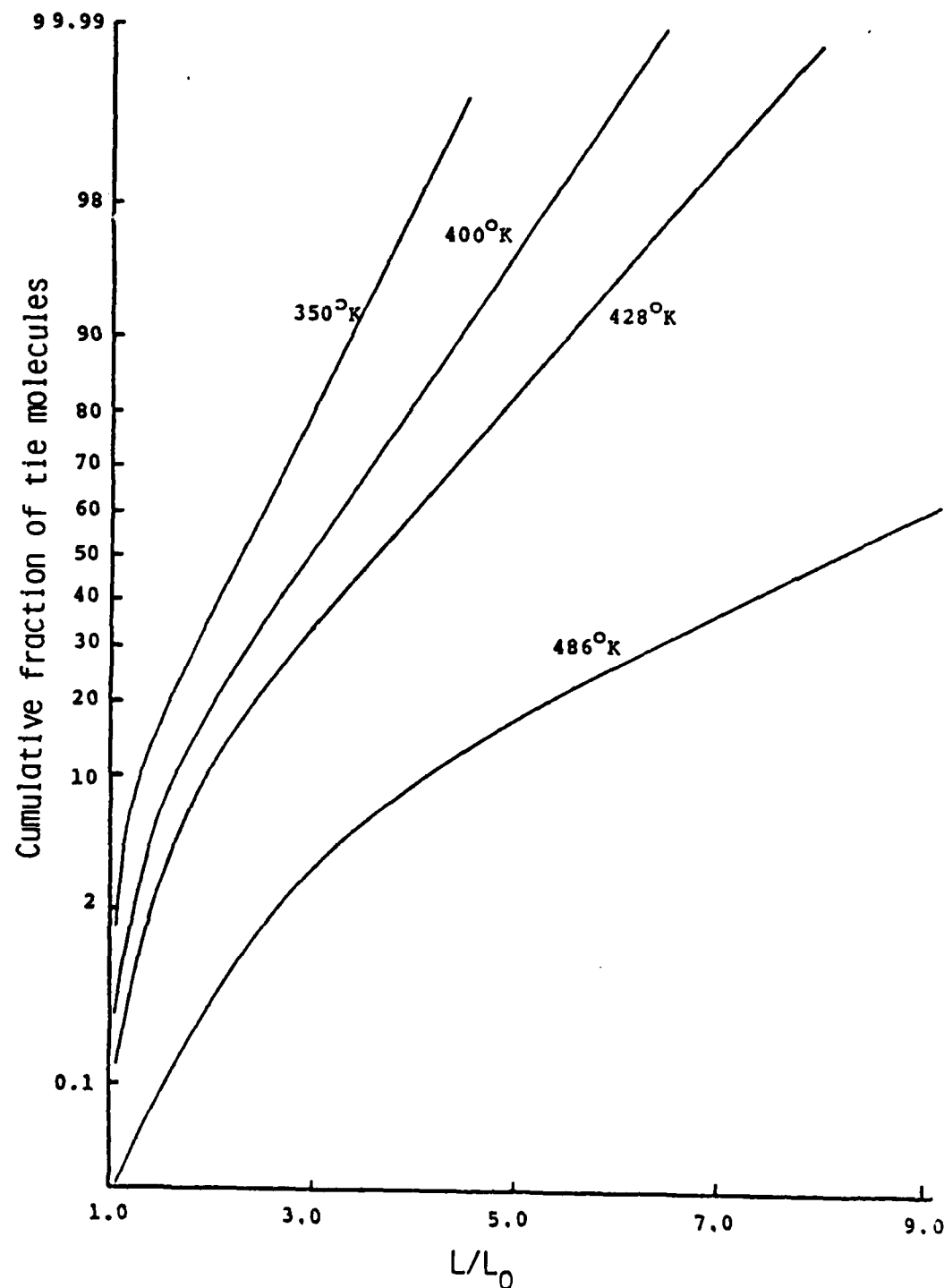


Figure 42: Cumulative fraction of tie molecules versus ratio of tie chain length to minimum tie chain length ( $L/L_0$ ).



#### 4.1.3 Critical Review

The model for calculation of the tie chain length distribution has been obtained on the minimization of free energy in a thermodynamic equilibrium situation. This might seem inappropriate since the characteristics of amorphous state are established during crystallization, a kinetic process.

Consider an amorphous polymer melt in equilibrium at certain temperature  $T_1$  is cooled down to another temperature  $T_2$  above the melting temperature. The chains in this case will start rearranging themselves as soon as the melt is cooled, towards a new thermodynamic equilibrium state of temperature  $T_2$ . Given enough time for chains to rearrange, the thermodynamic equilibrium configurations of chains at temperature  $T_2$  will be obtained; but now consider the other possibility that  $T_2$  is below melting temperature and enough time is not given for a complete rearrangement before the melt was quenched. The molecular state in which the solid will be locked is an equilibrium state between temperatures  $T_1$  and  $T_2$ . An exactly similar situation exists during crystallization where the chains in the amorphous region are striving toward thermodynamic equilibrium state at the temperature of the environment, but this rearrangement is impeded by crystallization. Therefore the thermodynamic equilibrium theory used to obtain the nature of amorphous state will only provide an approximation to the actual state of affairs. Keeping this in mind, the tie chain length distribution have also been calculated at temperatures about  $75^{\circ}\text{C}$  above and below the measured processing temperature. The crystallization kinetics in nylon 6 being slow, it is expected that the tie chain length distribution will be close to that calculated for the processing temperature, but almost certainly within the extremes of other temperatures for which the distributions are calculated and shown in Figures 41 and 42.

Looking back into the calculation of the tie chain length distribution, one observes absence of any consideration for the effects of drawing on the derived tie chain length distribution. Such effects will be small and will result in small increase in the concentration of the taut tie chains. Some increase in concentration of the interfibrillar tie molecules may also occur. These changes will be small as follows

from the cold drawing process of nylon 6, where a lamella may break up, but the amorphous material between the successive broken lamella is not terribly altered. This has been shown to be the case for nylon 6 fibers which are melt spun; the draw direction being the fiber direction as established during crystallization. The long period of these fibers does show a very small change on drawing (21). Thus the tie chains connecting adjacent crystalline blocks are not modified in any major way as a result of drawing. The exception is the formation of new interfibrillar tie molecules during drawing, and the calculated distribution is not applicable to this. Therefore the width of the tie chain length distribution in the drawn material will be approximately the same, as obtained from the model presented in this study.

#### 4.2 Calculation for Number of Tie Molecules

The calculation here for obtaining the number of tie molecules present per a gram of the nylon 6 material is derived on the basis of following assumptions and assertions:

- 1) The probability that any molecule present in the polymer can contribute to the formation of a tie chain is independent of the length of the molecule provided it is above a certain minimum required molecular length ( $L_{min}$ ). The minimum required molecular length will be the length of two crystalline blocks plus the length of an amorphous region.
- 2) The number of tie molecules resulting from a given polymer molecule is directly proportional to the length of the molecule.
- 3) The average length of the polymer molecule  $L$ , required to form a tie molecule is the length of a crystalline block  $L_c$  plus an average length for the tie molecule  $L_T$

$$L = L_c + L_T$$

where

$$I_T = \left[ \left\{ \sum_i L_T(i) * G(L(i)) \right\} \right] / \left[ \left\{ \sum_i G(L(i)) \right\} \right]$$

and  $G(L(i))$  is the density distribution function for the length of the tie molecule as obtained in the previous section.

4) The molecular chains that return to the same crystalline block (chain loops, switch board concept) or chain fold, represent molecules that do not cross over from one crystalline block to another and therefore do not contribute to the tie chain population. The reduced number of tie molecules obtained due to the formation of loops or chain folds can be taken into account by including a factor  $X$ . The factor  $X$  is the fraction of the chains in the crystalline block that contribute to formation of tie molecules. Note:  $w(i)$  is the fractional weight in grams of a molecular weight species MW(i) such that the total weight of the specimen under the chromatogram is one gram.  $N(i)$  is the number of molecules present of molecular weight MW(i) in one gram of the specimen.

5) Divide the molecular weight axis in Figure 28 into a certain number of segments, say  $M$  (100 in our case). The ordinate  $w(i)$  in Figure 28 can be changed to  $N(i)$  according to following manipulation:

$$N(i) = [w(i) * 6.023 \times 10^{23}] / MW(i)$$

6) Calculate the extended length  $L(i)$  of the molecule for the molecular weight segment of MW(i). The length  $L(i)$  is

$$L(i) = \{MW(i) * \text{Length (extended) of monomer}\} / \text{Molecular Weight of Monomer Unit}$$

For nylon 6,

$$L(i) = \{MW(i) * 8.62 \Lambda^0\} / 113.16$$

7) The total number of tie molecules resulting from a segment of molecules of molecular weight MW(i) is given by

AD-A092 241

MASSACHUSETTS INST OF TECH CAMBRIDGE DEPT OF MATERIALS ETC F/6 11/9  
MOLECULAR FRACTION BEHAVIOR IN ORIENTED POLYMERS. (U)

JUN 80 R K POPLI, D K ROYLANCE

DAA629-76-C-0044

ML

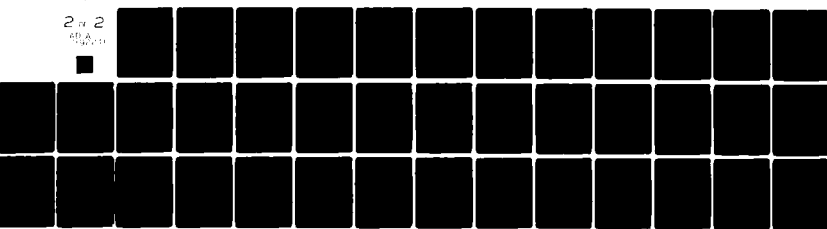
UNCLASSIFIED

ARO-13630.3-MSX

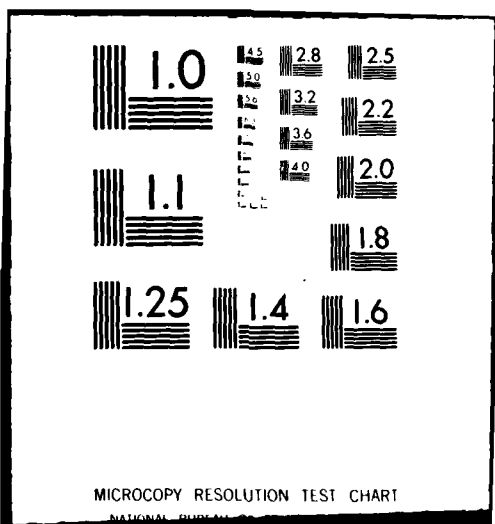
2 x 2

AR A

1981



END  
DATE  
FILED  
1-81  
DTIC



$$NT(i) = \{N(i) * L(i) * \chi\} / L$$

8) Calculate NT(i) for each segment for  $i = 1, 2, \dots, M$ .

The total number of tie molecules 'NT' is

$$NT = \sum_i NT(i)$$

The total number of tie molecules per gram has been found to be  $1 * 10^{20}$  per gram, which is in agreement with the generally expected value.

#### 4.3 Discussion

GPC measurements on nylon 6 show a bond scission ' $\beta$ ' of  $2.3 * 10^{18}/\text{cm}^3$ . This is in excellent agreement with  $\beta$  of  $3.3 * 10^{18}/\text{cm}^3$  measured by Crist (13) from decrease in the viscosity average molecular weight assuming random scission of chains and  $\bar{M}_w/\bar{M}_n = 2$  for nylon 6. These observations of GPC and viscometry are also in close agreement with the number of free radicals detected by ESR. The observed ratio of ' $\beta_{gpc}$ /free radicals' of approximately 5 very likely results from the decay of reactive free radical species, as suggested by Chapiro (60). The confirmation of these results by GPC is of significance since the results of viscometry and ESR are questionable due to the inherent uncertainties of the latter two techniques for such an analysis. The importance of an accurate value for  $\beta_{gpc}$  cannot be underestimated because to a large extent the acceptance of a fracture model has been based on its prediction of the bond scission per  $\text{cm}^3$ ; this being the most direct experimental evidence available at this time for fathoming the molecular nature of the fracture processes in highly drawn fibrous materials.

Zhurkov and Zakrevskii (24a, 24b) proposed a mechanism for submicroscopic crack nucleation from their studies of free radicals and of newly formed end groups. According to their observations, a single free radical undergoes secondary radical reactions to produce as many as 4000 bond scissions

before it decays. GPC observations of bond scission of  $2.3 \times 10^{18}$  per  $\text{cm}^3$  in nylon 6 and IR measurements of bond scission in fractured PE film of less than  $3 \times 10^{17}$  per  $\text{cm}^3$  cannot possibly be explained on the basis of Zhurkov-Zakrevskii mechanism. Viscometry data of Crist (13) and IR observations of De Vries (61) reinforce the observations made in this study. Therefore, the experimental observations of Zhurkov and his colleagues can only be attributed to some peculiar characteristics of their polyethylene specimens.

GPC observations of Figures 28 and 34 show that the higher molecular weight component is preferentially ruptured during fracture. The statistics of mechanically induced scission are therefore biased in favor of larger molecules. This would seem to follow logically from the consideration that a longer molecule generally has a greater probability of participating in the formation of a tie molecule. The positive and negative portions of Figure 34 have been summed over separately to obtain the number of molecules per gram that have ruptured and the ones that have formed. These numbers are  $1.35 \times 10^{17}$  and  $2.7 \times 10^{18}$  per gram respectively. The ratio of 20 (of number formed to those ruptured) means that a single long molecule, on an average, may be ruptured as many as 20 times. How is this achieved? It is generally believed that the tie molecules in the amorphous regions are the ones to rupture. Therefore, the observed behavior can only be explained if a long molecule were to form a large number of tie molecules. (Consider a molecule of molecular weight 500,000; the contour length of such a molecule is  $38000 \text{ \AA}^0$ . If only one tenth of the molecules in the crystalline block were to form tie molecules, one obtains 40 or so tie chains resulting from such a polymer molecule.) Such behavior would suggest a switch-board rather than a folded-chain model of the crystal morphology.

Comparison of the concentration or the number of molecules per gram as a function of molecular weight for virgin and fractured specimens of Figures 28 and 33 presents some interesting aspects regarding the role of different molecular weight components. In Figure 43, the fractional change in concentration (ratio of change in concentration at a given molecular weight to the concentration of virgin

specimen of that molecular weight) is plotted. This plot shows a maximum decrease in fractional concentration at molecular weight  $3 \times 10^5$ , but the fractional concentration increases from zero at molecular weight of  $5.5 \times 10^4$  to a maximum fractional increase of 0.24. The change in the number of molecules per gram at any molecular weight 'X', is resultant of the two effects of the amount added due to rupture of higher molecular weight 'Y' onto 'X', and the amount lost from rupture of 'X' into lower molecular weight species. It has not been possible to deconvolute these two effects to obtain an absolute conversion of each molecular weight species from its initial concentration. Such a deconvolution, if possible, will be helpful in providing the statistics of the scission of molecules in nylon 6.

Earlier mentioned observation of the preferential rupture of the high molecular weight molecules into a number of small segments was explained to suggest that a large molecule forms a great number of tie molecules. If the relative concentration of the high molecular weight component be increased, an increased number of tie molecules will be formed. Therefore, assuming fracture obeys the same statistics as before, a greater number of tie chain ruptures will be observed on fracture. This will slow down the crack propagation mode, thereby increasing the lifetime of the solid under stress. The greater number of tie molecules also implies a higher fracture strength and an increase in the total energy absorbed before macroscopic failure occurs.

This hypothesis can be checked from a comparison of the fracture behavior of two fibers of nylon 6 of similar morphology, with same number average molecular weight but different weight average molecular weights.

The plot of Figure 43 has a maximum in the fractional concentration decrease at a molecular weight of  $3 \times 10^5$ . The significance of this maximum, the molecular weight at which it occurs, and its role in determining the fracture properties is not understood at this time.

Amorphous Morphology: The mechanical behavior of drawn polymers is determined essentially by the nature of amorphous content and, in particular, the fraction of taut tie molecules (or, continued

crystallites through amorphous regions (62, 63, 64)). Peterlin (65) indicated a taut tie molecular fraction of 1 - 4 % derived from the elastic modulus and tensile strength, whereas etching of the polyethylene specimen with nitric acid provided for an amorphous tie chain content of 20 - 30 %. McCrum (66) estimated a concentration of only 0.25 % for tie chains (taut, apparently) to explain the anisotropy of the relaxation. Fischer (67) indicated about 1 % of the material in the cross-links. Ward (62) reports a maximum crystalline content of 0.6 for PE from the ratio of apparent lattice modulus to crystal modulus, implying that 40 % of the material in amorphous region is in disordered phase. The contribution of taut tie chains to the disordered phase in this case is not known. Nagou (63) has obtained from their experimental results on highly drawn polypropylene a concentration of taut tie molecules of approximately 2 % in a total concentration for the amorphous phase of 25 %.

A calculation performed by the author (details are given in Appendix III) for nylon 6 fiber specimens of 50 % crystallinity obtains the concentrations of chain loops (folds), chain ends, tie chains, and cilia. The results of this calculation are presented in Table 7. Some of the amorphous content of tie molecules might be accounted by interfibrillar tie molecules (69), connecting adjacent microfibrils or distant crystalline blocks within a microfibril. The contribution of the interfibrillar to the amorphous material has not been resolved. From Table 7, if the tie chain contribution of 0.254 gram were used up in obtaining the interfibrillar tie molecules (which are generally taut) and taut tie molecules only, the resulting modulus of the fiber based on Takayanagi's approach (71) will be much higher than the observed value. Therefore, one concludes that only a small fraction of the amorphous tie chains exist as taut tie chains and a major fraction comprises the tie molecules in non-extended conformations.

Non-extended tie molecules do not contribute significantly to the modulus of the fiber, except for the small entropic effect. However, void formation requires rupture of all the tie chains in that cross-section. As a result, all the non-extended tie chains in that cross-section are also ruptured. The rupture of the non-extended tie chains requires large local strains which will be present only in the

vicinity of a flaw.

Therefore, any fracture model must include the contribution of the non-extended tie chains to the number of molecules ruptured and to the formation of the microflaws.

A theoretical calculation described earlier gives the distribution of the tie chain lengths and the results of this calculation are presented in Figure 41. The cumulative distribution plot of Figure 42 gives an approximate value of 2 - 5 % for the fraction of taut tie molecules. This number is in good agreement with the fraction of taut tie molecules calculated by researchers from other studies discussed earlier.

A comparison of the tie chain length distribution of Lloyd - DeVries model with the theoretical distribution of the tie chain lengths calculated shows that the difference in the width of the two distributions along the axis (72) of ' $L/L_0$ ' is large. The Kausch's experimental results are between 1.07 and 1.18 whereas the theoretical model values vary from 1.03 through 6.0 or so. The initial portion of the cumulative tie chain length distribution from theory and the distribution of tie chain lengths of Kausch's observations are plotted in Figure 44. This plot suggests that the distribution of tie chain lengths obtained from experimental ESR observations of Kausch may have resulted partly from the taut tie molecules component of the theoretically calculated distribution. The apparent suggestion is that Lloyd - DeVries distribution does not represent the distribution of tie chain lengths but possibly reflects a contribution from the distribution of taut tie molecules only. This seems reasonable in light of the fact that Lloyd - DeVries distribution has been obtained from a histogram of the free radical obtained on fracture which is a result of the presence of taut tie molecules and the not-so-obvious effects of the variation of stress-intensity factor in the vicinity of the submicrocracks.

A major problem with the Lloyd - DeVries model is that the experimentally observed chain rupture of ( $5 \times 10^{17}$  per  $\text{cm}^3$  of free radicals from ESR)  $2.3 \times 10^{18}$  per  $\text{cm}^3$  from GPC is only a small fraction of the  $5 \times 10^{19} - 1 \times 10^{20}$  per  $\text{cm}^3$  of the tie molecules present in nylon 6. Another problem with Lloyd - DeVries model is the presence of inhomogeneities through submicrocrack formation which have been

observed by Zhurkov from SAXS of the loaded fibrous specimens of nylon, polyethylene, and other materials. Lloyd - DeVries model makes no provision for the formation of submicroscopic cracks. Notwithstanding the other drawbacks of Peterlin's model, submicroscopic crack formation follows directly as a result of the retraction of the microfibril ends. The formation of microcracks also enables a logical explanation for the rupture of only a small number of tie molecules. Lloyd-DeVries model can easily explain the observed stress-strain behavior, of Figure 45, if the number of tie chains experiencing the stress is taken to be about 20 times the number of free radicals observed (23).

A new approach for the formation of the microcracks in the fibrous morphology is suggested here:

The fibrous structure is assumed to consist of an almost continuous fibril of alternating crystalline and amorphous regions. The long period and the cross-section of the fibril is typically of the order of  $100 \text{ \AA}^0$  and  $(100 \text{ \AA}^0)^2$  respectively. The major question to be addressed is, what is the nature of the weak region where the submicrocracks can be initiated? Considering the amorphous regions, the number of tie chains are not the same in every amorphous block. An amorphous block of  $(100 \text{ \AA}^0)^2$  will have, on an average, about 50 tie chains or so, assuming a cross-section for the tie chain of  $20 \text{ \AA}^0$  and that only one-tenth of the chains in the crystalline lattice will form tie molecules. Thus the number of tie chains in the amorphous regions being statistically distributed, few of these regions will have a greater number of tie molecules than the average of 50, whereas some others will have a much smaller number of tie chains. The amorphous regions with a small number of tie chains are relatively weak and the stress experienced by the individual chains will be higher than for the chains in other amorphous regions. As a result, the tie chains in weak amorphous regions break and a submicrocrack is initiated. Comparing the experimentally observed submicrocrack density with the approximate number of amorphous regions present, it turns out that an upper limit for the amorphous regions classified as weak will be one out of every hundred amorphous regions present.

The main features of this model, which is similar to Lloyd - DeVries model in many respects, are:

- (1). Consists of alternating regions of crystalline and amorphous blocks.
- (2). In loading, the tie molecules and, in particular, the taut tie molecules in almost every amorphous region experience the stress.
- (3). The stress experienced by the tie molecules in the weaker regions, where fewer tie chains are available, is considerably higher.
- (4). These weaker regions and sometimes the adjacent amorphous regions open up as microcracks due to the rupture of the tie chains.
- (5). All the tie chains in the weaker regions, their neighborhoods that open up as microcracks, and some of the taut chains in other amorphous regions are ruptured on loading the specimen to failure.
- (6). Macroscopic fracture occurs when accumulation of a large number of microcracks at a site produces a large critical crack.

This model does not require the rupture of all the tie chains present as is the case with Lloyd - DeVries model. Further, many more taut tie chains than those ruptured experience the stress. (It is not possible to calculate this number presently.) Therefore, the discrepancy of a ratio of 5 between the number of tie chains needed to obtain the stress-strain behavior based on Lloyd - DeVries model as shown in Figure 45 and the number of tie chains ruptured can possibly explained.

The amorphous regions in the fibrous structure are strained commensurate with the modulus of the amorphous blocks, when stressed. The weak amorphous regions, as mentioned above, will experience large local strains. Therefore, all the tie chains in these regions will break and the amorphous region will open up as a submicrocrack. The formation of submicrocracks will cause redistribution of the applied load. The amorphous material in the immediate vicinity of the microcrack will be under higher stress due to the redistribution of load and the stress intensity concentration effect in front of a crack tip. As a result, some of the chains (particularly, the extended tie chains) in the neighborhood of the submicrocracks are also ruptured. The propagation of cracks in these neighboring regions will be to

some extent inhibited by presence of other crystalline and strong amorphous blocks. The strong intermolecular hydrogen bonding between fibrils and molecules of nylon 6 prevents any major slippage of fibrils past each other. Therefore, every (almost) region will be under stress and some of the taut tie molecules will be close to their breaking stress.

Within experimental error of observation, the stress-strain behavior of the fibers loaded to a stress below the fracture stress is unchanged from the first cycle to the second cycle of loading. The modulus of the fibers is believed to be governed by the taut chain molecules present. Therefore, a comparison of the stress-strain behavior between the first and the second cycle suggests that the concentration of taut tie chain molecules is practically unchanged in loading of fibers. The majority of the broken chains will be formed in the weak regions and their vicinity. Only a very small fraction of the taut tie chains in all the remaining amorphous regions are expected to break.

This is further verified from observations of no additional chain rupture during the second load cycle. This follows from the consideration that all the weak regions, their neighborhoods, and the tie molecules present in these regions and few of the taut tie chains in other amorphous blocks have been ruptured in the first loading cycle. During the second cycle, these regions open up without any additional chain rupture; some of the taut tie chains may be close to their breaking stress and a few may break, but their number is very small. If the highest load in the second cycle is applied for a long time, additional bond rupture due to breaking of taut tie chains or further propagation of the defects may be seen. The breakage of a large number of taut tie chains will be expected to result in lower modulus.

Two halves of the broken fiber have the same fracture strength as the original fiber. It seems likely that the breakage concentration of the tie chains of the order of 2 % or so of all the amorphous chain segments does not weaken the polymer network decisively. Subsequent loading of the fiber does not produce additional detectable chain scission (as observed from ESR); but a small chain scission will be expected on the basis of the morphology of the fibrous structure. In fatigue where the damage

accumulates over a large number of repeated loadings, a definitive decrease in the fracture strength of the fiber is observed.

Table 7.

Crystalline Contribution = 50.0%

Contributions of different amorphous components to the total amount:

<u>Chain Ends</u>	<u>Chain Loops(folds)</u>	<u>C111a</u>	<u>Tie Chain</u>
2.6%	22.0 (5.5)%	0.0%	25.4 (41.9)%

Figure 43 : Fractional change in concentration vs.  
 $\log_{10}$  (molecular weight).

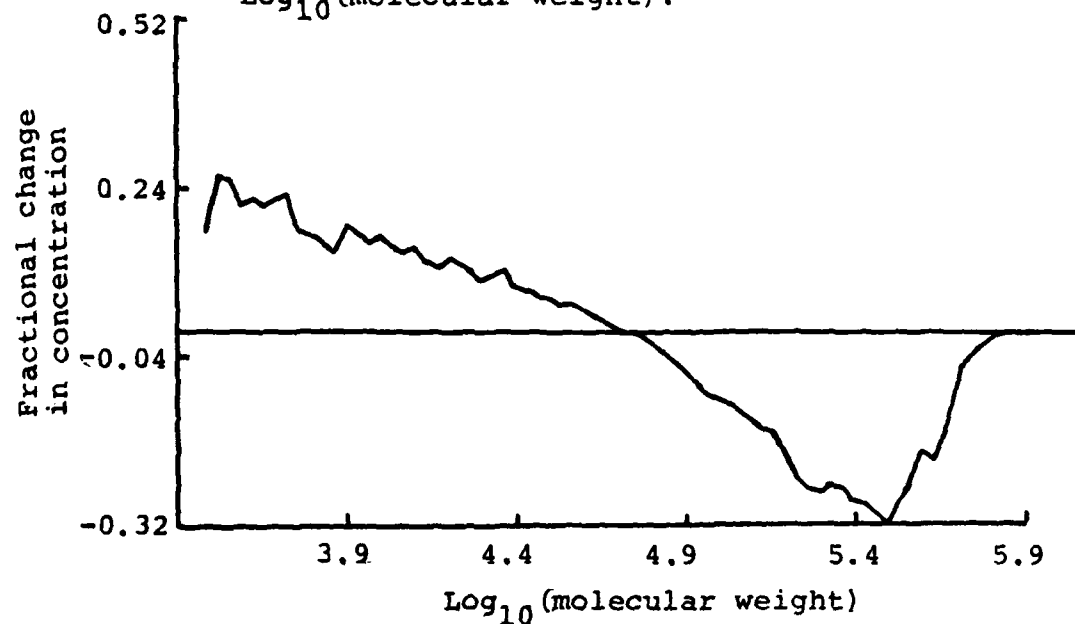
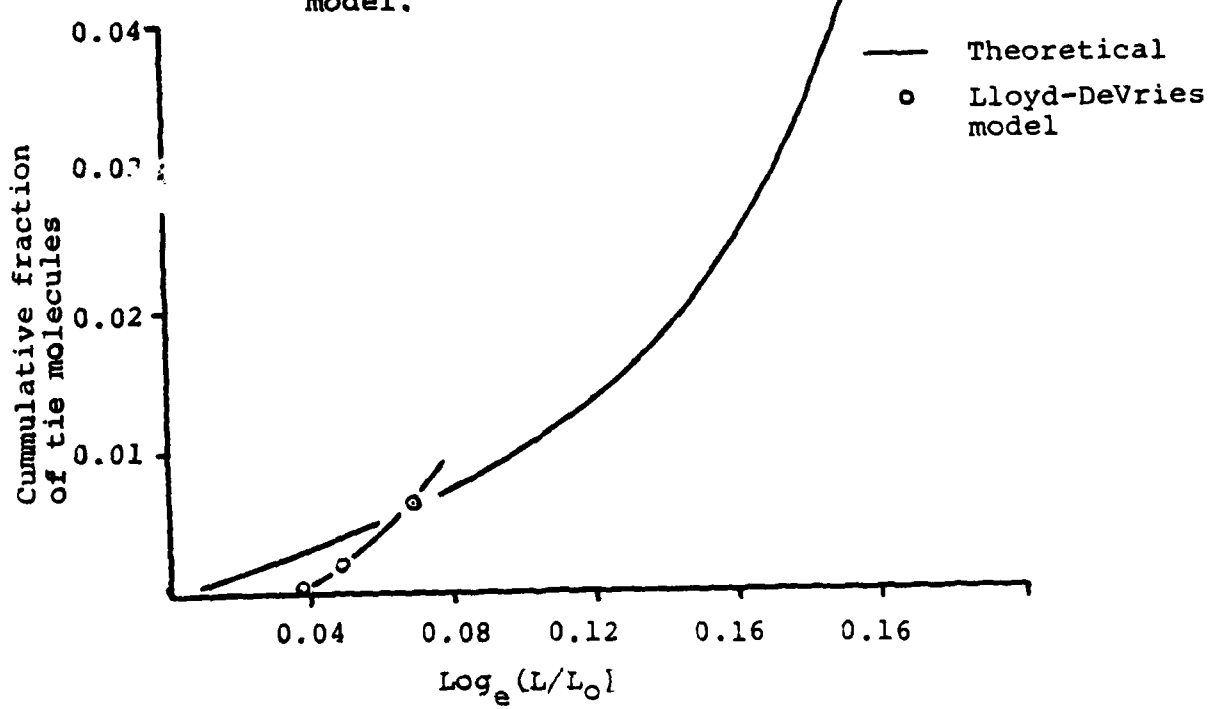


Figure 44 : Comparison of the cumulative tie chain distribution from Lloyd-DeVries model and theoretical model.



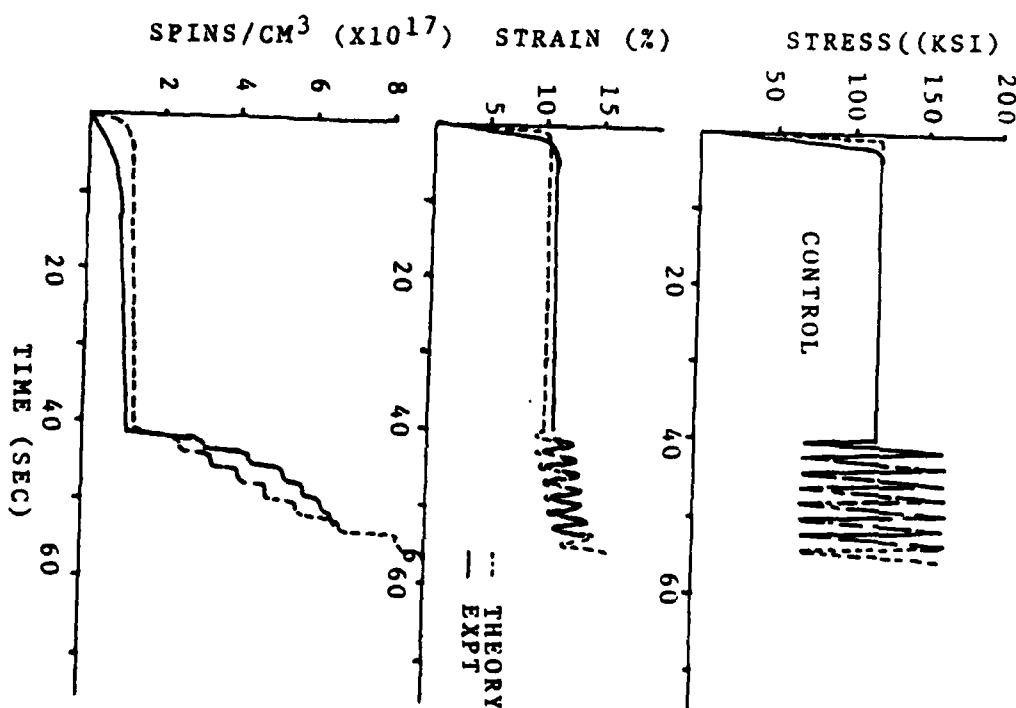
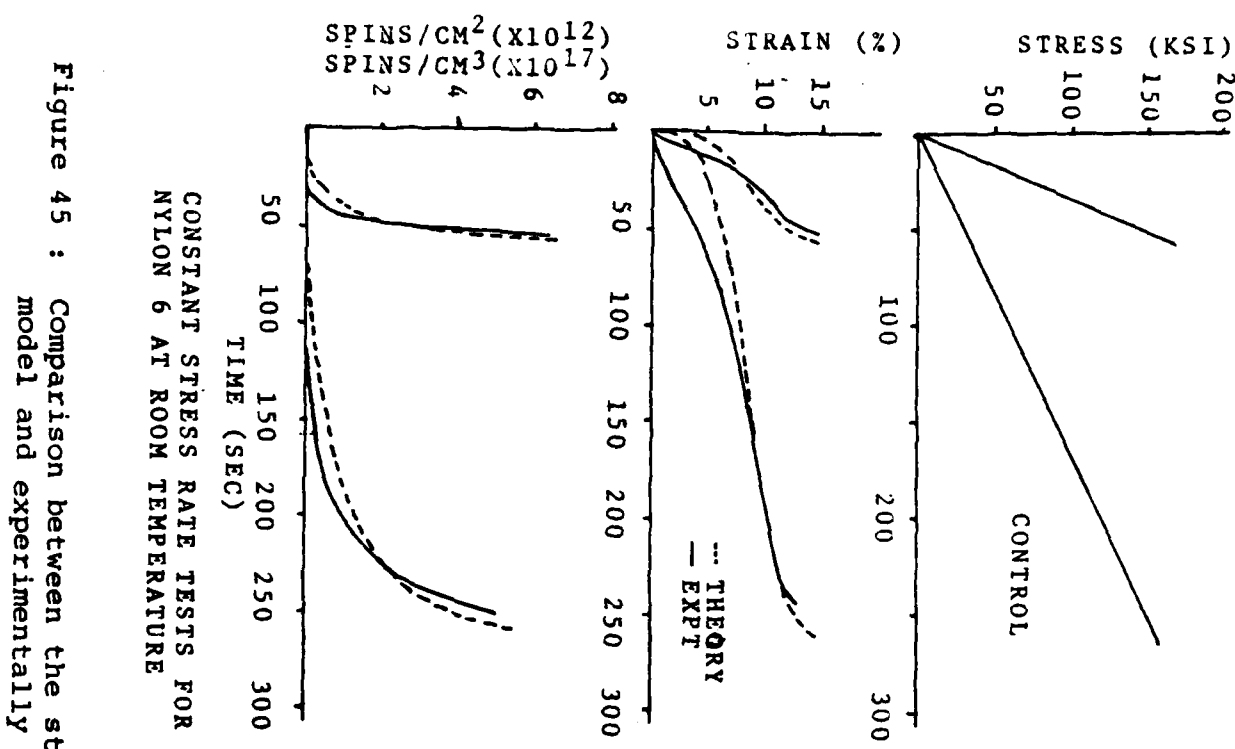


Figure 45 : Comparison between the stress-strain behaviour predicted by Lloyd-DeVries model and experimentally measured.

## Appendix I - Calculation for P(N,r)

$$P(N,r) = \sum_{m=-\infty}^{\infty} \{W(N-1, r(m)) - W(N-1, r'(m))\} * a^3$$

$$P(N,r)/a^3 = \sum_{m=-\infty}^{\infty} W(N-1, (x_A - \lambda - 2md, y, z)) - W(N-1, (x_A + \lambda - 2md, y, z))$$

Let  $P'(N,r) = P(N,r)/a^3$

Assuming that gaussian statistics are appropriate for the description of tie chains in the amorphous regions of the semi-crystalline polymer,

$$W(r) = \{3/2\pi \langle r^2 \rangle_0\}^{3/2} * \exp \{-3r^2/2 \langle r^2 \rangle_0\}$$

where  $r^2 = x^2 + y^2 + z^2$

For a gaussian chain of N - 1 units,

$$\langle r^2 \rangle_0 = (N-1)a^2$$

$$P'(N,r) = \{3/2\pi \langle r^2 \rangle_0\}^{3/2} \sum_{m=-\infty}^{\infty} [\exp \{-3((x_A - \lambda - 2md)^2 + y^2 + z^2)/2 \langle r^2 \rangle_0\}$$

$$- \exp \{-3((x_A + \lambda - 2md)^2 + y^2 + z^2)/2 \langle r^2 \rangle_0\}]$$

Let RSQR =  $y^2 + z^2$

$$P'(N,r) = \{3/2\pi \langle r^2 \rangle_0\}^{3/2} * \exp (-3RSQR/2 \langle r^2 \rangle_0) *$$

$$\sum_{m=-\infty}^{\infty} [\exp \{-3((x_A - 2md)^2 + \lambda^2 + 4md\lambda - 2x_A\lambda)/2 \langle r^2 \rangle_0\}$$

$$- \exp \{-3((x_A + 2md)^2 + \lambda^2 + 4md\lambda + 2x_A\lambda)/2 \langle r^2 \rangle_0\}]$$

Then,

$$P'(N,r) = \{3/2\pi \langle r^2 \rangle_0\}^{3/2} * \exp (-3RSQR/2 \langle r^2 \rangle_0) * \exp (-3\lambda^2/2 \langle r^2 \rangle_0) *$$

$$\sum_{m=-\infty}^{\infty} \exp \{-3((x_A - 2md)^2/2 \langle r^2 \rangle_0\} * [\exp \{(3/2)*2\lambda(x_A - 2md)/\langle r^2 \rangle_0\}$$

$$- \exp\{- (3/2) * 2\lambda(x_A - 2md)/\langle r^2 \rangle_0\}]$$

$$\begin{aligned} P(N,r) &= \{3/2 \pi \langle r^2 \rangle_0\} * \exp(-3(RSQR + \lambda^2)/2\langle r^2 \rangle_0) * \\ &\quad \sum_{m=-\infty}^{\infty} \exp\{-3(x_A - 2md)^2/2\langle r^2 \rangle_0\} * 2\sinh\{3\lambda(x_A - 2md)/\langle r^2 \rangle_0\} \\ &= 2C \sum_{m=-\infty}^{\infty} \exp\{-3(x_A - 2md)^2/2\langle r^2 \rangle_0\} * \sinh\{3\lambda(x_A - 2md)/\langle r^2 \rangle_0\} \end{aligned}$$

where  $C = \{3/2 \pi \langle r^2 \rangle_0\}^{3/2} * \exp(-3(RSQR + \lambda^2)/2\langle r^2 \rangle_0)$

Consider the summation

$$\sum_{m=-\infty}^{\infty} = \sum_{m=-\infty}^{-1} + P(N,r)|_{m=0} + \sum_{m=1}^{\infty}$$

Also consider

$$\sum_{m=1}^{-1} \exp\{-3(x_A - 2md)^2/2\langle r^2 \rangle_0\} * \sinh\{3\lambda(x_A - 2md)/\langle r^2 \rangle_0\}$$

Changing the variable  $m = -n$ ,

$$\begin{aligned} \sum_{m=-\infty}^{-1} &= \sum_{n=\infty}^1 \exp\{-3(x_A + 2nd)^2/2\langle r^2 \rangle_0\} * \sinh\{3\lambda(x_A + 2nd)/\langle r^2 \rangle_0\} \\ &= - \sum_{m=1}^{\infty} \exp\{-3(x_A + 2nd)^2/2\langle r^2 \rangle_0\} * \sinh\{3\lambda(x_A + 2nd)/\langle r^2 \rangle_0\} \end{aligned}$$

$$\text{Also, } P(N,r)|_{m=0} = 2C \exp(-3x_A^2/2\langle r^2 \rangle_0) * \sinh(3\lambda x_A/\langle r^2 \rangle_0)$$

Therefore,

$$\begin{aligned} P(N,r) &= 2C \{\exp(-3x_A^2/2\langle r^2 \rangle_0) * \sinh(3\lambda x_A/\langle r^2 \rangle_0)\} \\ &\quad + \sum_{m=1}^{\infty} [\exp\{-3(x_A - 2md)^2/2\langle r^2 \rangle_0\} * \sinh\{3\lambda(x_A - 2md)/\langle r^2 \rangle_0\}] \\ &\quad - \exp\{-3(x_A + 2nd)^2/2\langle r^2 \rangle_0\} * \sinh\{3\lambda(x_A + 2nd)/\langle r^2 \rangle_0\}] \end{aligned}$$

For the molecules,  $x_A = d \cdot \lambda$ .

Thus, for the molecules, the previous equation is

$$P(N,r) = 2C \left\{ \exp \left( -3(d-\lambda)^2 / 2\langle r^2 \rangle_0 \right) * \sinh \left( 3\lambda(d-\lambda) / \langle r^2 \rangle_0 \right) \right. \\ \left. + \sum_{m=1}^{\infty} \left[ \exp \left\{ -3(-\lambda + (1-2m)d)^2 / 2\langle r^2 \rangle_0 \right\} * \sinh \left\{ 3\lambda(-\lambda + (1-2m)d) / \langle r^2 \rangle_0 \right\} \right. \right. \\ \left. \left. - \exp \left\{ -3((1+2m)d-\lambda)^2 / 2\langle r^2 \rangle_0 \right\} * \sinh \left\{ 3\lambda((1+2m)d-\lambda) / \langle r^2 \rangle_0 \right\} \right] \right\}$$

Considering the summation in above equation explicitly,

$$\sum_{m=1}^{\infty} = \exp \left\{ -3(\lambda+d)^2 / 2\langle r^2 \rangle_0 \right\} * \sinh \left\{ -3\lambda(\lambda+d) / \langle r^2 \rangle_0 \right\} \\ - \exp \left\{ -3(3d-\lambda)^2 / 2\langle r^2 \rangle_0 \right\} * \sinh \left\{ 3\lambda(3d-\lambda) / \langle r^2 \rangle_0 \right\} \\ + \exp \left\{ -3(3d+\lambda)^2 / 2\langle r^2 \rangle_0 \right\} * \sinh \left\{ -3\lambda(d+\lambda) / \langle r^2 \rangle_0 \right\} \\ - \exp \left\{ -3(5d-\lambda)^2 / 2\langle r^2 \rangle_0 \right\} * \sinh \left\{ 3\lambda(5d-\lambda) / \langle r^2 \rangle_0 \right\} \\ + \dots \dots \dots$$

In the summation the zeroth and first order terms are significant and others drop out very rapidly with increasing  $m$ . Thus, to a first order approximation,

$$P'(N,r) = 2C \left\{ \left[ \exp \left( -3(d-\lambda)^2 / 2\langle r^2 \rangle_0 \right) * \sinh \left( 3\lambda(d-\lambda) / \langle r^2 \rangle_0 \right) \right] \right. \\ \left. + \exp \left\{ -3(\lambda+d)^2 / 2\langle r^2 \rangle_0 \right\} * \sinh \left\{ -3\lambda(\lambda+d) / \langle r^2 \rangle_0 \right\} \right]$$

$$\text{Or, } P'(N,r) = 2 \left\{ 3/2\pi \langle r^2 \rangle_0 \right\}^{3/2} * \exp \left( -3(RSQR + \lambda^2) / 2\langle r^2 \rangle_0 \right) * \left[ \left\{ \exp \left( -3(d-\lambda)^2 / 2\langle r^2 \rangle_0 \right) * \right. \right. \\ \left. \left. \sinh \left( 3\lambda(d-\lambda) / \langle r^2 \rangle_0 \right) \right\} - \exp \left\{ -3(\lambda+d)^2 / 2\langle r^2 \rangle_0 \right\} * \right. \\ \left. \sinh \left\{ 3\lambda(\lambda+d) / \langle r^2 \rangle_0 \right\} \right]$$

Also, substituting  $\langle r^2 \rangle_0 = (N-1)a^2$

$$P(N,r) = P'(N,r)a^3 = 2 \left\{ 3/2\pi(N-1) \right\}^{3/2} * \exp \left( -3(RSQR + \lambda^2) / 2(N-1)a^2 \right) *$$

$$\begin{aligned} & \left[ \left\{ \exp \left( -3(d-\lambda)^2/2(N-1)a^2 \right) * \sinh \left( 3\lambda(d-\lambda)/(N-1)a^2 \right) \right\} \right. \\ & \quad \left. - \exp \left\{ -3(\lambda+d)^2/2(N-1)a^2 \right\} * \sinh \left\{ 3\lambda(\lambda+d)/(N-1)a^2 \right\} \right] \end{aligned}$$

Taking logarithms,

$$\begin{aligned} \log_e P(N,r) = & \log_e 2 + 3/2 \log_e \{3/2\pi(N-1)\} - 3(RSQR + \lambda^2)/2(N-1)a^2 \\ & + \log_e \left[ \left\{ \exp \left( -3(d-\lambda)^2/2(N-1)a^2 \right) * \sinh \left( 3\lambda(d-\lambda)/(N-1)a^2 \right) \right\} \right. \\ & \quad \left. - \exp \left\{ -3(\lambda+d)^2/2(N-1)a^2 \right\} * \sinh \left\{ 3\lambda(\lambda+d)/(N-1)a^2 \right\} \right] \end{aligned}$$

Using  $\lambda = 2a$ ,

$$\begin{aligned} \log_e P(N,r) = & -0.4158 - 1.5 \log_e (N-1) - 1.5(RSQR + 4a^2)/(N-1)a^2 \\ & + \log_e \left[ \exp \left( -3(d-2a)^2/2(N-1)a^2 \right) * \sinh \left( 6(d-2a)/(N-1)a \right) \right. \\ & \quad \left. - \exp \left( -3(d+2a)^2/2(N-1)a^2 \right) * \sinh \left( 6(d+2a)/(N-1)a \right) \right] \end{aligned}$$

## Appendix II • Calculation for X

Crystallinity = Z (fraction)

Length of crystalline block =  $L_c$

Average length of tie molecule =  $L_A$

Average length of loop or fold =  $L_f$

Consider 1 gm. of the polymer. Then Z gm. is the weight of crystalline component.

Total number of crystalline chains per gram = N, say.

$$\text{Then, } Z = N \cdot L_c \cdot w \quad (40)$$

where w is the weight of unit length ( $\text{\AA}^0$ ) of the polymer chain.

### Amorphous Region:

$$L_A \cdot w \cdot N \cdot X + L_f \cdot w \cdot N \cdot (1 - X) = 1 \cdot Z$$

$$L_A \cdot X + L_f \cdot L_f X = (1 - Z)/wN$$

$$\text{From equation (40), } wN = Z/L_c$$

$$\text{Therefore, } (L_A + L_f)X = (1 - Z) \cdot L_c / Z \cdot L_f$$

$$\text{i.e., } X = \{(1 - Z)(L_c + L_f)\} / Z(L_A + L_f)$$

### Choice of Parameter for 'X' calculation:

Crystallinity Z = 0.500

$$L_c = 60 \text{\AA}^0$$

$$L_A = 120 \text{\AA}^0$$

$$L_f = q$$

Then,

$$X = \{(0.5/0.5) * (60 - q)\} / (120 - q) = (60 - q) / (120 - q)$$

Since chain fold length  $q$  is only a few  $\text{\AA}^0$ , much less than  $100 \text{\AA}^0$ ,

$$X = 60/120 = 0.5$$

If instead of folds, chain loops are present, a value (expected) for average loop length on the higher side will be, say,  $30 \text{\AA}^0$ . Then,

$$X = (60 - 30) / (120 - 30) = 0.33$$

Therefore, a value between 0.33 and 0.5 for  $X$  would be a good approximation.

### Appendix III - Calculation of Amorphous Components

Length of nylon 6 repeat unit =  $8.64 \text{ \AA}^0$

Mass of nylon 6 repeat unit = 113 gm./mole

Therefore, mass of nylon 6 repeat unit per  $\text{\AA}^0$  of length

$$= 113/(8.64 \times 6.0225 \times 10^{23})$$

$$= 2.17 \times 10^{-23} \text{ gm./\AA}^0$$

Crystallinity of nylon 6 (density measurement) = 50.0 %

Therefore, mass of amorphous component per gram of nylon 6 specimen = 0.50 gm.

#### Chain End Contribution:

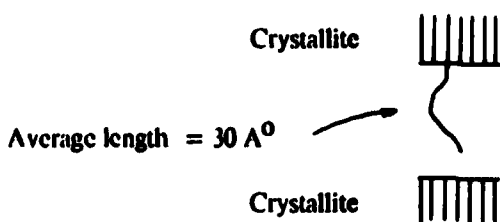
Number average molecular weight of nylon 6 = 30,000.

Number of chain ends per gm. of material =  $(2 \times 6.023 \times 10^{23})/30,000$

$$= 4.02 \times 10^{19}/\text{gm.}$$

The thickness of the amorphous region in nylon 6 has been determined experimentally as  $30 \text{ \AA}^0$ .

As an approximation, assume the average length for a loose chain in the amorphous region with chain end (as shown in the figure below) to be  $30 \text{ \AA}^0$ .



Total mass due to chain ends/gm. of nylon 6 =  $4.02 \times 10^{19} \times 30 \times 2.17 \times 10^{-23}$

$$= 2.62 \times 10^{-2} \text{ gm./gm. of nylon}$$

#### Chain Loop (Fold) Contribution:

From dimensions for the crystal structure (58, 59) of nylon 6, the average cross-section of a chain in the crystalline region is

$$= 19.1 \text{ } \text{\AA}^2$$

Long period of nylon 6 specimen fiber =  $90 \text{ } \text{\AA}$

Number of crystallite chains/gm. of the material =  $1/(19.1 \times 90 \times 10^{-24}) = 5.8 \times 10^{20}/\text{gm.}$

It takes two crystallite ends to form a tie molecule or chain loop (fold), but each chain has two ends.

Therefore, one crystallite chain forms a tie molecule or chain loop (fold).

Number of tie molecules and chain loops (folds)/gm. of nylon 6

$$= (\text{Number of crystallite chains/gm.} \cdot (\text{Number of chain ends/2}))$$

$$= 5.8 \times 10^{20} \cdot 2.01 \times 10^{19}$$

$$= 5.6 \times 10^{20}/\text{gm. of nylon 6}$$

Estimates (25, 28) for ratio of tie chains to crystallite units present have varied from  $1/10$  to  $1/3$  or even  $1/2$  as in the calculation in Appendix II. A value of  $1/10$  will be used, which might overestimate contribution of chain loops (folds) to the amorphous region.

$$\text{Number of chain loops (folds)/gm. of nylon 6} = 5.6 \times 10^{20} \times 9/10 = 5.04 \times 10^{20}/\text{gm. of nylon 6.}$$

The average length for a chain loop (fold) in an amorphous region of thickness  $30 \text{ } \text{\AA}$  may be taken as, on a higher side, as  $20 \text{ } \text{\AA}$  ( $5 \text{ } \text{\AA}$ ).

Thus, mass of chain loops (folds) per gm. of nylon 6

$$= (5.0 \times 10^{20}/\text{gm. of nylon 6}) \cdot (2.17 \times 10^{-23} \text{ gm./}\text{\AA}^3) \cdot 20 \text{ } \text{\AA}^3 (\text{or, } 5 \text{ } \text{\AA}^3)$$

$$= 0.22 (0.055) \text{ gm./gm. of nylon}$$

Thus a higher estimate for mass of chain loops (folds) will be  $0.22$  ( $0.055$ ) gm. per gm. of nylon 6 material.

#### Cilia Contribution:

GPC analysis of nylon 6 specimen did not indicate presence of any low molecular weight additive or any other species. The lowest molecular weight concentration seen in the main molecular weight distribution was about 2000. This will be incorporated into the crystalline lamella formed during crystallization. Therefore, we do not expect any substantial contribution from cilia to the amorphous region. In light of this observation and the lack of any other definite information in this regard, this contribution will be assumed to be zero.

**Tie Chain Contribution:**

Since the amorphous region consists of tie chains, cilia, chain loops (folds), and loose chain ends, the contribution due to tie chains will be the difference between the amorphous material present and the sum of contributions due to cilia, chain loops (folds) and chain ends.

Tie chain contribution/gm. of nylon 6

$$= 0.500 - 0.22 - 0.0 - 0.026$$

$$= 0.254 \text{ gm./gm. of nylon 6}$$

Thus tie chains contribute substantially to the amorphous region.

On this basis, one can also estimate the average tie chain length, assuming a concentration for tie molecules at  $1*10^{20}$  per gm. of nylon 6 material.

$$\begin{aligned} \text{Average tie chain length} &= (0.254 \text{ gm./gm. of nylon 6}) * (\Lambda^0 / 2.17 * 10^{-23} \text{ gm.}) * (gm. of nylon \\ &6 / 1 * 10^{20}) \\ &= 117 \Lambda^0 \end{aligned}$$

## Appendix IV - GPC Calibration

GPC is a polymer fractionation technique which depends upon molecular size in solution. Very large molecules will have sizes in solution greater than the size of the gel pores and will be confined to solvent between the particles. The small molecules have access to solvent both inside and outside the particles and will be retarded in their progress through a column.

From an analytical GPC fractionation one seeks information on molecular weight distribution (cumulative and differential) as a function of molecular weight M. These normalized distributions are:

$$W(M) = dC(M)/dM = (dC(V)/dV) * (dV/d \log_e M) * (d \log_e M/dM)$$

where  $dC(V)/dV = h(V)$  is the ordinate of chromatogram. For the calculation of  $W(M)$  one needs to know the relationship

$$\log_e M = f(V) \quad (41)$$

which is dependent on polymer type, its structure, and interaction with the solvent.

The calibration procedure consists of obtaining the relationship of equation (41) experimentally or theoretically for various polymer and solvent combinations.

These calibration procedures can be divided into two major classes:

- (1). Direct calibration: This procedure requires fractions of known molecular weight for the polymer under analysis.
- (2). Indirect calibration: This does not require narrow fractions of polymer under analysis, but needs a relation between solute size in solution and molecular weight, assuming that molecular size in solution is the controlling separation parameter.

**Direct Method:** If fractions with  $\bar{M}_w/\bar{M}_n < 1.1$  are available for the polymer under consideration, then gel permeation chromatograms are obtained for each of the fractions in a solvent for the given

system. From the chromatograms, elution volume (the peak retention volume) for the different molecular weight fractions are obtained and from a knowledge of the molecular weight of the corresponding fraction, a plot of  $\log_e M$  against elution volume  $V$  is made. Generally, a linear plot for a large-molecular-weight range described by the following equation is obtained:

$$\log_e M = a - bV$$

This calibration plot can be used in conjunction with the gel permeation chromatogram of the unknown polymer to find  $W(M)$ .

Narrow calibration standards for polystyrene are the only ones available commercially. For other polymers well-characterized, narrow molecular weight distribution fractions are exception rather than the rule. Also, in the few cases where available, it does not cover a wide elution volume range.

Universal Calibration: Calibration curve ( $\log_e M$  versus  $V$ ) obtained from direct methods for narrow molecular weight polystyrene samples cannot be expected to hold for other polymers, particularly if the material under consideration is structurally different.

It is therefore desirable to find a way of transforming a primary calibration curve (as obtained for PS) in such a manner that it can be used with structurally different polymers. One such approach is commonly known as 'Universal Calibration'. These methods are based on the assumption that GPC separation is controlled by molecular size parameters that relate to the viscosity of dilute solution of these polymers. The suggested parameters are hydrodynamic volume  $V$ , unperturbed radius of the molecule, and size of the molecule in solution. The equations and parameters plotted are as in Table 8. These calibration parameters differ only in their response to variations in solvent power.

The elution volume  $V_e$  in GPC is directly proportional to these parameters. Thus, validity of these different approaches can be confirmed by plotting  $[M]M$ ,  $[\eta]M/\Phi(c)$ , or  $\langle L_o^2 \rangle^{1/2}$  against elution volume for a wide range of flexible, random coil polymers (linear or branched) in good solvents.

At low molecular weights, the gaussian distribution of chain lengths as used in the above-mentioned equations is not valid. Therefore, wide variation from these relations may be expected. One is generally interested in relative values for two polymers, so the deviations may not be as striking as they sound.

Using the universal calibration parameters, one obtains from different equations the following expression (for a given solution volume):

$$\log_e \{[\eta]_p M_p\} = \log_e \{[\eta]_{ps} M_{ps}\}$$

$$\text{or, } \log_e \{[\eta]_p M_p / \phi_p(\epsilon)\} = \log_e \{[\eta]_{ps} M_{ps} / \phi_{ps}(\epsilon)\}$$

A molecular weight calibration for a polymer P can thus be established by using molecular weight calibration for polystyrene, provided the dependence of  $[\eta]_{ps}$  and  $[\eta]_p$  on elution volume can be established. If the intrinsic viscosity of each of the fractions separated by an analytical GPC from the polymer being analyzed is determined with a viscometer,  $M_p$  can be obtained from the above equation.

Alternatively, the equations in the table above can be combined with the Mark-Houwink equation:

$$[\eta] = KM^a$$

to obtain the following set of relationships:

$$(1). \log_e M_p = \{(1 + \alpha_{ps})/(1 + \alpha_p)\} \log_e M_{ps} + \{(\log_e K_{ps}/K_p)/(1 + \alpha_p)\}$$

$$(2). \log_e M_p = \{(1 + \alpha_{ps})/(1 + \alpha_p)\} \log_e M_{ps} + \{(\log_e K_{ps}/K_p)/(1 + \alpha_p)\}$$

$$(3). \log_e M_p = \log_e M_{ps} + \log_e \{\langle L_o^2 \rangle / M\}_{ps} \{M / \langle L_o^2 \rangle\}_p$$

The relationships in Table 8 for calculating polymer molecular weight calibration curves from a basic polystyrene calibration are valid in good solvents. Relations (1), (2) and (3) above are derived by equating  $[\eta]M$ ,  $[\eta]M/\phi(\epsilon)$ , or  $\langle L_o^2 \rangle^{1/2}$  for two polymers at a given retention volume and combining with Mark-Houwink equation.

Mark-Houwink constants for certain polymer-solvent combinations are listed in the literature but must be used with caution since many of the reported constants are only valid over a short molecular weight range. Deviations at low and high molecular weight ends are particularly striking.

It has been generally observed that none of the universal calibration parameters give valid calibration predictions if the appropriate Mark-Houwink exponent is less than about 0.65.

Empirical Calibration: The calibration procedure used here is based on a linear relationship between  $\log_{10}(\text{molecular weight})$  and the elution volume  $V$ .

$$V = C_1 \cdot C_2 \log_{10}(M) \quad (42)$$

The constants  $C_1$  and  $C_2$  in the linear calibration of equation (42) are obtained using a number and weight average molecular weight of one broad molecular weight distribution of a standard nylon 6 specimen. The constants  $C_1$  and  $C_2$  are determined in a manner described below, using an iteration procedure on the computer.

From equation (42),

$$M = 10^{\{(C_1 \cdot V)/C_2\}} = 10^{(C_1/C_2)} \cdot 10^{(V/C_2)}$$

Or,  $M = C \cdot 10^{(-V/C_2)}$  (43)

where  $C = 10^{(C_1/C_2)}$

Number average and weight average molecular weights  $M_n$ ,  $M_w$  are, respectively,

$$\bar{M}_n = \frac{\sum w(i) / \{\sum w(i)/M(i)\}}{\sum w(i)} = W / \{\sum w(i) / C \cdot 10^{(-V(i)/C_2)}\}$$

$$\bar{M}_n = CW / \{\sum w(i) \cdot 10^{(V(i)/C_2)}\} \quad (44)$$

and  $W = \sum w(i)$

$$\bar{M}_w = \frac{\{\sum w(i)M(i)\} / \sum w(i)}{\sum w(i)} = \{\sum w(i) \cdot C \cdot 10^{(-V(i)/C_2)}\} / W$$

$$\bar{M}_w = (C/W) * \{\sum w(i) \cdot 10^{(-V(i)/C_2)}\} \quad (45)$$

Dividing equation (45) by (44)

$$\bar{M}_w/\bar{M}_n = \left\{ \sum_i w(i) * 10^{(-V(i)/C_2)} \right\} \left\{ \sum_i w(i) * 10^{(V(i)/C_2)} \right\} / W^2 \quad (46)$$

Define

$$A = \bar{M}_w/\bar{M}_n - \left\{ \sum_i w(i) * 10^{(-V(i)/C_2)} \right\} \left\{ \sum_i w(i) * 10^{(V(i)/C_2)} \right\} / W^2 \quad (47)$$

According to equation (46), the  $C_2$  value that describes the calibration of equation (42) will make 'A' zero. This is achieved using an iterative procedure on the computer. The outline for the procedure is to choose a representative ' $C_2$ ' value; 'A' is calculated according to equation (47). A new ' $C_2$ ' is chosen depending upon the sign and the magnitude of 'A'. 'A' is calculated, compared and new less than a certain minimum specified value is obtained. This ' $C_2$ ' is the constant for the equation (42). Once ' $C_2$ ' is known, equation (44) or (45) can be used to obtain 'C'. Then,

$$C_1 = C_2 \log_{10} C \quad (48)$$

For the nylon 6 fiber specimen the calibration equation obtained according to this procedure for  $\bar{M}_w$  and  $\bar{M}_n$  of 69,760 and 30,200 is

$$V_c = 52.52 - 4.75 \log_{10}(M) \quad (49)$$

Equation (49) has been used to calculate the MWDs of nylon 6 in this study.

Table 8.

	Equation	Plotted	Variables
Einstein - Simha	$[\eta] = \frac{\phi V_h}{M}$	$V_h$	$[\eta] M$
Flory - Fox	$[\eta] = \frac{\Phi_0 [ L^2 ]^{3/2}}{M}$	$[ L^2 ]^{1/2}$	$[\eta] M$
		$[ L_o^2 ]^{1/2}$	$[\eta] M$
Ptitsyn - Eisner	$[\eta] = \frac{\Phi(\epsilon) [ L^2 ]^{3/2}}{M}$	$[ L^2 ]^{1/2}$	$\frac{[\eta] M}{\Phi(\epsilon)}$

## Appendix V - Median Rank Plotting

Consider a parameter whose actual value is 'a'. Supposing N experimental measurements have been performed to estimate the parameter. These N measured values of the parameter will generally be scattered around the actual value 'a' according to a gaussian distribution  $f(z)$ , with a standard deviation determined by the experimental error.

$$f(z) = (1/2\pi)^{0.5} \exp\{-((z-a)/2\mu)^2\}$$

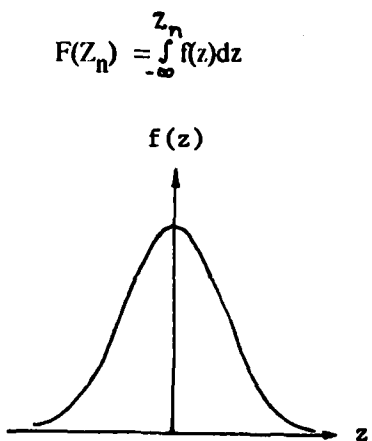


**Figure A**

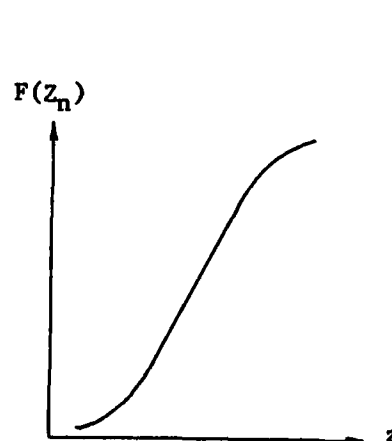


**Figure B**

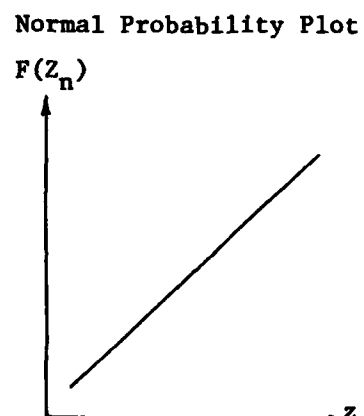


**Figure C**

Figures A and B are plots of function  $f(z)$  and the cumulative function  $F(z)$  on a linear plot. Figure C is a plot of the cumulative function  $F(z)$  on a normal probability function paper. The characteristics of the latter plot are such that if  $f(z)$  is gaussian,  $F(z)$  will be a straight line plot on the normal probability function paper.

In an actual analysis a finite number of data points are available. The data are processed through following steps to obtain the median rank plot:

1. Rank the N measured data points  $z(i)$  in order of increasing magnitude, i.e., rank  $z(i)$  such that

$$z(1) < z(2) < z(3) < \dots < z(N)$$

2. F(z) axis: Assign  $F(z(i))$  according to the following equation

$$F(z(i)) = (100/2N) + (100/N)*(i - 1)$$

for  $i = 1, 2, \dots, N$ .

For example, for  $N = 5$

z	$F(z)$
---	--------

z(1)	10
------	----

z(2)	30
------	----

z(3)	50
------	----

z(4)	70
------	----

z(5)	90
------	----

#### t-statistics test:

The statistical test compares two similar experimentally measured parameters and gives a measure of the probability that the two observed parameters have the same value.

t-statistics test starts with a hypothesis that the difference between the 'actual mean value', say  $U_1$  and  $U_2$  of two parameters under consideration is zero, i.e.,

$$\text{Hypothesis: } H_0 = U_1 - U_2 = 0$$

sample used to obtain these were to be infinitely large. Let  $x_1$  and  $x_2$  be the observed means for the finite sample.  $S_{(x_1 - x_2)}$  is the standard deviation for the sampling distribution of the differences between the sample means:

$$S^2_{(x_1 - x_2)} = \{(N_1 - 1)S_1^2 + (N_2 - 1)S_2^2\}/(N_1 + N_2 - 2) * \{(N_1 + N_2)/(N_1 N_2)\}$$

where  $S_1$ ,  $N_1$  and  $S_2$ ,  $N_2$  are the standard deviation and the size of each sample individually.

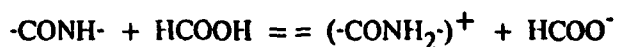
Next,  $t_\alpha$  given by the following equation is calculated.

$$t_\alpha = \{(x_1 - x_2)/S_{(x_1 - x_2)}\}$$

Having calculated  $t_\alpha$ ,  $\alpha$  is obtained from set of tables for t-statistics. The ' $\alpha$ ' value so obtained gives a probability of ' $2\alpha$ ' that the hypothesis  $H_0$  can be rejected, i.e.,  $U_1 = U_2$ . For example, an ' $\alpha$ ' value of 0.03 implies that the probability of making an error in rejecting the hypothesis  $U_1 = U_2$  is 0.06. The probability of that  $U_1 = U_2$  is 0.94.

## Appendix VI - Viscosity of Nylon 6 in Dilute Solutions

Polyamides (PA) show polyelectrolyte behavior in dilute solutions with many solvents (57, 72). A possible mechanism for the formation of ions in 100 % anhydrous formic acid has been proposed (72):



Addition of water to formic acid suppresses such behavior and the mechanism proposed is that water preferentially is able to take  $\text{H}^+$  ions, thereby  $\text{-CONH-}$  remains neutral.

A similar electrolyte behavior has been observed for nylon 6 in hexafluoro iso-propanol (HFIP). GPC analysis of nylon 6 in HFIP resulted in some very late eluting distribution of molecules (beyond the elution volume where all molecular weight components are expected to have eluted out). This indicates another separation mechanism besides the size exclusion of polymer molecules. A rather likely mechanism might be an ionic interaction between column material and the polymer molecules. It has been suggested that addition of sodium trifluoroacetate salt in HFIP to a concentration of 0.1 molar suppresses the polyelectrolyte effect (73) and the polymer chain has a random chain configuration in solution. The GPC analysis of nylon 6 in such a solution showed an expected molecular weight distribution. Therefore, a 0.1 molar sodium trifluoroacetate solution in HFIP has been used for all subsequent GPC analysis. This mobile phase will be referred to as S-HFIP for future reference.

The hypothesis of a random coil configuration for nylon 6 in S-HFIP has been checked by measuring the viscosities of nylon 6 polymer solutions using Ubcholde capillary viscometer. Plots of inherent viscosity  $(\log_e \eta_r)/C$  and reduced viscosity  $\eta_{sp}/C$  against the concentration C of solution are made for three different nylon 6 specimens in Figures 46 and 47. From these plots the intrinsic viscosity, the constants ' $k_1$ ' and ' $k_2$ ' for Huggins and Kraemer equations are obtained as shown in Table 9.

$$\eta_{sp}/C = [\eta] + k_1[\eta]^2 C \quad \text{Huggins Equation}$$

$$(\log_e \eta_r)/C = [\eta] - k_2[\eta]^2 C \quad \text{Kraemer Equation}$$

These determinations of intrinsic viscosity, constants  $k_1$  and  $k_2$  are also made for other solvents: (a) 0.1 molar sodium trifluoroacetate in tetra fluoro-ethanol 2, 2, 2 (S-TFE); (b) aqueous formic acid containing 88 % formic acid. The results of these analyses are shown in Figures 48 through 51. The  $k_1$  and  $k_2$  values measured for nylon 6 in S-HFIP and S-TFE are not typical of a polymer in good solution. Therefore, nylon 6 does not have a random coil configuration in dilute solutions of S-HFIP and S-TFE. The values of the constants  $k_1$  and  $k_2$  in aqueous formic acid are of the order expected for a polymer in good solvent, and  $k_1 \cdot k_2 = 0.5$  implies a random coil configuration for nylon 6 in this solvent.

It is possible that S-HFIP and S-TFE will act as good solvents for nylon 6 if the concentration of sodium trifluoroacetate were increased. This is not feasible due to the limited solubility of the salt in HFIP and TFE. The behavior of nylon 6 molecules in S-HFIP and S-TFE is neither of a random coil nor of a polyelectrolyte (in which case the viscosity of polymer solution increases greatly at low concentrations). Thus one can state that nylon 6 possibly has a rod-like chain configuration in S-HFIP and S-TFE. It is believed that the observed molecular weight distribution will not be affected since the calibration equation is obtained by fitting the known number and weight average molecular weight of a nylon 6 specimen to its MWD obtained from GPC analysis.

Another interesting aspect of viscosity results is the difference between  $k_1$  and  $k_2$  for S-HFIP and S-TFE being consistently close to 0.6.

Figure 46 : Viscosity of nylon 6 fibers in dilute solutions.

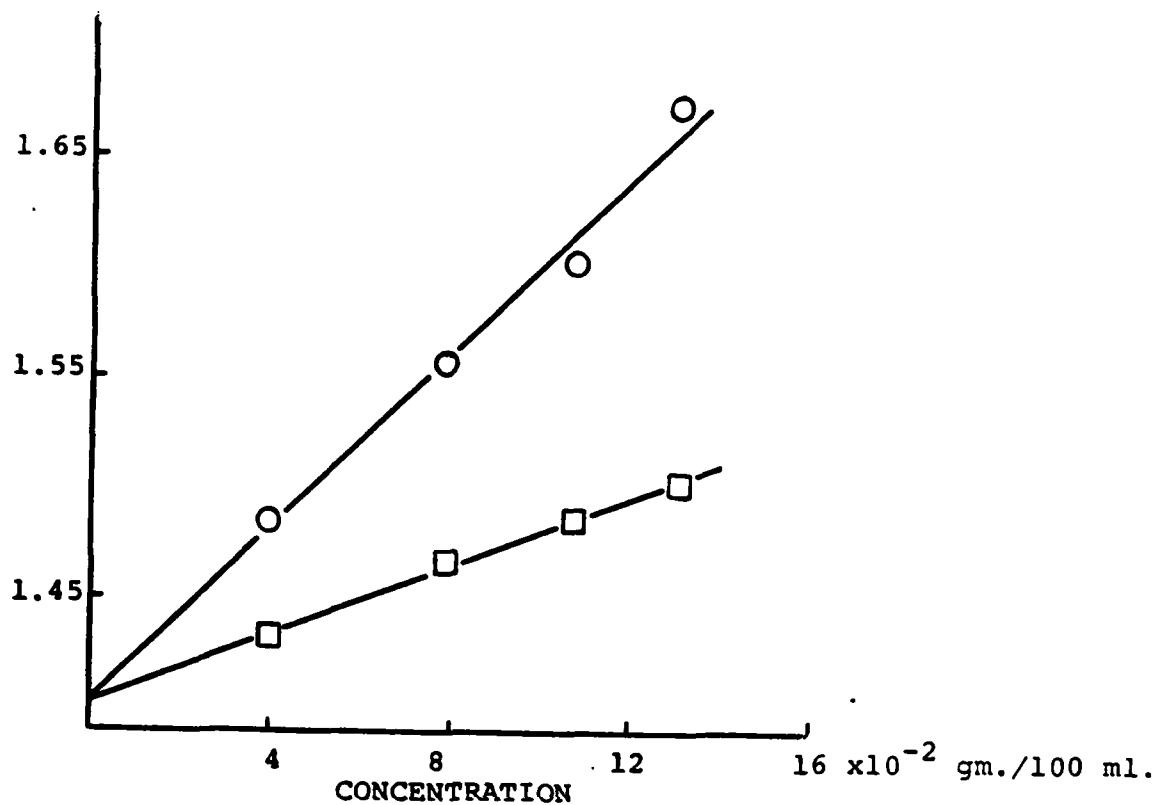


Figure 47 : Viscosity of Allied nylon 6 in dilute solution.

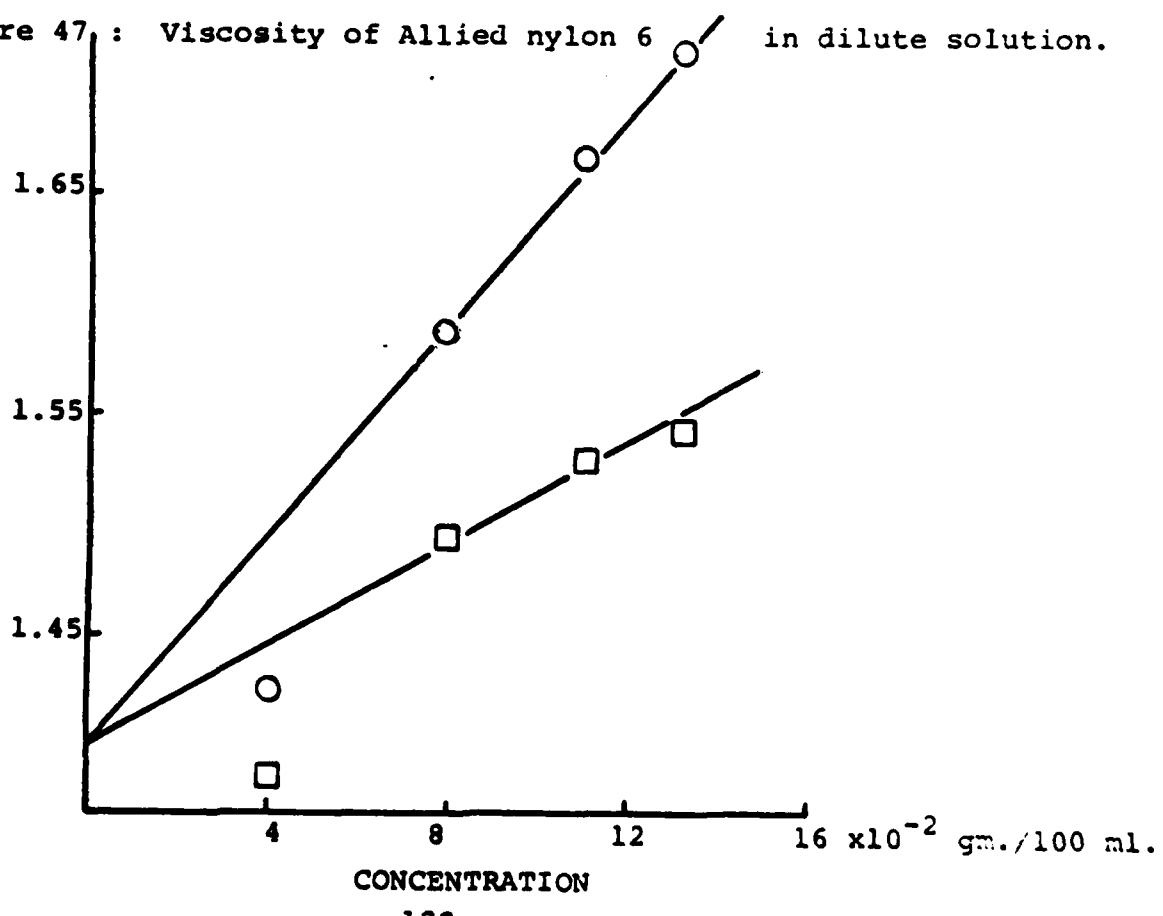


Figure 48 : Viscosity of nylon 6 fibers  
in tetrafluoroethanol (S-TFE).

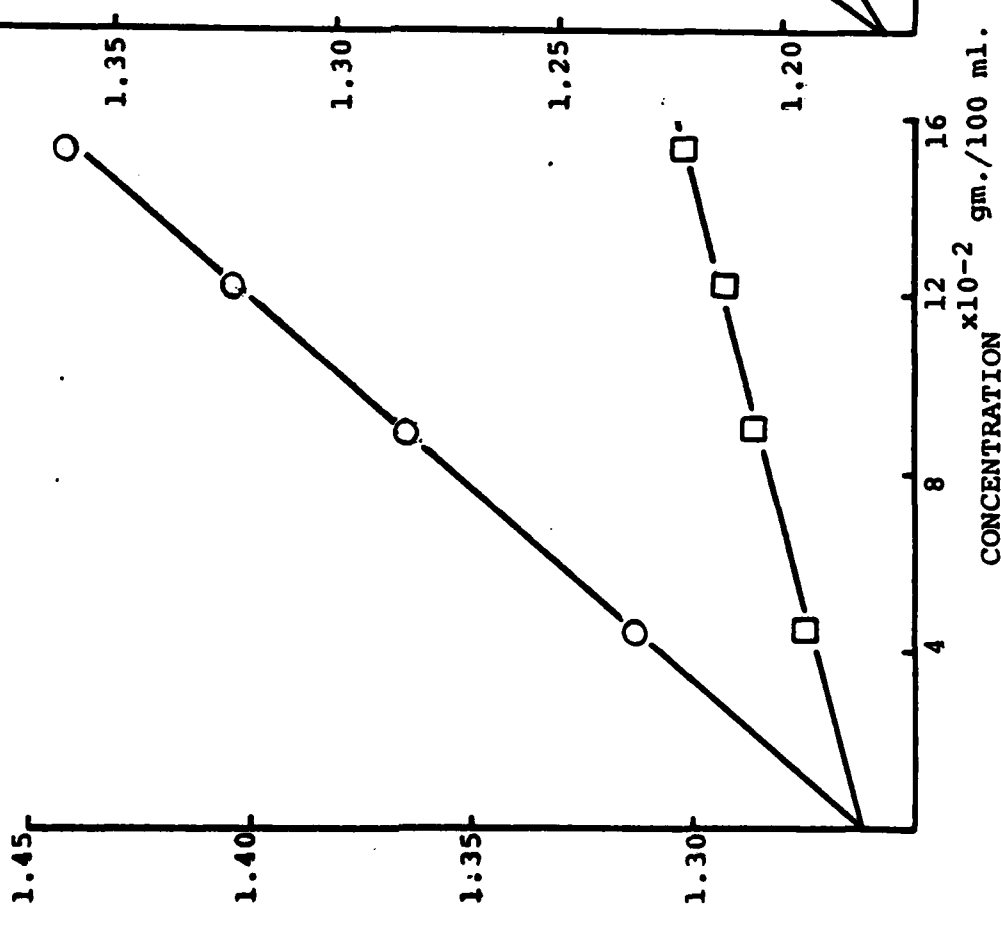


Figure 49 : Viscosity of Allied nulon 6  
in tetrafluoroethanol (S-TFE).

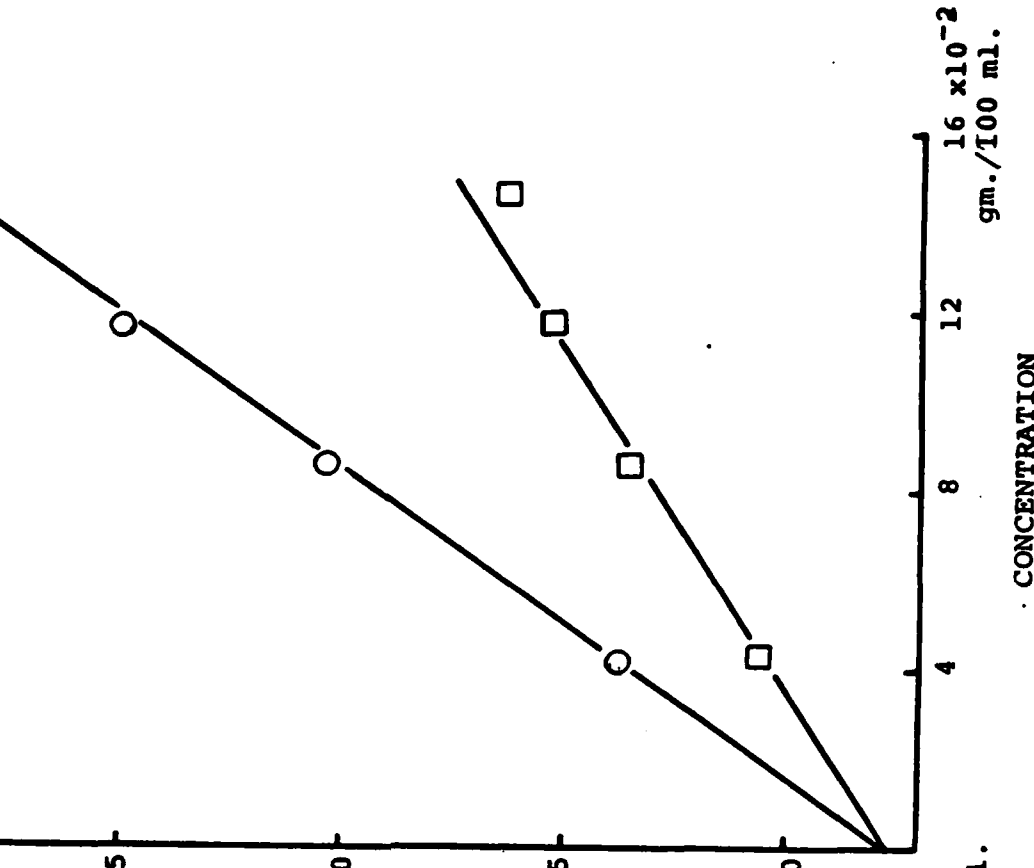


Figure 50 : Viscosity of nylon 6 fibers in  
formic acid (88%).

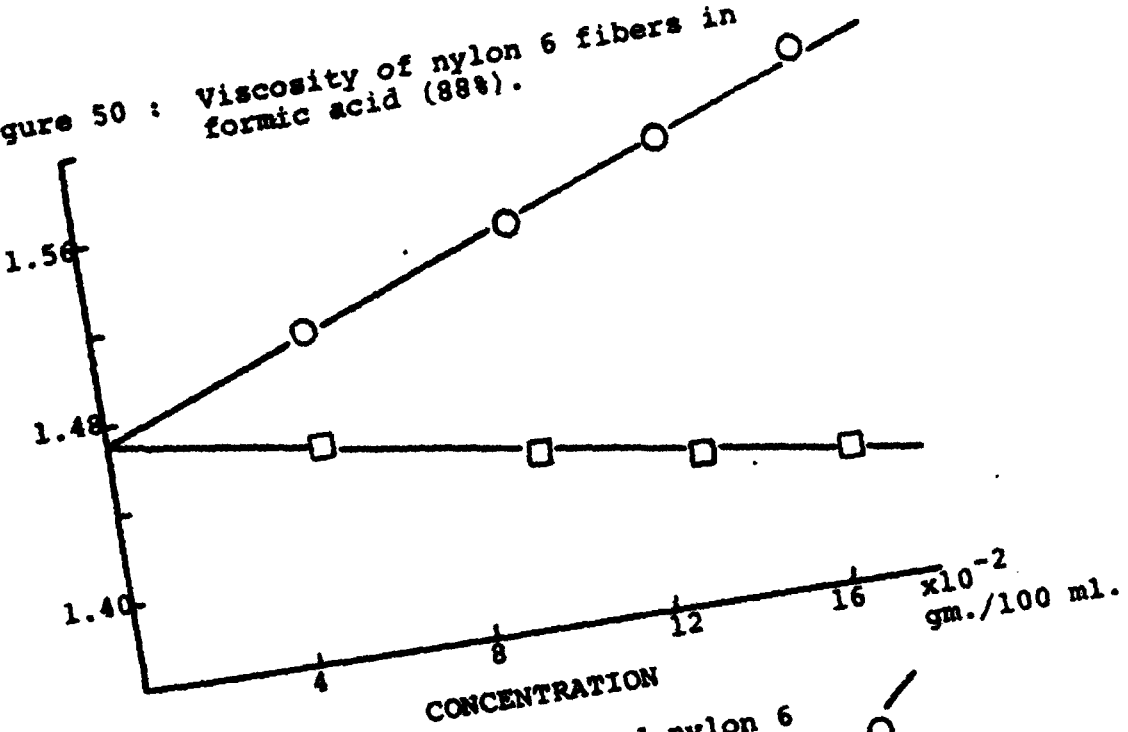


Figure 51 : Viscosity of Allied nylon 6  
in formic acid (88%).

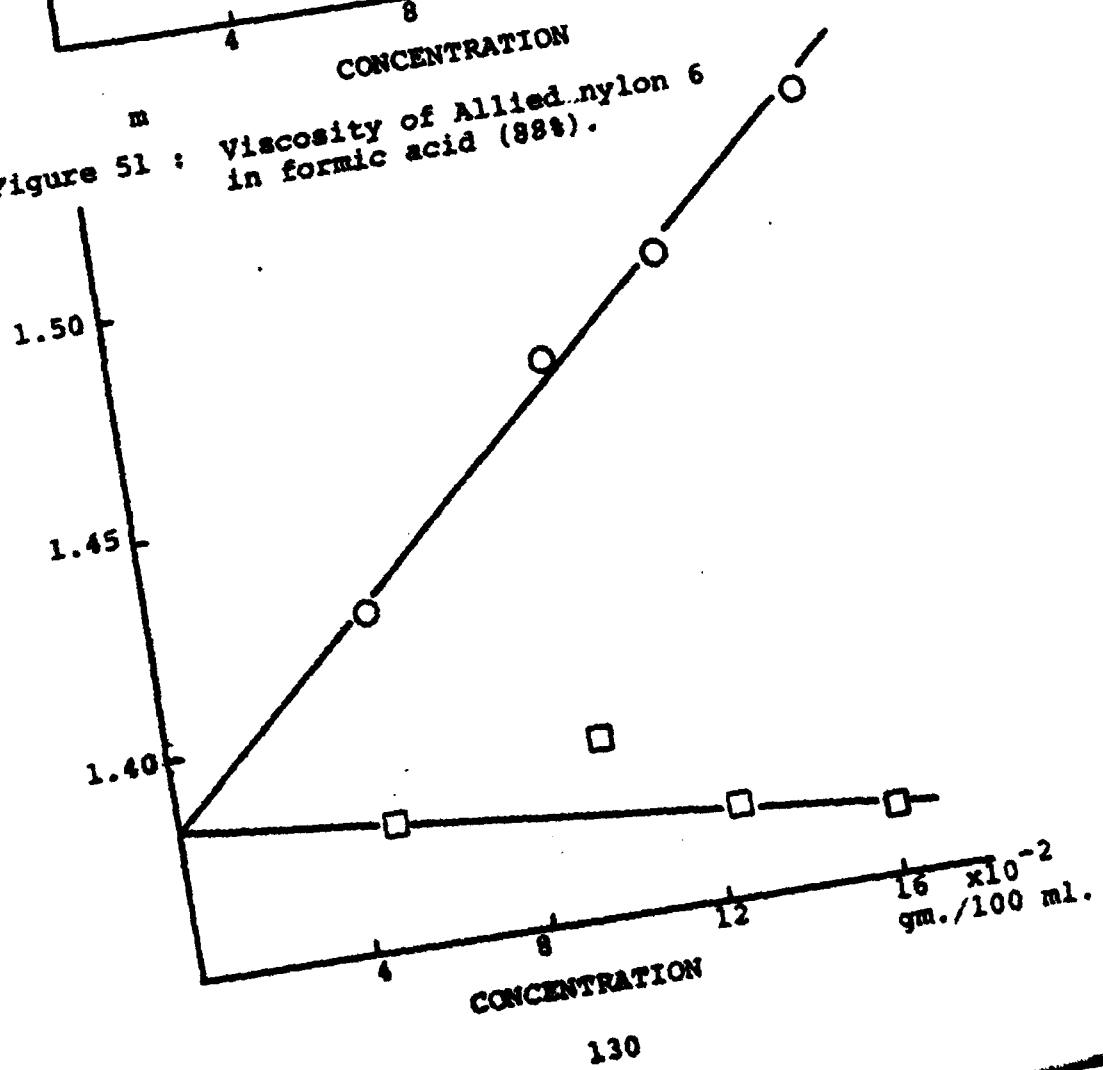


Table 9.

Specimen Type	Solvent: Hexafluoro Isopropanol and Sodium Trifluoroacetate	Solvent: Tetrafluoro- ethanol (2,2,2) and Sodium Trifluoroacetate	Solvent: Aqueous Formic Acid (88%)
---------------	--	---	---------------------------------------

	[ $\eta$ ]	$k'$	$k''$	$k'-k''$	[ $\eta$ ]	$k'$	$k''$	$k'-k''$	[ $\eta$ ]	$k'$	$k''$	$k'-k''$
Nylon 6 fiber	1.404	0.987	0.384	0.603	1.262	0.719	0.163	0.556	1.471	0.348	-0.146	0.494
Allied Nylon 6	1.400	1.194	0.578	0.616	1.170	1.088	0.482	0.606	1.384	0.474	-0.057	0.531
Potter Great Nylon 6	1.274	0.867	0.293	0.574								

## References

1. Griffith, A. A., Phil. Trans. Royal Soc., A221, 163 (1920).
2. Smith, T. L., Stedry, P. J., J. Appl. Phys., 31, 11, 1892 (1962).
- 2b. Smith, T. L., J. Appl. Phys., 35, 1, 27 (1964).
3. Bueche, F., Halpin, J. C., J. Appl. Phys., 30, 1492 (1959).
4. Tobolsky, A., Eyring, H., J. Chem. Phys., 11, 125 (1943).
5. Coleman, B., J. Poly. Sci., 20, 447 (1956).
6. Bueche, F., Halpin, J. C., J. Appl. Phys., 35, 1, 36 (1964).
7. Zhurkov, S. N., Int. J. Fracture, 1, 311 (1965).
8. Hsiao, C. C., J. Appl. Phys., 30, 1 (1959).
9. Kausch, H. H., Hsiao, C. C., J. Appl. Phys., 39, 4915 (1968).
10. Kausch, H. H. Polymer Fracture. Springer-Verlag: New York. 61 - 62. (1979).
11. Gotlib, Y. Y., Dobrodumov, A. V., El'syashevich, A. M., Svetlov, Y. E., Soviet Physics : Solid State, 15, 555 (1973).
- 11a. Dobrodumov, A. V., El'syashevich, A. M., Soviet Physics : Solid State, 15, 6, 1259 (1973).
12. Roylance, D. K., Ph. D. thesis - unpublished, University of Utah (1968).
13. Stoeckel, T. M., Blasius, J., Crist, B., J. Poly. Sci. : Phys., 16, 485 (1978).
14. Kausch, H. H., Bccht, J., Rheological Acta, 9, 137 (1970).
15. Lloyd, B. A. Ph. D. thesis - unpublished, University of Utah (1972).
16. See reference 10, pp. 141 - 150.
17. Zhurkov, S. N., Vettergen, V. I., Korsukov, V. E., Novak, I. I., Fracture, paper 4/47 (1969).
18. Wool, R. P., J. Poly. Sci., 13, 1795 (1975).

19. Roylance, D. K., DeVries, K. L., Polymer Letters, 9, 443 (1971).
20. See reference 10, pp. 148.
21. Nagamura, T., Fukitani, K., Takayanagi, M., J. Poly. Sci. - Phys., 13, 1515 (1975).
22. DeVries, K. L., Lloyd, B. A., Williams, M. L., J. Appl. Phys., 42, 4633 (1971).
23. Klinkenberg, D., Ph. D. dissertation, Technische Hochshule Darmstadt (1978). Referred to in reference 10.
- 24a. Zakrevskii, V. A., Korsukov, Y. Y., Polymer Science - USSR, 10, 1064 (1972).
- 24b. Zhurkov, S. N., Zakrevskii, V. A., Korsukov, V. E., Kuksenko, V. S., Soviet Phys. - Solid State, 13, 7, 1680 (1972).
25. Peterlin, A., J. Material Sci., 6, 490 (1971).
26. Peterlin, A., Textile Res. J., 42, 20 (1972).
27. Yoon, D. Y., Flory, P. J., Polymer, 18, 509 (May 1977).
28. Peterlin, A., J. Poly. Sci. A - 2, 7, 1151 (1969).
29. Peterlin, A., J. Macromolecular Sci., B7, 705 (1973).
30. Peterlin, A., Int. J. Fracture, 11, 761 (1975).
31. Zhurkov, S. N., Kuksenko, V. S., Int. J. Fracture, 11, 629 (1975).
32. Kuksenko, V. S., Slutsker, A. I., J. Macromolecular Sci.: Phys., B12 (4), 487 (1976).
33. Peterlin, A., Polymer Engg. & Sci., 18, 14, 1062 (1978).
34. See reference 10, pp. 196 - 198.
35. Kausch, H. H., Int. Conf. on Deformation, Yield and Fracture of Polymers, Cambridge, 27.1. (April, 1979).
36. Godovskii, Y. K., Papkov, V. S., Slutsker, A. I., Tomashevskii, E. E., Slonimskii, G. L., Soviet Phys. - Solid State, 13, 8, 1919 (1972).
37. Van Krevelen, W. P., Properties of Polymers, Elsevier Publishing Co. New York. pp. 72 (1972).

38. Tobolsky, A., Eyring, H., J. Chem. Phys., 11, 125 (1943).
39. Verma, G. S. P., Peterlin, A., Polymer Preprints, 10, 1051 (1969).
40. Becht, V. J., Fischer, H., Kolloid Z. u. Z. Polymere, 240, 766 (1970).
41. Park, J., Ph. D. thesis - unpublished, University of Utah (1972).
- 42a. Bresler, S. E., Zhurkov, S. N., Kasbekov, E. N., Saminskii, E. M., Tomashevskii, E. E., Soviet Phys. - Tech. Phys., 4, 321 (1959).
- 42b. Zhurkov, S. N., et al., Soviet Phys. - Solid State, 9, 986 (1965).
- 42c. Zhurkov, S. N., Int. J. Fracture, 1, 311, (1965).
- 42d. Zhurkov, S. N., Tomashevskii, E. E., Proc. Conf. on the Physical Basis of Yield and Fracture, Oxford University Press, London, pp. 200 (1976).
- 43a. DeVries, K. L., Roylance, D. K., Williams, M. L., Presentation at the Sixth ICRPG meeting, Pasadena, California.
- 43b. See reference 12.
44. See reference 10, pp. 156.
45. Zakrevskii, V. A., Baptizmanskii, V. V., Tomashevskii, E. E., Soviet Phys. - Solid State, 10, 6, 1341 (1968).
46. Zakrevskii, V. A., Korsukov, V. E., Polymer Sci. - USSR, 14, 1064 (1972).
47. See reference 12.
48. Zakrevskii, V. A., Tomashevskii, E. E., Baptizmanskii, V. V., Soviet Phys. - Solid State, 9, 5, 1118 (1967).
49. Koenig, J. I., Applied Spectroscopy, 29, 4, 293 (1975).
50. DeVries, K. L. (Private communication).
51. Flory, P. J., Yoon, D. Y., Nature, 272, 16, 226 (1978).
52. Kausch, H. H., DeVries, K. L., Int. J. Fracture, 11, 727 (1975).
53. Hoffman, J. D., SPE Transactions, 315 (October 1964).

54. Zachman, H. G., Peterlin, A., J. Macromolecular Sci. - Phys., B3(3), 495 (1969).
55. Chandrasekhar, S., Rev. Mod. Phys., 15, 1, 1 (1943).
56. Gaylord, R. J., Lohse, D. J., J. Chem. Phys., 65, 7, 2779 (1976).
57. Flory, P. J., Principles of Polymer Chemistry, Cornell University Press, Ithaca, New York, (1953).
58. Prevorsek, D. C., Harget, P. J., Sharma, R. K., Reimschussel, A. C., J. Macromolecular Sci. - Phys., B8(1 - 2), 127 (1973).
59. Prevorsek, D. C., Kwon, Y. D., Sharma, R. K., J. Material Sci., 12, 2310, (1977).
60. Chapiro, A., Discussion in the paper - Peterlin, A., Proc. 22nd Nobel Symposium, Sweden, pp. 235 (June, 1972).
61. See reference 50.
62. Clements, J., Jakeway, R., Ward, I. M., Polymer, 19, 63, 9 (1978).
63. Clements, J., Jakeway, R., Ward, I. M., Longman, W., Polymer, 20, 295 (1979).
64. Gibson, A. G., Davies, G. R., Ward, I. M., Polymer, 19, 683 (1978).
65. Peterlin, A., J. Poly. Sci. A - 2, 7, 1151 (1969).
66. Buckley, C. P., Gray, R. W., McCrum, N. G., J. Poly. Sci. B, 7, 835 (1969).
67. Fischer, E. W., Godder, H., Piesczech, W., J. Poly. Sci. C, 32, 149 (1971).
68. Nagou, S., Azuma, K., J. Macromolecular Sci. - Phys., B16 (3), 435 (1979).
69. Perkins, W. G., Porter, R. S., J. Material Sci., 12, 2355 (1977).
70. Takayanagi, M., Imada, K., Kajiyama, T., J. Poly. Sci. C, 15, 263 (1966).
71. Becht, J., DeVries, K. L., Kausch, H. H., European Polymer J., 7, 105 (1971).
72. Schaeffgen, J. R., Trivisonno, C. F., J. Am. Chem. Soc., 73, 4580 (1951); 74, 2715 (1952).
73. Eckmannis, J., Waters Associates, Medford, Mass. (Private communication).